Improving Brain Slice Methodology

Charles E. Miller

A dissertation submitted to the faculty of the University of North Carolina at Chapel Hill in partial fulfillment for the degree of Doctor of Philosophy in the Department of Chemistry

Chapel Hill
2008

Approved by:

Dr. R. Mark Wightman

Dr. Royce Murray

Dr. Gary Glish

Dr. Garegin Papoian

Dr. Greg McCarty

ABSTRACT

Charles E. Miller: Improving Brain Slice Methodology
(Under the direction of Dr. R. Mark Wightman)

Brain slices are an *in vitro* preparation used to simplify the complexity of the brain by isolating particular regions of interest. Dopamine neurons have been found to function differently under current brain slice protocols than *in vivo*. To improve the worth of the information gained from brain slice experiments, it must be determined which elements of the *in vivo* environment are important to normal function. Making these determinations is central to this dissertation. Carbon-fiber microelectrodes were used to monitor electrically stimulated dopamine release in brain slices with fast-scan cyclic voltammetry (FSCV). The first question asked is what role extracellular dopamine tone plays in controlling dopamine release. Basal dopamine tone *in vivo* stimulates D_2 autoreceptors, which regulate dopamine release; however, in brain slices, there is no dopamine tone. Therefore, determining proper autoreceptor activation is important to making release biologically relevant. Second, neurons fire action potentials along their axons to cause release at their terminals. In brain slice experiments stimulation occurs at the nerve terminals. To stimulate at the axons requires visualization of the dopamine neurons. Two transgenic mouse models that make dopaminergic cells visible due to their fluorescence are evaluated. Lastly, electrochemical and immunohistochemical methods are used to account for norepinephrine and serotonin in these brain slices. D_2 autoreceptor stimulation, proper electrode placement, and the appropriate electrochemical approach are found to be important for improving current brain slice methodology.

ACKNOWLEDGEMENTS

The research in this dissertation was made possible with the support and advice of Dr. Mark Wightman. Dr. Lorraine Iacovitti, Thomas Jefferson University, created the GFP transgenic mice on which much of my research relied. The Michael Hooker Microscopy Facility, particularly Wendy Salmon, deserve credit for training and guidance on the confocal microscope and in immunohistochemical technique. Present and past members of the Wightman lab provided assistance in many forms. NIH provided funding.

I would also like to acknowledge the role the North Carolina Air National Guard played in providing financial support, a mental/physical outlet, and an opportunity to serve. My family, fiancé, and friends provided the emotional support necessary to persevere through graduate school.

Table of Contents

List of Tables

List of Figures

List of Abbreviations and Symbols

AADC	aromatic amino acid decarboxylase
AC	anterior commissure
ANCOVA	analysis of covariance
cAMP	cyclic adenosine monophosphate
CCD	charge coupled device
CFME	carbon-fiber microelectrode
CP	caudate putamen
CV	cyclic voltammogram
DA	dopamine
DAT	dopamine transporter
DβH	dopamine-β-hydroxylase
Desi	desipramine
DOPA	dihydroxyphenylalanine
EC_{50}	median effective concentration
EEDQ	2-ethoxy-1-ethoxycarbonyl-1,2-dihydroquinoline
FIA	flow injection analysis
FSCV	fast-scan cyclic voltammetry
GABA	γ-aminobutyric acid
GBR	GBR-12909
GIRK	g-protein coupled inward rectifying potassium channel
HPLC	high performance liquid chromatography
iMLF	interstitial nucleus of the medial longitudinal fasciculus
ip	intraperitoneal
K_d	dissociation constant

K_I	inhibition constant
K_M	Michaelis-Menton constant
MFB	medial forebrain bundle
NAc/Acb	nucleus accumbens
NET	norepinephrine transporter
PLAP	placental alkaline phosphatase
RN	red nucleus
sem	standard error of the mean
SERT	serotonin transporter
SNc	substantia nigra compacta
SNr	substantia nigra reticulate
TH	tyrosine hydroxylase
TPH	tryptophan hydroxylase
TTX	tetrodotoxin
VMAT	vesicular monoamine transporter
V_{MAX}	maximal rate of uptake
VTA	ventral tegmental area
WT	wild-type

Chapter 1

Electrochemistry in Brain Slices

Introduction

The brain is the most complex and least understood organ of the body. Although much has been learned, there is still no overall theory that describes brain function to guide research. There are many reasons to pursue an understanding of the brain. There are a number of diseases/disorders that have eluded description and cures, such as Alzheimer's, Parkinson's, Huntington's, depression, schizophrenia, etc. Additionally, the brain affects the entire body, so many of these diseases/disorders have wide-ranging physical symptoms. Psychologists and cognitive neuroscientists are interested in the mind-body connection. How do the firing of neurons and chemicals acting on receptors translate to behavior and thought? Studying the actions of biogenic amines including dopamine, serotonin, and norepinephrine are central to understanding the brain. The primary excitatory and inhibitory neurotransmitters are glutamate and γ–aminobutyric acid (GABA), respectively. However, biogenic amines are neuromodulators, substances that change the neuronal response to neurotransmitters such as glutamate and GABA. For example, dopamine inhibits glutamate release at its synapse with GABAergic cells in the striatum (Tang et al., 2001). In other words, dopamine is modulating synaptic strength between the glutamatergic and GABAergic neurons.

Neurons are electrically excitable cells in the nervous system that process and transmit information. These cells contain ionic channels that are responsive to the voltage

across the cell's plasma membrane. The traffic of ions through these channels provides the electrical excitability that defines neurons and allows information to be transmitted from one end of the cell to the other. A schematic of a neuron is shown in Figure 1.1. A typical unipolar neuron receives inputs from other cells at the dendrites. These inputs are summed in the cell body where action potentials are generated if the inputs provide a sufficient excitation. An action potential is the wave-like propagation of membrane voltage changes down the axon to the terminals caused by the opening and closing of voltage gated ion channels (Figure 1.2). When the action potential reaches the terminal, it causes the opening of calcium channels (Ca^{2+}, Figure 1.3). The influx of extracellular calcium initiates a cascade of events that results in the release of neurotransmitters (DA, for dopamine) from the neuron into the extracellular space. The released contents can then diffuse across the synapse to act on post-synaptic receptors (D1 and D2), provide feedback to the releasing neuron through pre-synaptic autoreceptors (D_2) and be taken up into the releasing neuron by membrane bound transporters (DAT) (Figure 1.3).

A neuron exists within a network of neurons that form circuits, which constitute a subsystem of the brain. It is the connections made by large numbers of neurons that allow them to store, process, and direct responses to information. For example, the dopamine neurons are shown in Figure 1.4, by labeling tyrosine hydroxylase (TH). Two major pathways are present in this panel (Zeiss, 2005). The mesolimbic pathway consists of dopamine cell bodies in the ventral tegmental are (VTA) that project axons along the medial forebrain bundle (MFB) to terminate in the nucleus accumbens (Acb). The nigrostriatal pathway consists of dopamine cell bodies in the substantia nigra compacta (SNc) that project axons along the MFB and terminate in the caudate putamen (CP). The neurons of the nigrostriatal pathway are part of the basal ganglia motor loop (Hoover and Strick, 1999).

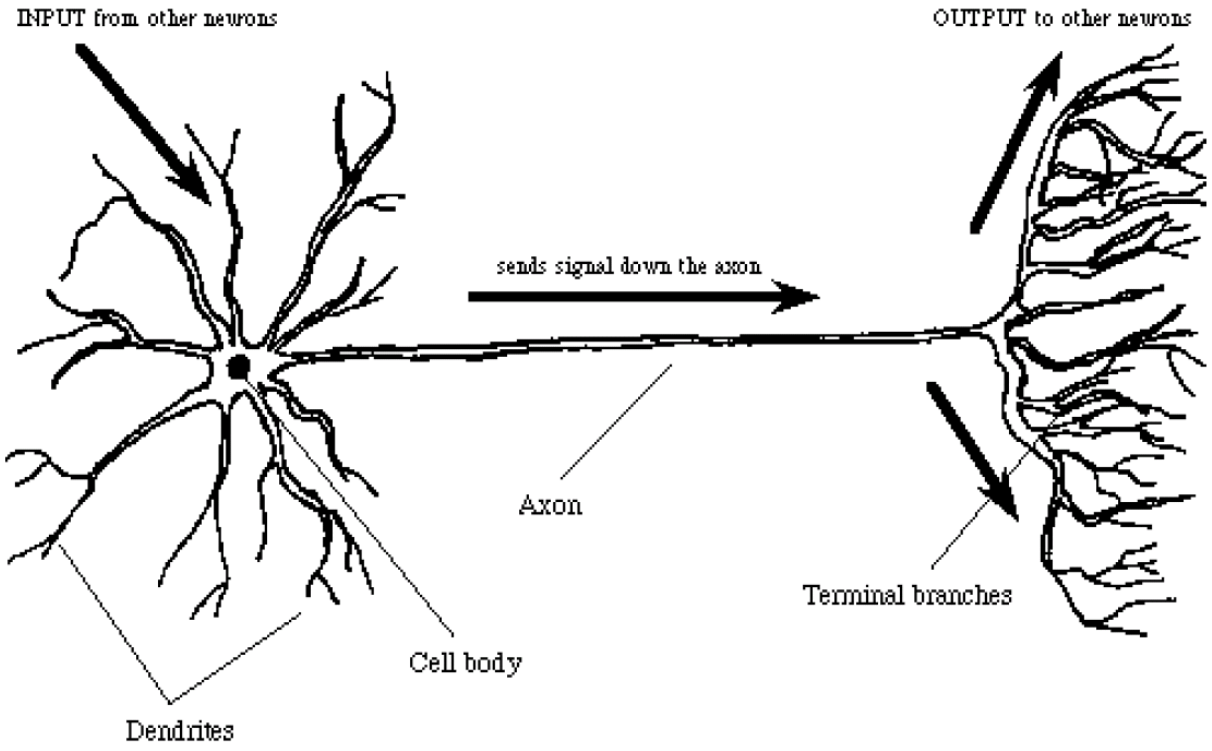

Figure 1.1. Schematic of a neuron. Dendrites receive inputs, which are summed in the cell body. If the inputs provide sufficient excitation, an action potential propagates to the terminals, where substances are released and can interact with other cells.

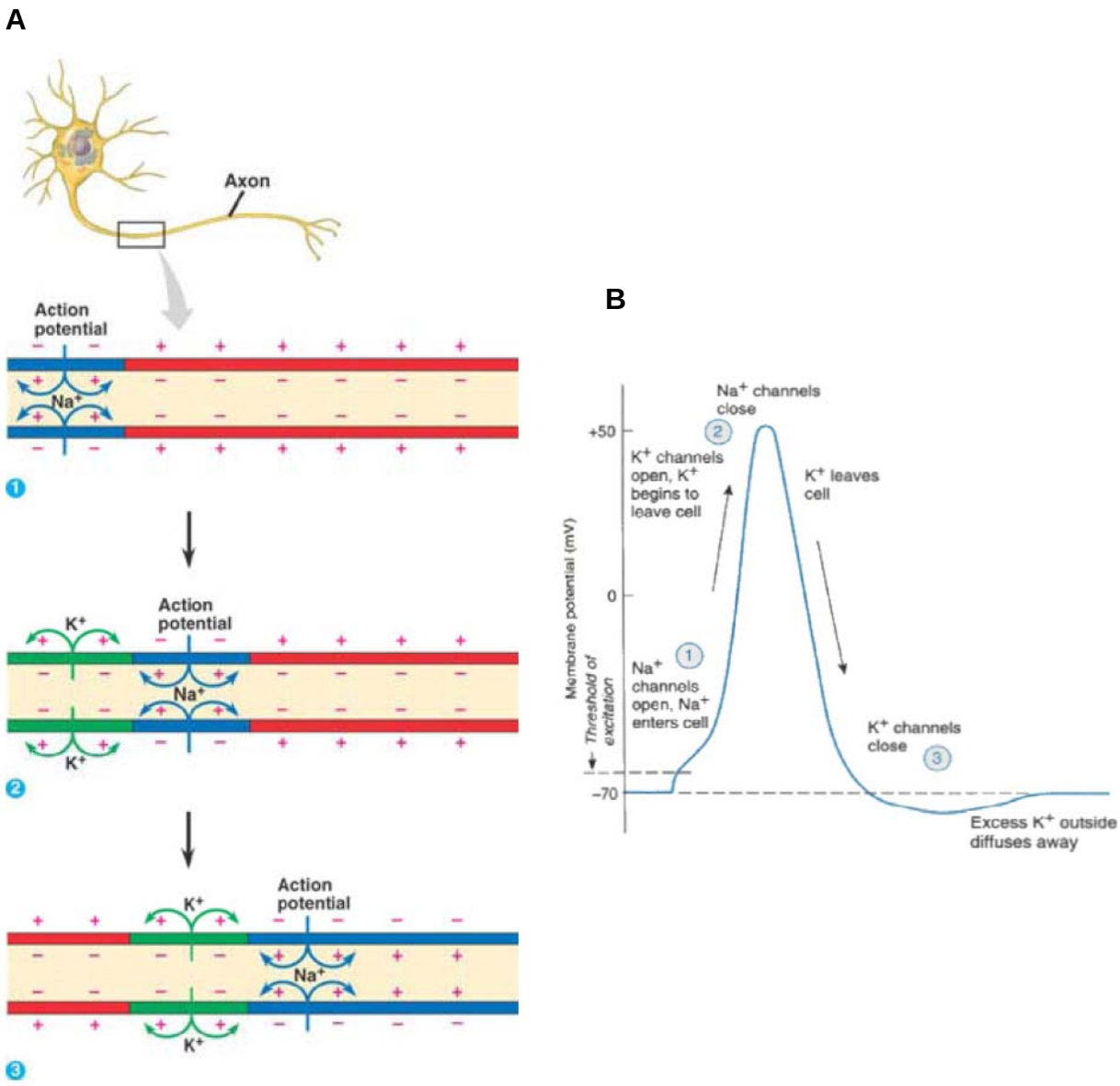

Figure 1.2. Action potential mechanism. A.) 1.Upon depolarization of the plasma membrane, voltage-dependent sodium channels open allowing sodium to diffuse into the neuron along its concentration gradient. 2. As the neuron continues to depolarize, potassium channels open and diffuse out of the cell along its concentration gradient. Adjacent sodium channels open, and immediate sodium channels close. 3. Sodium/potassium pumps re-establish membrane resting potential as the action potential propagates. B.) The membrane potential changes at a fixed position along the axon as an action potential passes. The corresponding changes in ion channel status that cause these potential changes are noted. Images at kvhs.nbed.nb.ca/gallant/biology/action_potential_propagation.html.

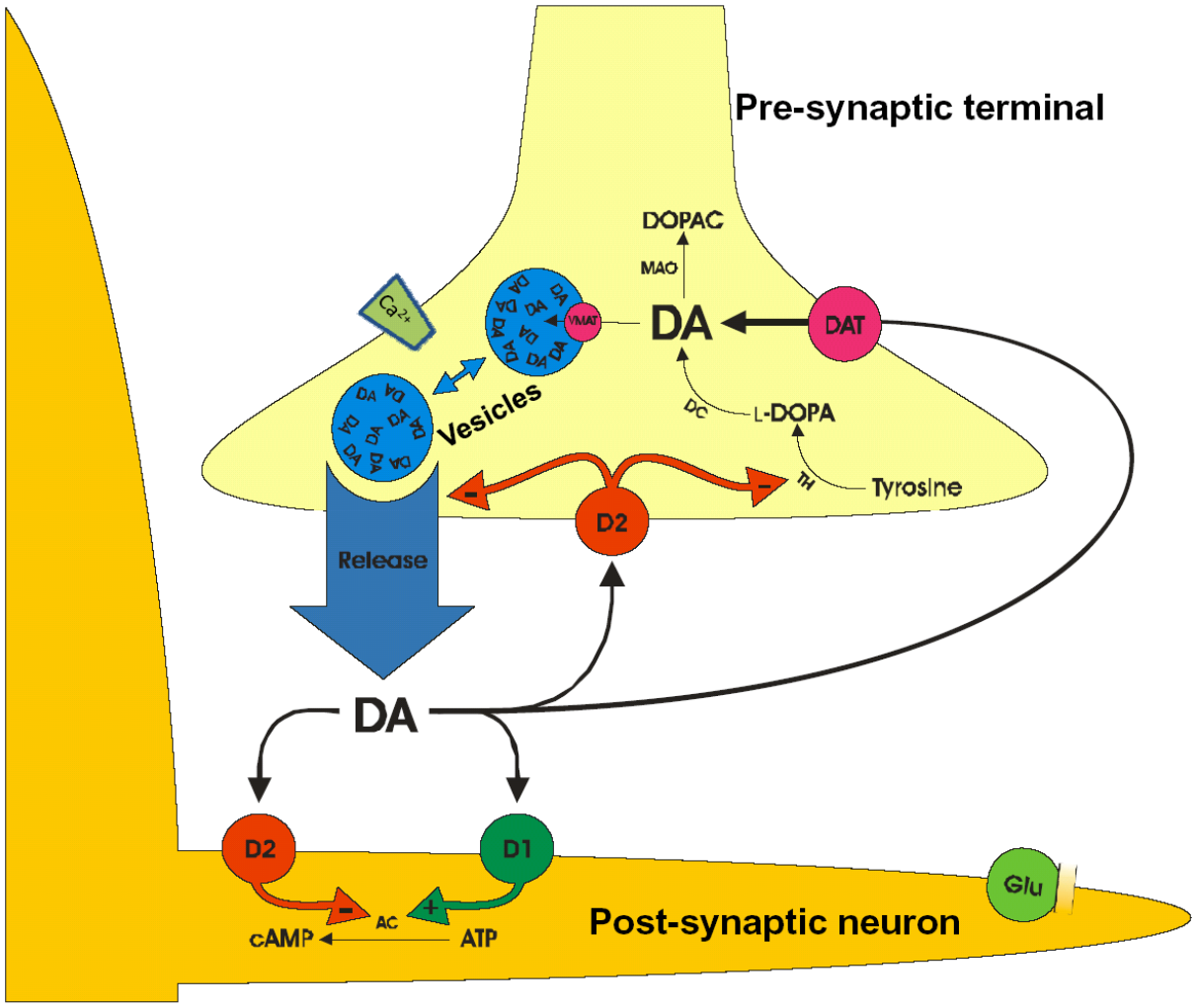

Figure 1.3. Synaptic structure of a dopamine terminal. Dopamine (DA) is synthesized from tyrosine and packaged into vesicles by VMAT. Upon stimulation by an action potential calcium channels (Ca^{2+}) open, causing an influx of calcium that triggers vesicle fusion with the plasma membrane. This fusion event causes release. DA can then bind autoreceptors (D2) to inhibit release, post-synaptic receptors (D1 and D2) to transmit the signal, and the dopamine transporter (DAT) which takes DA up into the terminal.

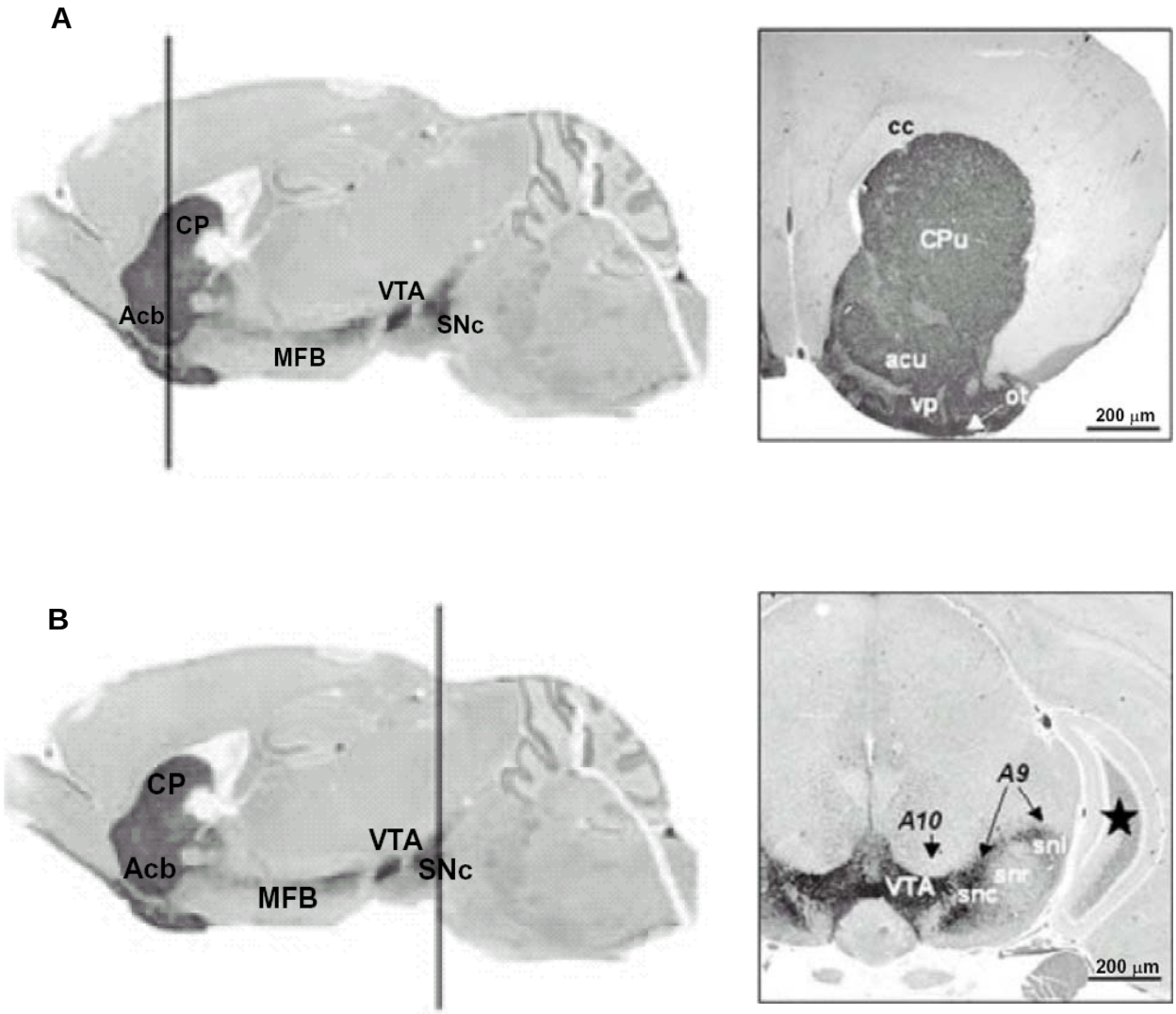

Figure 1.4. TH labeling of the mouse brain visualizes two major dopamine pathways. The nigrostriatal pathway includes the SNc, MFB, and CP. The mesolimbic pathway includes the VTA, MFB, and Acb. These regions are dark in the images. To the left is a side-view of the dopamine neurons in a mouse brain. The vertical line through this view indicates where a slice has been taken to produce the image shown on the right. A.) The line passes through the terminal region of these pathways. In the image on the right heavy TH labeling can be seen in these large terminal regions. B.) The line passes through the cell body region of these pathways. In the image on the right, the VTA and SNc can be seen labeled for TH (Zeiss 2005).

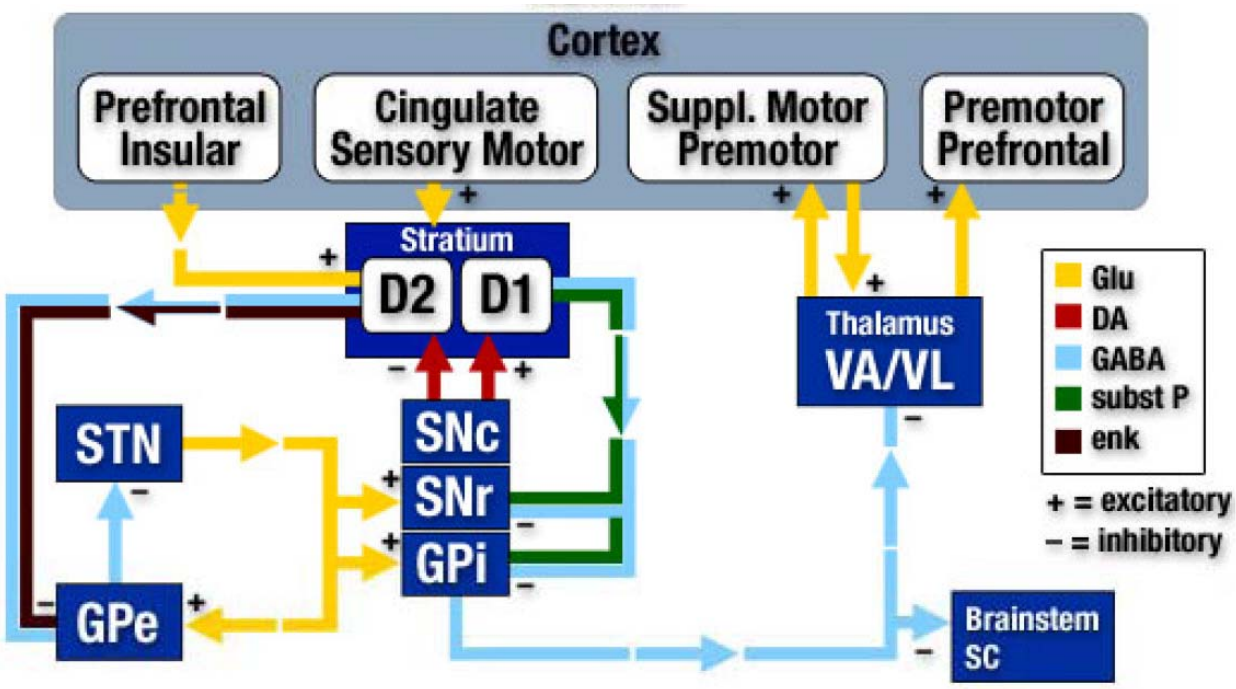

Figure 1.5. The connections within the basal ganglia motor loop. The DA nigrostriatal neurons from SNc to striatum (CP) are in red and provide both inhibitory and excitatory inputs based on the receptors expressed post-synaptically. These neurons operate within a larger circuit of neurons with complex interconnectivity. Image at www.mdvu.org/library/disease/pd/par_path.html.

A flow chart of the circuits that form the basal ganglia are shown in Figure 1.5. The complexity of these circuits makes explaining a change in DA signaling *in vivo* difficult. *In vitro* brain slice experiments isolate the neuron from the circuits and systems to investigate the properties of the neuron that regulate its activity. In our lab, we can measure the activity of pre-synaptic mechanisms that control the amount of neurotransmitter released, such as feedback from autoreceptors and uptake by transporters.

Brain slices

The mammalian brain can be described in reference to three axes (Figure 1.6a). Dorsal-ventral describes the axis from the top of the brain to the bottom. Lateral-medial describes the axis from the sides of the brain inward to the center. Anterior-posterior is the axis from the front of the brain backward. Likewise, brain slices can be made along these three axes (Figure 1.6b). The experiments in this thesis involve coronal and horizontal brain slices. Coronal slices are made along the lateral-medial axis at different distances from bregma, a point of reference on the skull used to measure anterior-posterior distances in the brain. Horizontal slices are made along the anterior-posterior axis at different depths from dura, a membrane covering the top of the brain. Referring to the dopamine pathways described above, coronal slices of the striatum would sever dopamine nerve terminals from the rest of the neuron. Since this slice isolates dopamine terminals, it is commonly used to investigate presynaptic mechanisms that control extracellular concentrations of dopamine. A horizontal brain slice taken from the correct depth can include the complete mesolimbic pathway. Since most of a dopamine neuron is present within this slice, the cell can be stimulated at different locations and release and uptake can be investigated at different recording sites throughout the slice.

A

B

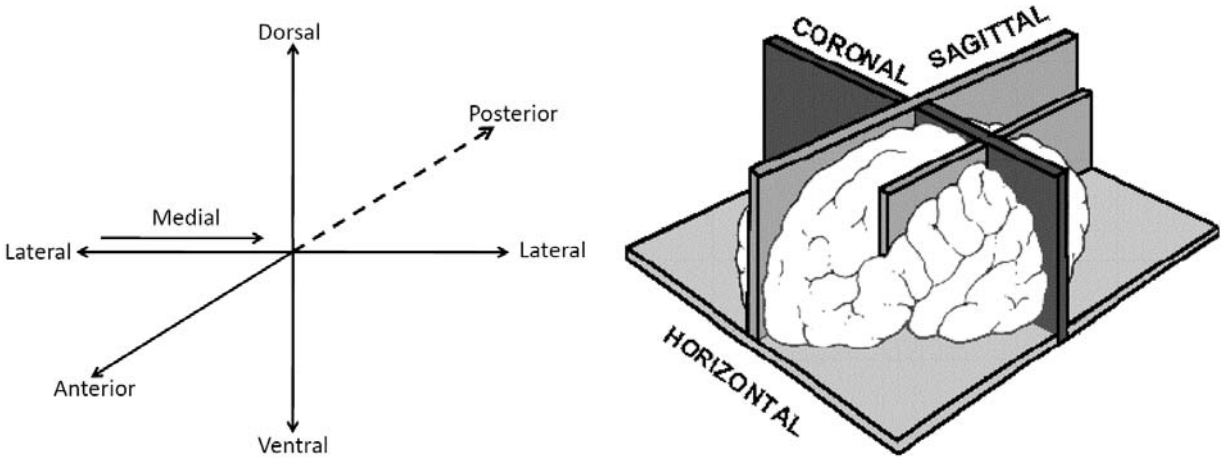

Figure 1.6. Anatomical axes and slice orientations. A.) Three anatomical axes are shown within the context of the human central nervous system. These axes apply within the mouse brain as well. B.) These axes are redrawn for comparison to the three brain slice orientations that are taken along these axes. Coronal slices contain the medial-lateral axis and are taken at different anterior-posterior positions. Horizontal slices encompass the anterior-posterior axis and are taken at different dorsal-ventral positions. Sagittal slices are run along the anterior-posterior axis and are taken at different lateral-medial positions.

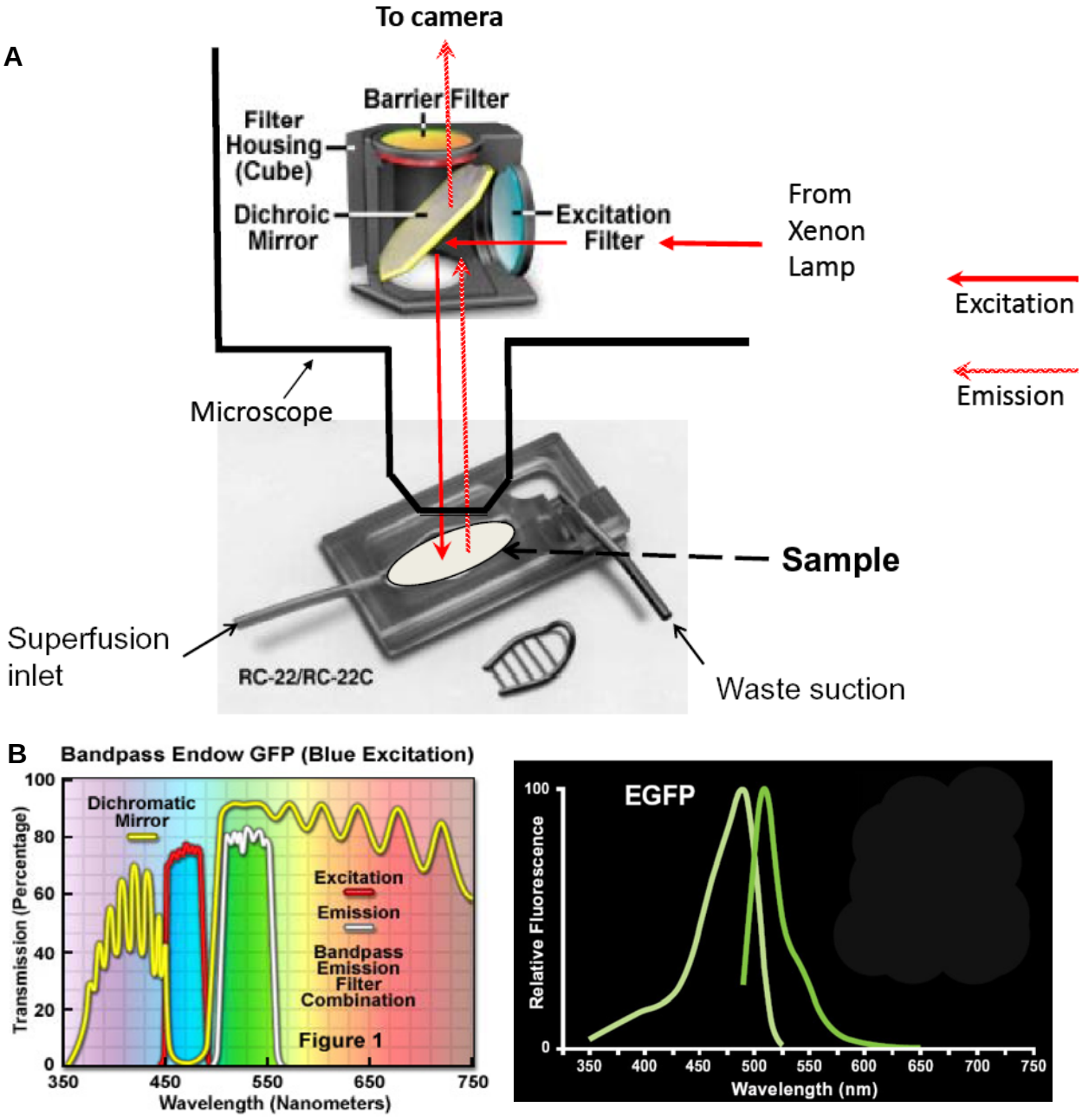

Figure 1.7. Brain slice samples in a tissue chamber (Warner Instruments). A.) Superfusion buffer is used to sustain the sample and administer pharmacological agents. Prior to the tissue chamber an in-line heater maintains buffer temperature (not shown). A microscope is used to aid placement of the stimulating electrode and microelectrode with micromanipulators. With the use of a Xenon lamp source and the appropriate filters, fluorescence from samples can be viewed. For example, fluorescence from green fluorescent protein (GFP) is observed in many samples throughout the thesis. B.) The GFP filter spectral characteristics and the GFP spectra.

To slice the brain, the extracted brain is mounted in a vibratome (World Precision Instruments, Sarasota, FL, USA) according to the orientation desired. The brain is then sliced to a desired thickness (200-300 μm) and placed in a tissue chamber (Figure 1.7). The brain slice is kept functional by a superfusion of buffer. If brain tissue is sliced to thickly, then nutrients within the buffer will not reach interior cells as nutrients are consumed by cells closer to the surface of the slice. The brain slice thickness used provides the structural robustness necessary to withstand sustained manipulation. Under these conditions, slices can remain viable 8-10 hours. This highlights additional benefits of using brain slices. The environment is controlled by the experimenter such that temperature and buffer composition, including pharmacological agents, can be finely controlled. Additionally, the system has an overhead microscope to aid precise electrode placement with micromanipulators. Other spectroscopic microscopy methods can be used as well, including fluorescence and infrared imaging.

Measurement

The bulk of what is known about brain function has been discovered by electrophysiologists, who use electrodes to measure the changes in voltage that indicate the "firing" of action potentials. The action potential was first described in 1952 by Hodgkin and Huxley using the squid axon. Since that time it has been found that much of the information conveyed in the brain is encoded in the frequency of neuron firing (Heine et al., 2008). Which neurons fire is controlled by the molecules being released from firing neurons and the distribution of corresponding receptors on target neurons. To study the concentration and time course of these release events most investigators have used two primary techniques: microdialysis and electrochemistry.

Microdialysis is a technique for sampling the extracellular brain fluid using a probe with a semi-permeable membrane (Watson et al., 2006). The fluid can be analyzed off-line, typically with high-pressure liquid chromatography (HPLC). This approach allows one to monitor changes of many extracellular components simultaneously and with high sensitivity. However, microdialysis is relatively slow (collections times of several minutes) and the probe is large (200-400 μm wide) relative to electrodes (<10 μm wide).

The electrochemical approach used in this work is fast-scan cyclic voltammetry (FSCV). The temporal resolution of this technique allows collection rates of 10-60 Hz to be used. Carbon-fiber microelectrodes (CFME's) used here are 25 μm long and 5-7 μm in diameter (Figure 1.8) and are made as described previously (Kawagoe et al., 1993). To the electrode a triangle waveform is applied. Figure 1.9 shows the waveform used for detecting dopamine in this work. In the absence of analyte, the high scan rate generates a large background current caused by capacitive charging and oxidation of surface groups. Over short time intervals, this background is stable and can be subtracted from the signal when the analyte is present. Dopamine adsorbs to the electrode at the holding potential, oxidized on the forward scan, and reduced on the return scan. The resulting cyclic voltammogram identifies the analyte and measures the concentration present, following a calibration of the electrode. A similar approach is used to detect serotonin. Serotonin can be detected with the same waveform as dopamine but will lead to electrode fouling. A modified waveform that avoids fouling is shown in Figure 1.10. The portion of the waveform at more negative potentials than the holding potential serves to clean the electrode surface. The very fast scan rate is used to out-run side reactions that serotonin oxidation products undergo.

While FSCV with CFME's provides spatial and temporal resolution superior to microdialysis, it is more limited in selectivity and sensitivity. Only electroactive substances

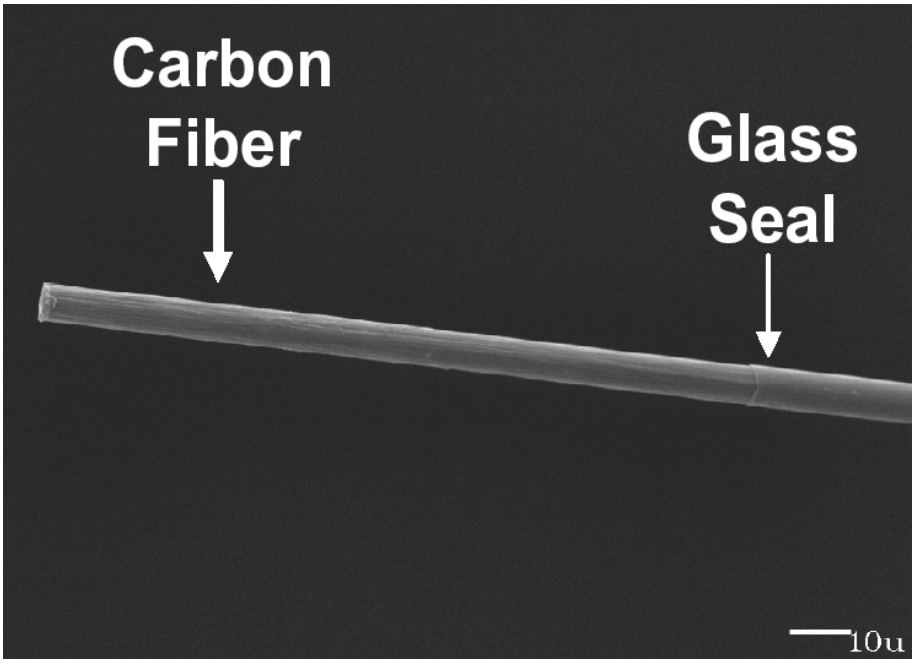

Figure 1.8. An SEM image of a cylinder carbon-fiber microelectrode. The carbon fiber is encapsulated in a pulled glass capillary to form a seal less than 10 μm in diameter. The portion of the fiber extending from the seal is cut to a length about 25 μm (Kawagoe et al., 1993).

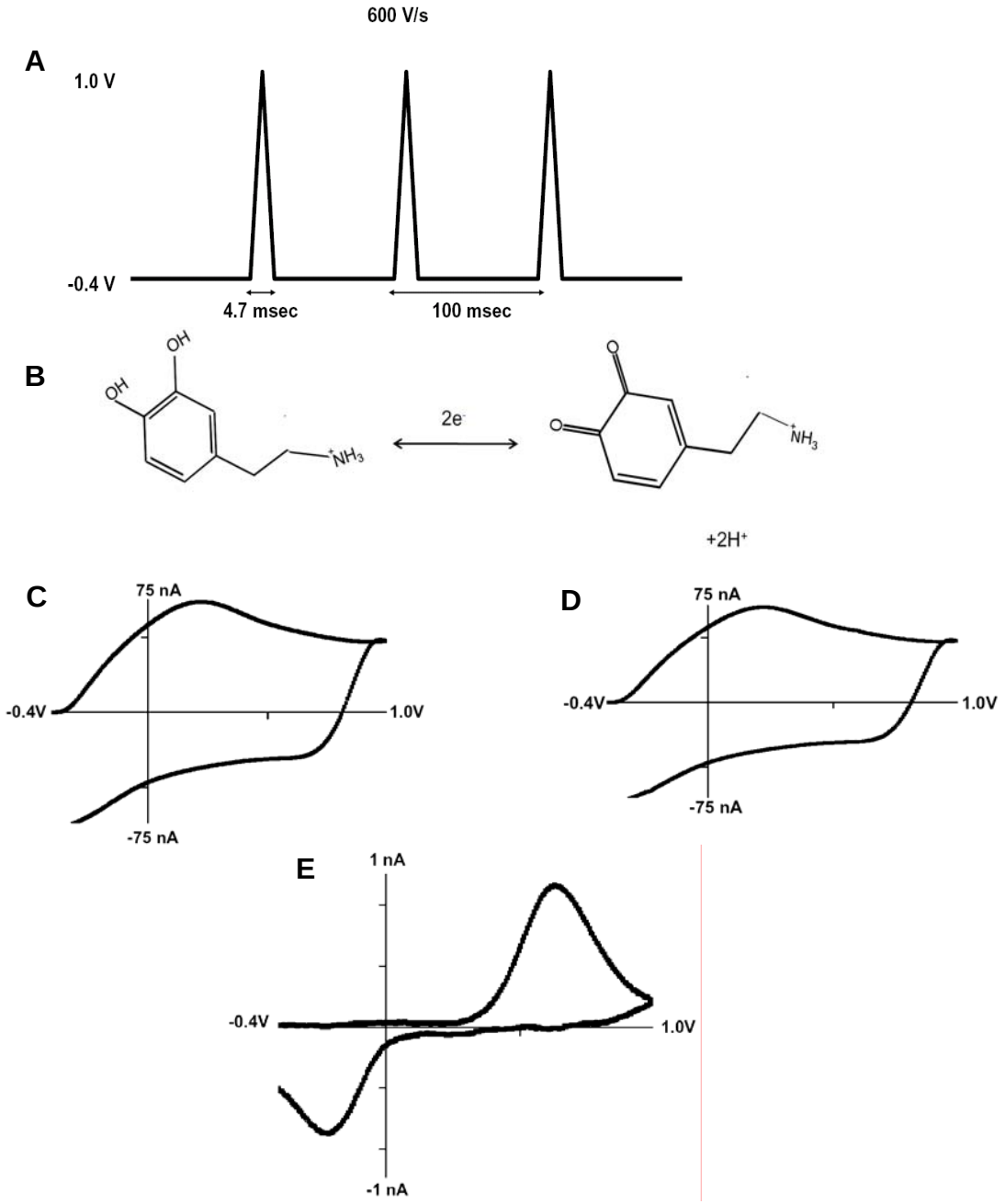

Figure 1.9. DA detection. A.) The triangle waveform used to detect DA. B.) The oxidation-reduction reaction of dopamine that causes the faradaic current measured. C.) The background current generated by applying the waveform to the microelectrode. D.) The current obtained in the presence of dopamine. E.) The background subtracted cyclic voltammogram of dopamine.

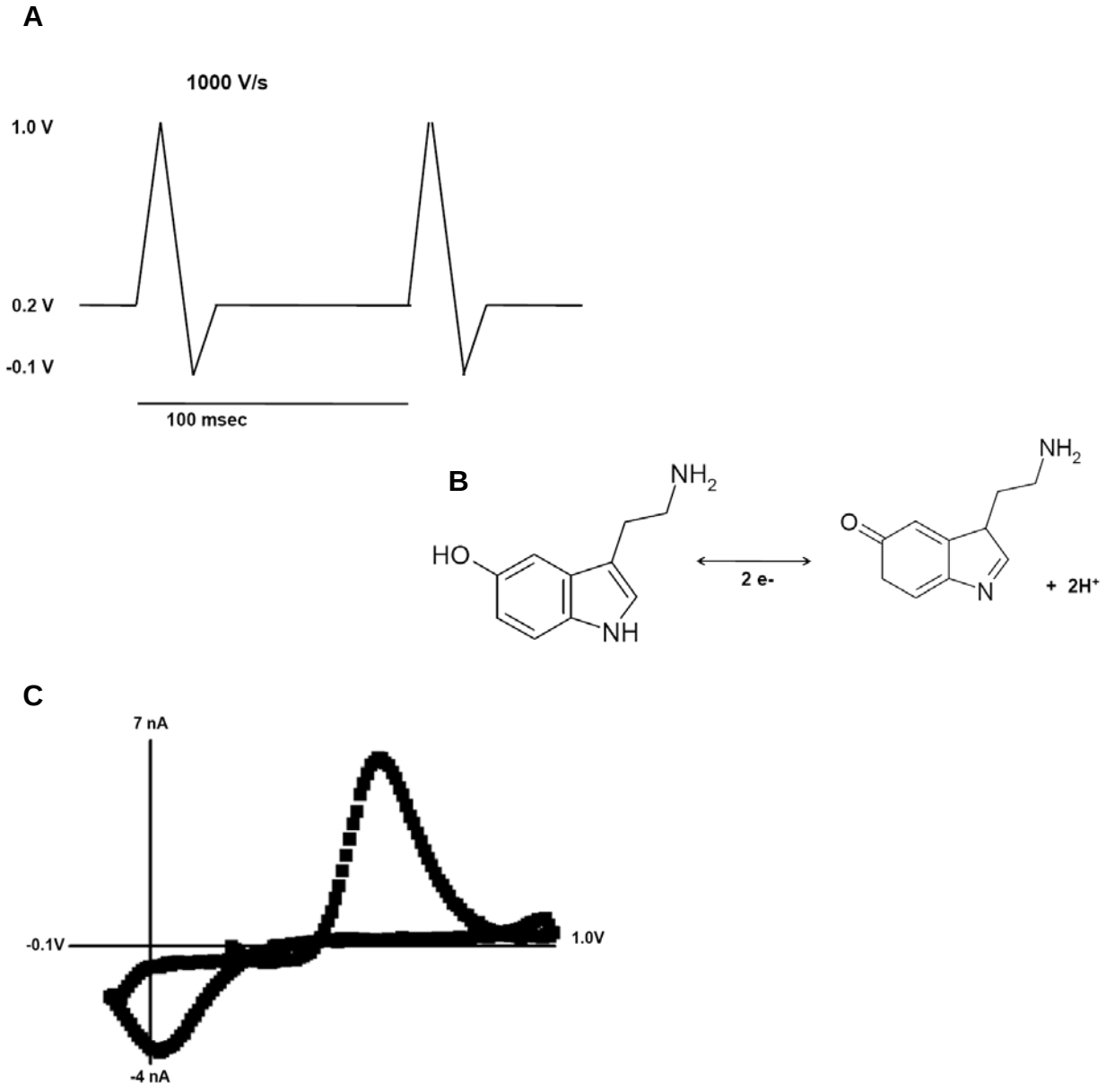

Figure 1.10. 5-HT detection. A.) The triangle waveform used to detect 5-HT. B.) The oxidation-reduction reaction of 5-HT that causes the faradaic current measured. C.) The background subtracted cyclic voltammogram of 5-HT .

can be detected with FSCV, while offline analysis with microdialysis allows one to analyze many neurochemicals. Moreover, FSCV is limited in the number of analytes that can be simulataneously measured. Generally, the potential window is so small that it is best when only one analyte is monitored at a time, but newer data analysis approaches, such as principle component regression, are improving the resolution of multi-component signals (Heien et al., 2005).

Additionally, FSCV is sensitive to changes in the surface of the microelectrode that affect the response to an analyte. This includes fouling which reduces electrode sensitivity, but also includes substances that increase electrode sensitivity. Quinpirole and quinelorane, commonly used pharmacological agents, increase the microelectrodes response to dopamine. Using flow-injection analysis (FIA) to analyze electrode sensitivity to a bolus of 2 μM dopamine, it was found that quinpirole increases electrode sensitivity to dopamine despite the fact that quinpirole is not electroactive itself. This increase in sensitivity is blocked by coating the electrode in Nafion, a cation exchange membrane. Quinpirole increase the signal by 120 $\pm$6% of control with a bare electrode, but a Nafion-coated electrode's sensitivity does not change with the presence of quinpirole (98 $\pm$2%). Quinelorane, an analog of quinpirole, also increases the sensitivity to the same bolus (118 $\pm$5%, Figure 1.12). While it is not known at this time what the mechanism of this change in sensitivity is, it may be that Nafion is blocking adsorption of quinepirole/quinelorane to the surface of the electrode or preventing it from changing the double layer structure near the electrode.

While microdialysis can look at slow changes in the extracellular concentration of brain fluid components, FSCV is sufficiently fast (millisecond temporal resolution) to investigate the components of a release event. Shown in Figure 1.13 is the typical release

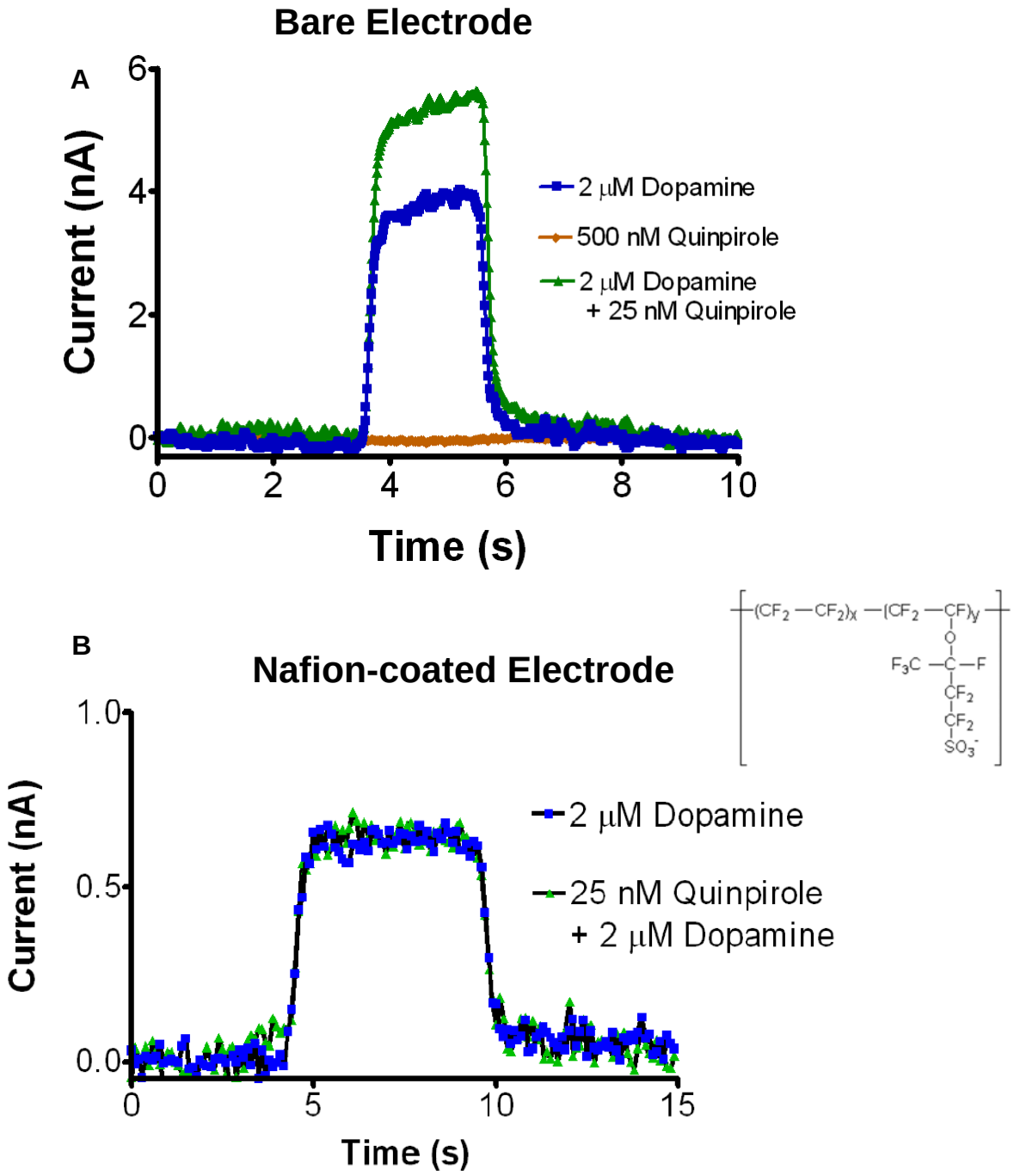

Figure 1.11. In a flow-cell apparatus, a bolus of dopamine was injected in the presence and absence of quinpirole. A.) Quinpirole enhances a bare electrode's current response to dopamine, although quinpirole itself is not electroactive. B.) This enhancement of sensitivity is absent when the electrode is coated with Nafion, the perfluorinated sulfonate polymer shown on the right.

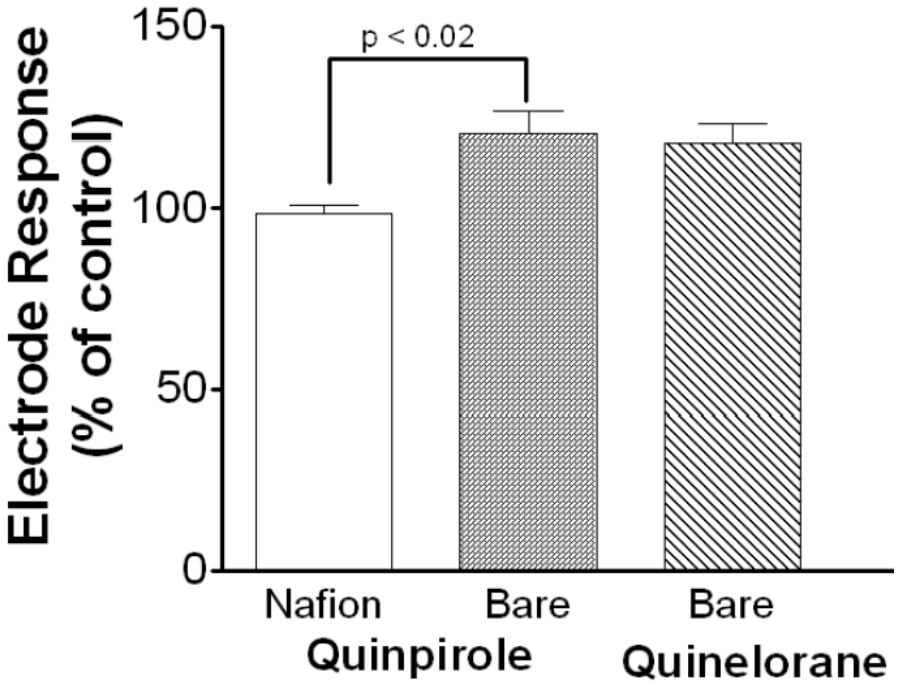

Figure 1.12. Effect of quinpirole and quinelorane on DA sensitivity. In a flow-cell apparatus, a bolus of dopamine was injected in the presence and absence of quinpirole and quinelorane. Quinpirole increases a bare electrode's sensitivity to dopamine (120 $\pm$6% of control) but does not increase a Nafion-coated electrode's sensitivity to dopamine (98 $\pm$2% of control). There is a significant difference in the increase in sensitivity to dopamine in the presence of quinpirole between Nafion-coated and bare electrodes ($n = 5$, $p < 0.02$). Quinelorane, an analog of quinpirole, increases a bare electrode's sensitivity to dopamine by a similar amount (118 $\pm$5% of control).

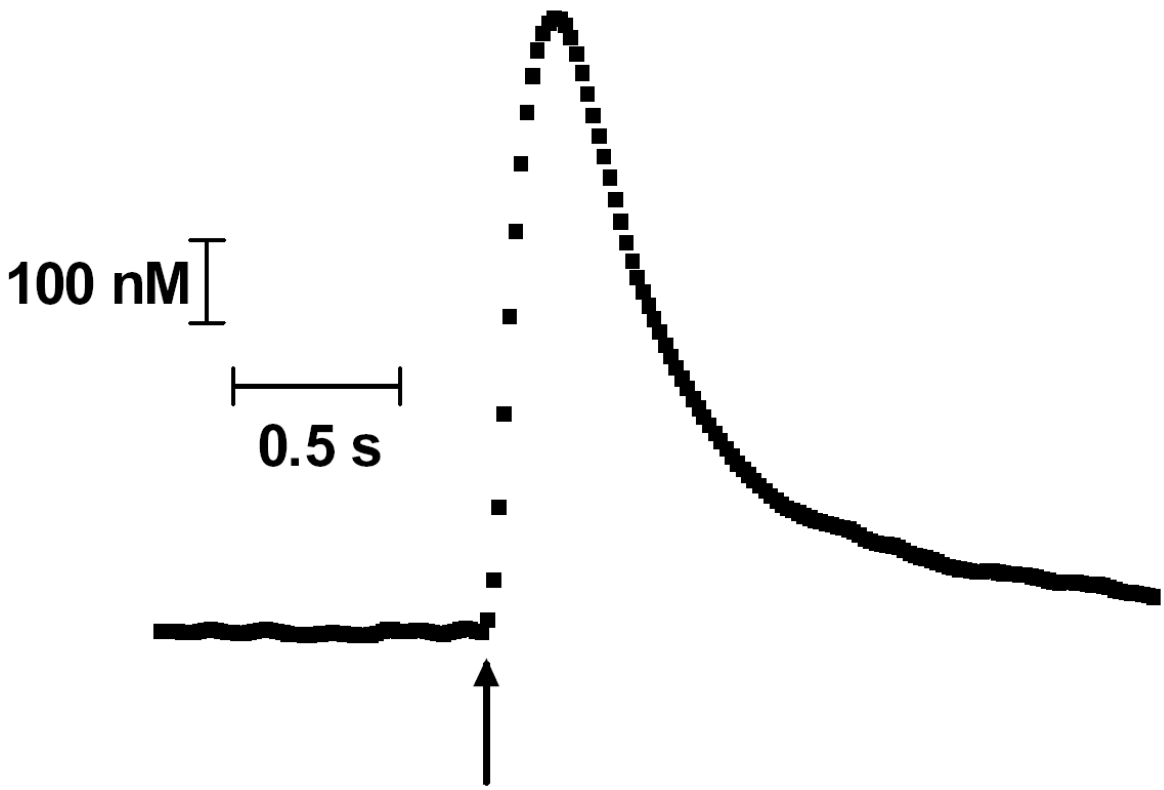

Figure 1.13. Representative trace of stimulated release in the CP of a mouse brain slice. Single-pulse stimulation applied at the time indicated by the arrow. The concentration of extracellular dopamine increases immediately upon stimulation. This increase indicates the release of dopamine from the terminals. The concentration decreases more slowly and is due to the uptake by DAT as DA is cleared from the extracellular space.

profile elicited by a single current pulse stimulation in a brain slice. This profile contains a rapidly increasing segment indicating release followed by a slower descending component indicating clearance of the substance. The signal is on the second time scale that can be best measured by electrochemical approaches.

Pre-synaptic controls

Neurons synthesize biogenic amines, package them into vesicles, and release them to the extracellular space upon stimulation. The release of dopamine from neurons is very similar to that of the other biogenic amines (Cooper et al., 2003) and is briefly described here (see Figure 1.3). Dopamine is synthesized from the amino acid tyrosine. TH, the rate-limiting enzyme in catecholamine synthesis, converts tyrosine to dihydroxyphenylalanine (L-DOPA). L-DOPA is then converted to dopamine by aromatic amino acid decarboxylase (AADC). Dopamine is then packaged into vesicles by the vesicular monoamine transporter (VMAT). When an action potential reaches a nerve terminal, it causes the opening of voltage-gated calcium channels and a large influx of extracellular calcium. There are a number of calcium sensitive proteins both on the surface of vesicles and the inner surface of the plasma membrane. They respond to the influx of extracellular calcium by fusing the vesicle with the plasma membrane, thus causing dopamine within the vesicle to be released to the extracellular space. There are several pharmacological points of control in this process. One can inhibit TH, VMAT, and calcium channels. One could remove calcium from the extracellular buffer being superfused. One could also remove sodium or use a sodium channel blocker, such as tetrodotoxin (TTX), to inhibit the initiation of action potentials.

The D_2-autoreceptor is a receptor found on dopaminergic terminals that provide negative feedback to the cell (Figure 1.3). It is a metabotropic receptor, which means it is coupled to G-proteins that serve as second messengers within the cell. Substances that

bind to a receptor and activate it are called an agonist. Dopamine, quinpirole, and quinelorane are D_2-receptor agonists. When these agonists bind the autoreceptor, they activate a second messenger system that targets several points in the cell to lower the amount of dopamine. First, it leads to the phosphorylation of TH, which reduces the rate of dopamine synthesis (Wolf et al., 1986). Second, it leads to the phosphorylation of GIRK channels (G protein activated inward rectifying potassium channels) (Einhorn et al., 1991). By increasing potassium conductance, the terminal membrane potential is made less positive and thus lowering the probability of opening sodium and calcium channels, i.e. lowering the chance and magnitude of release.

Once dopamine is released, it can return to the interior of the neuron by being taken up by the dopamine transporter (DAT). DAT uptake is driven by the sodium gradient across the plasma membrane. Two sodium ions are transported into the cell with each molecule of dopamine. One chloride ion is transported in as well to avoid a charge buildup. Since dopamine is being measured on the outside of the neuron, its uptake causes a disappearance of signal and is primarily responsible for the descending portion of the trace in Figure 1.13. The rate of uptake can be modeled using Michaelis-Menton kinetics (Wightman et al., 1988; Kawagoe et al., 1992; Jones et al., 1995). Thus, the presumed scheme is (Matthews and Holde, 1996):

$$(DA)_o + T \leftrightarrow (DA)T \rightarrow (DA)_I + T$$

where $(DA)_o$ is extracellular dopamine, $(DA)_i$ is intracellular dopamine, and T is the dopamine transporter. DA binds the transporter, which then changes conformation to expose DA to the inside of the cell, and DA dissociates from the transporter. The Michaelis–Menten rate equation for dopamine uptake may be written as:

$$d[DA]/dt = [DA]_p - V_{max}/(K_M/[DA] + 1)$$

where [DA] is the brain extracellular concentration of dopamine and $[DA]_p$ is the change in concentration of dopamine at the electrode produced by each stimulus pulse. V_{max} is the maximal rate of uptake, which is dependent on DAT concentration. K_M is the concentration of DA at which the rate of uptake is half of V_{max}.

The kinetics of uptake by DAT can be slowed by adding an uptake inhibitor, such as cocaine, methamphetamine, or nomifensine. This change in kinetics can be understood as that of a competitive inhibitor, which competes with the endogenous ligand to bind the protein. In this case, the uptake inhibitors bind DAT and thus interfere with DA uptake. In the presence of a competitive inhibitor (I), the additional equilibrium must be considered:

$$I + T \leftrightarrow IT$$

Under this paradigm $(K_M)_{app}$, the apparent K_M, is defined as $K_M(1 + [I]/K_i)$, where K_i is the dissociation constant for the above reaction, and is defined as $K_i = [I][T]/[IT]$. Therefore, the introduction of an uptake inhibitor will increase the apparent K_M, thus increasing the time DA persists in the extracellular space (Figure 1.14).

Animals

The experiments described here are conducted in mice. Therefore, conclusions from this data provide information useful in basic research on rodents and are not extendable to other species, including humans, although some similarities may exist. Rodents are commonly used in brain research. They have a highly evolved mammalian brain but are still simple enough for necessary *in vitro* experiments, such as brain slice experiments. While many different types of rodents are used in brain research, including rats and guinea pigs, mice

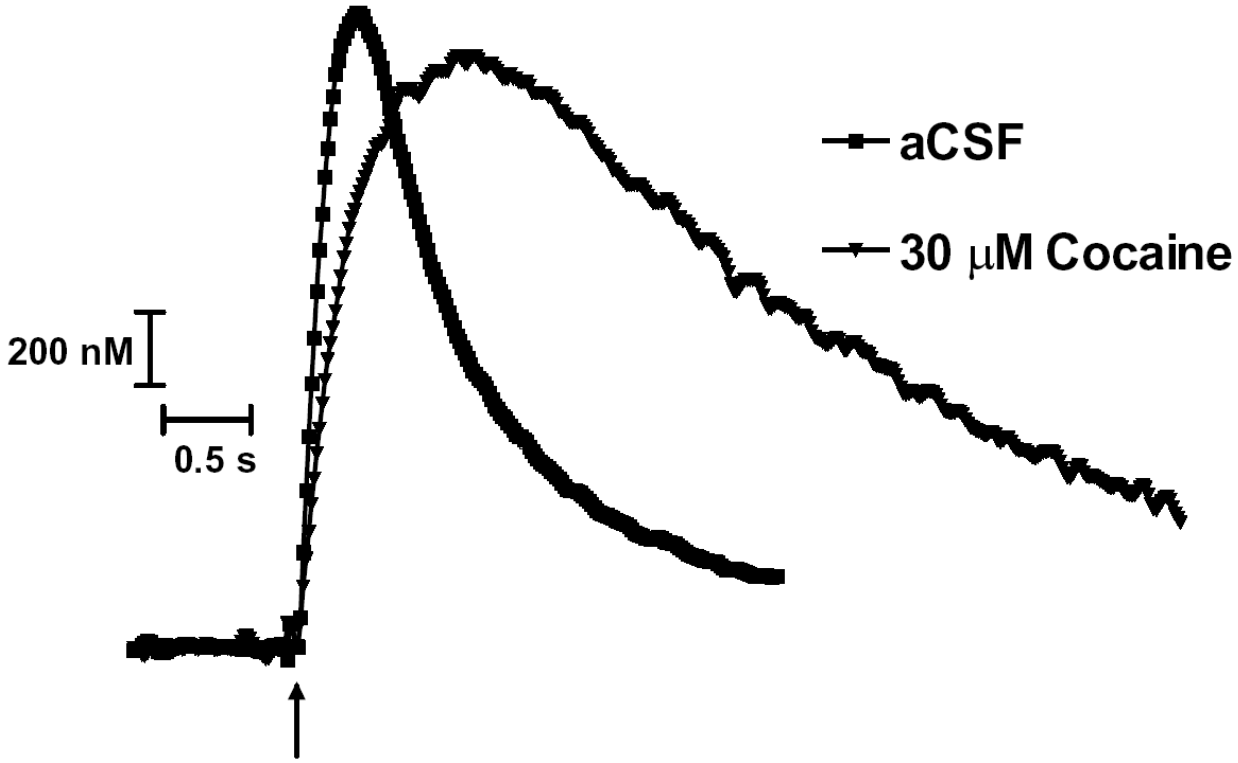

Figure 1.14. Representative trace of uptake inhibition after incubation with 30 μM cocaine. Single-pulse stimulation applied at the time indicated by the arrow. Application of cocaine increases the time needed for DAT to clear DA from the extracellular space. Since cocaine competitively binds to DAT, the kinetics of DA clearance are slowed.

were used here because many transgenic models exist that aid brain slice experiments. Specifically, GFP transgenic mice are used in this work. They express green fluorescent protein (GFP) in their dopaminergic neurons (Kessler et al., 2003). Due to their intrinsic fluorescence, dopaminergic neurons are easily identified in a brain slice and aid electrode placement. They have been generated on a C57BL/6 background strain, which is referred to as wild-type (WT) mice throughout this thesis. This is a strain of mouse that has been used in the Wightman lab since 1998 (Jones et al., 1998). The C57BL/6 is the most widely used inbred strain, and in fact, was the DNA source for the sequencing of the mouse genome (Jackson Laboratory, www.jax.org). Adults are used to ensure the cessation of cell migration and rapid change inherent to development of the mature brain. Males have been used to simplify controls. Female mice could be used, but one must account for any effect of their estrous cycle. Gender studies have shown that female mice release more dopamine and have greater uptake (Walker et al., 2000). The species, strain, and gender are all relevant variables that are controlled for throughout these experiments and provide the context for the interpretation of results.

Thesis Overview

The action of D_2-autoreceptor agonists quinpirole and quinelorane to alter the short-term inhibition provided by the autoreceptor is investigated in Chapter 2. Then, the visualization of dopaminergic cells by fluorescent techniques using transgenic mice, specifically PLAP and GFP transgenic mice, are explored in Chapter 3. These GFP and WT mice are compared in terms of dopamine release, calcium sensitivity, dopamine tissue content, rates of uptake and cocaine inhibition in Chapter 4. Then, the GFP transgenic mice are used in Chapter 5 to develop remote stimulation, in which axons within horizontal slices of the mesolimbic pathway are stimulated in order to elicit release some distance away at the

terminals. The development of an electrochemical approach to determine the concentration of serotonin and dopamine in mixed solutions and in brain regions where mixed signals are measured is discussed in Chapter 6.

References

Cooper J, Bloom F, Roth RH, eds (2003) The Biochemical Basis of Neuropharmacology, Eigth Edition.

Einhorn LC, Gregerson KA, Oxford GS (1991) D2 dopamine receptor activation of potassium channels in identified rat lactotrophs: whole-cell and single-channel recording. J Neurosci 11:3727-3737.

Heien ML, Khan AS, Ariansen JL, Cheer JF, Phillips PE, Wassum KM, Wightman RM (2005) Real-time measurement of dopamine fluctuations after cocaine in the brain of behaving rats. Proc Natl Acad Sci U S A 102:10023-10028.

Heine M, Groc L, Frischknecht R, Beique JC, Lounis B, Rumbaugh G, Huganir RL, Cognet L, Choquet D (2008) Surface mobility of postsynaptic AMPARs tunes synaptic transmission. Science 320:201-205.

Hoover JE, Strick PL (1999) The organization of cerebellar and basal ganglia outputs to primary motor cortex as revealed by retrograde transneuronal transport of herpes simplex virus type 1. J Neurosci 19:1446-1463.

Jones SR, Garris PA, Kilts CD, Wightman RM (1995) Comparison of dopamine uptake in the basolateral amygdaloid nucleus, caudate-putamen, and nucleus accumbens of the rat. J Neurochem 64:2581-2589.

Jones SR, Gainetdinov RR, Wightman RM, Caron MG (1998) Mechanisms of amphetamine action revealed in mice lacking the dopamine transporter. J Neurosci 18:1979-1986.

Kawagoe KT, Zimmerman JB, Wightman RM (1993) Principles of voltammetry and microelectrode surface states. J Neurosci Methods 48:225-240.

Kawagoe KT, Garris PA, Wiedemann DJ, Wightman RM (1992) Regulation of transient dopamine concentration gradients in the microenvironment surrounding nerve terminals in the rat striatum. Neuroscience 51:55-64.

Kessler MA, Yang M, Gollomp KL, Jin H, Iacovitti L (2003) The human tyrosine hydroxylase gene promoter. Brain Res Mol Brain Res 112:8-23.

Matthews C, Holde Kv (1996) In: Biochemistry, 2nd Edition (Benjamin/Cummings, ed), p 1158. Menlo Park, CA: .

Tang K, Low MJ, Grandy DK, Lovinger DM (2001) Dopamine-dependent synaptic plasticity in striatum during in vivo development. Proc Natl Acad Sci U S A 98:1255-1260.

Walker QD, Rooney MB, Wightman RM, Kuhn CM (2000) Dopamine release and uptake are greater in female than male rat striatum as measured by fast cyclic voltammetry. Neuroscience 95:1061-1070.

Watson C, Venton B, Kennedy R (2006) In vivo measurements of neurotransmitters by microdialysis sampling. Analytical Chemistry 78:1391-1399.

Wightman RM, Amatore C, Engstrom RC, Hale PD, Kristensen EW, Kuhr WG, May LJ (1988) Real-time characterization of dopamine overflow and uptake in the rat striatum. Neuroscience 25:513-523.

Wolf ME, Galloway MP, Roth RH (1986) Regulation of dopamine synthesis in the medial prefrontal cortex: studies in brain slices. J Pharmacol Exp Ther 236:699-707.

Zeiss CJ (2005) Neuroanatomical phenotyping in the mouse: the dopaminergic system. Vet Pathol 42:753-773.

Chapter 2

Dynamics of Short-term Inhibition with D_2 Agonists

Introduction

How do tonic levels of dopamine effect the short-term dynamics of stimulated dopamine release? The normal, tonic firing of dopamine neurons provides a background of slowly changing (minutes scale) dopamine concentrations maintained in the extracellular space which provide tonic activation of dopamine receptors (Grace, 1991). In a coronal brain slice there is no dopamine tone. This has been proven by the lack of change in dopamine release elicited by a one-pulse stimulation upon addition of a D_2-receptor antagonist to the slice buffer (Kennedy et al., 1992). The lack of tone should have consequences on dopamine release dynamics. Differences in dopamine release measured in brain slices and *in vivo* have been reported. For example, in the intact brain the amount of dopamine released per stimulation pulse, $[DA]_p$, remains constant during stimulation of the medial forebrain bundle (May et al., 1988), while it decreases rapidly *in vitro* (Kennedy et al., 1992).

In brain slices, it has been shown that stimulated release of dopamine activates D_2-autoreceptors that inhibit subsequent stimulated release (Kennedy et al., 1992; Phillips et al., 2002). In awake-behaving rats as well as anesthetized rats it has been shown that the amount of dopamine released for a given stimulation is dependent upon the history of stimulation (Montague et al., 2004). Short-term factors controlling dopamine release

dynamics are mediated by D_2-autoreceptors (Kita et al., 2007). While it is impractical to remove dopamine tone *in vivo*, the *in vitro* setting provides an opportunity to monitor how these short-term dynamics change as the D_2-autoreceptors become tonically activated.

Unfortunately dopamine cannot be added to the buffer to provide this tone. First, it is the target analyte and could complicate measurements of dopamine release. Moreover if dopamine is applied to a brain slice, it is cleared from the extracellular space by a high-affinity uptake system and packed into vesicles. This could increase the amount of release but will not result in tonic activation of the autoreceptors. In the intact brain, dopamine tone is accomplished by asynchronous firing of dopamine neurons (Venton et al., 2003). However an electrical stimulation of the brain slice will cause synchronous release. To provide the tone desired, a D_2-autoreceptor agonist that is not electrochemically active is preferred. In this work, quinpirole and quinelorane are used to investigate changes in short-term inhibition under a paired-pulse paradigm.

Materials and methods

Chemicals

(-)-Quinpirole hydrochloride, quinelorane dihydrochloride, and 2-Ethoxy-1-ethoxycarbonyl-1,2-dihydroquinoline (EEDQ) was obtained from Sigma-Aldrich (St Louis, MO, USA). For administration of quinpirole and quinelorane to brain slices, 10 mM stock solutions were prepared by dissolving the appropriate weight into a known volume of deionized water. For dose-response curves, serial dilutions of the greatest concentration were used. EEDQ or vehicle were injected i.p. 24 hours prior to sacrifice and brain slicing.

Animals

Animals were handled in accordance with protocols approved by the Institutional Animal Care and Use Committee of the University of North Carolina. C57/BL6 (wild-type) mice were

obtained from The Jackson Laboratory (Bar Harbor,ME, USA) at 5–6 weeks of age. Upon receipt, mice were housed at the University of North Carolina Animal Husbandry Facility in Kerr Hall. Mice were provided food and water ad libitum and were kept under conditions of controlled temperature, humidity, and a 12-h light/dark cycle.

Brain slices

Mice were deeply anesthetized by ether inhalation and decapitated. The brain was immediately removed and placed in ice-cold aCSF. The aCSF solution consisted of (in mM): NaCl 126, KCl 2.5, NaH_2PO_4 1.2, $CaCl_2$ 2.4, $MgCl_2$ 1.2, $NaHCO_3$ 25, HEPES 20, D-glucose 11. The pH was adjusted to 7.4 with 5 M NaOH and the buffer was continuously saturated with 95% O_2/5% CO_2. The cerebellum was sliced off with a razor blade and the brain was mounted on a Teflon block using Krazy Glue ®. Brain slices were made using an NVSL vibratome (World Precision Instruments, Sarasota, FL, USA). Coronal slices containing the striatum were made 300-μm thick, obtained at +0.3 to +1.3 mm from bregma. Brain slices were stored in ice-cold aCSF. A single slice was submerged under aCSF maintained at 34°C and continuously flowing (2 mL/min) through a superfusion chamber (Warner Instruments, Hamden, CT, USA). Each brain slice was equilibrated for 30 min prior to obtaining measurements. To expose the brain slice to a given drug, the appropriate volume of drug stock solution was added to the buffer reserve and introduced by a peristaltic pump to the slice through a threeway valve. A cumulative dosing regimen was used to collect concentration-response data. Brain slices were allowed to equilibrate for 30 min at a given drug concentration prior to exposing the slice to the next higher concentration.

Electrochemistry

Carbon-fiber cylinder microelectrodes were made as previously described (Kawagoe et al., 1993) using T650 carbon fibers (Amoco, Greenville, SC, USA) cut to a length of 25 μm. Electrodes were epoxied (Miller-Stevenson, Danbury, CT, USA) to ensure a good seal, and

dipped immediately in acetone for a few seconds to remove residual epoxy from the carbon fiber. A triangular waveform, starting at -0.4 V, increasing to 1.0 V, and scanning back to -0.4 V, was applied to the carbon-fiber working electrode, versus a Ag/AgCl reference electrode, at a scan rate of 600 V/s. An update rate of 10 Hz was used for all experiments except the quinelorane dose-response for which a 60 Hz update rate was used.

The carbon fiber was inserted until the tip was 60-70 μm below the surface of the brain slice in the dorsolateral caudate region of the striatum between the prongs of a bipolar stimulating electrode (FHC, Bowdoinham, ME, USA), situated 200 μm apart. To evoke dopamine release, a single biphasic stimulating current pulse (2 ms each phase, 350 μA in amplitude) was applied to the stimulating electrode. The current arising from dopamine oxidation (at about 0.6 V) in successive voltammograms was measured and plotted versus time.

Statistics

The peak current arising from dopamine oxidation in response to each stimulation was adjusted with a correction factor to account for the change in sensitivity upon the introduction of quinpirole and quinelorane, see Chapter 1. This current is expressed as a percentage of the value obtained before drug application. Data were considered significant at the 95% confidence level and are reported as the mean ± SEM for n animals. Statistical significance was evaluated using an unpaired t-test. Dose-response curves were evaluated with non-linear regression to a sigmoidal dose-response curve (GraphPad Software Inc., San Diego, CA, USA).

Results

Short-term inhibition

Short-term inhibition is illustrated with FSCV measurements made during a 5 s stimulation pulse interval and a 30 s stimulation pulse interval (Figure 2.1). The difference in peak height following stimulation can be expressed as a ratio of release due to the second stimulation pulse (S_2) to the release due to the first stimulation pulse (S_1). At a short pulse interval, such as 5 s, there is much greater inhibition (S_2/S_1 = 0.42, Figure 2.1A) than at a longer pulse interval, such as 30 s (S_2/S_1 = 0.94, Figure 2.1B) under control conditions. Upon the addition of selective D_2 agonist quinelorane the magnitude of S_1 is reduced as expected. Moreover, the S_2/S_1 ratio decreases for both pulse intervals, but the percentage decrease is much greater for the short pulse interval (40% of control) than the longer pulse interval (23% of control).

Dose-Response curves

Quinelorane and quinpirole inhibit dopamine release in a dose-dependent manner (Figure 2.2). Quinelorane (EC_{50} = 5.3 $\pm$11 nM) is a potent analog of quinpirole (EC_{50} = 40 $\pm$11 nM). The Hill slope is not significantly different for these two drugs ($p > 0.05$), presumably due to their similar modes of action. The dashed line represents the presumptive curve for dopamine based on reported EC_{50} values (12 $\pm$12 nM).

Dose-Response of Short-term Inhibition

Quinpirole causes a decrease in the S_2/S_1 ratio for a 5 s pulse interval up to concentrations about its EC_{50} (Figure 2.3). Moreover, there is no change for a 30 s pulse interval. The difference between the 5 s and 30s pulse interval in percent change of the S_2/S_1 ratio is highly significant for several concentrations (25 nM $p < 0.01$, 50 nM and 100nM $p < 0.005$, Figure 2.3). As the quinpirole concentrations increase further, the S_2/S_1 ratio returns to pre-drug levels.

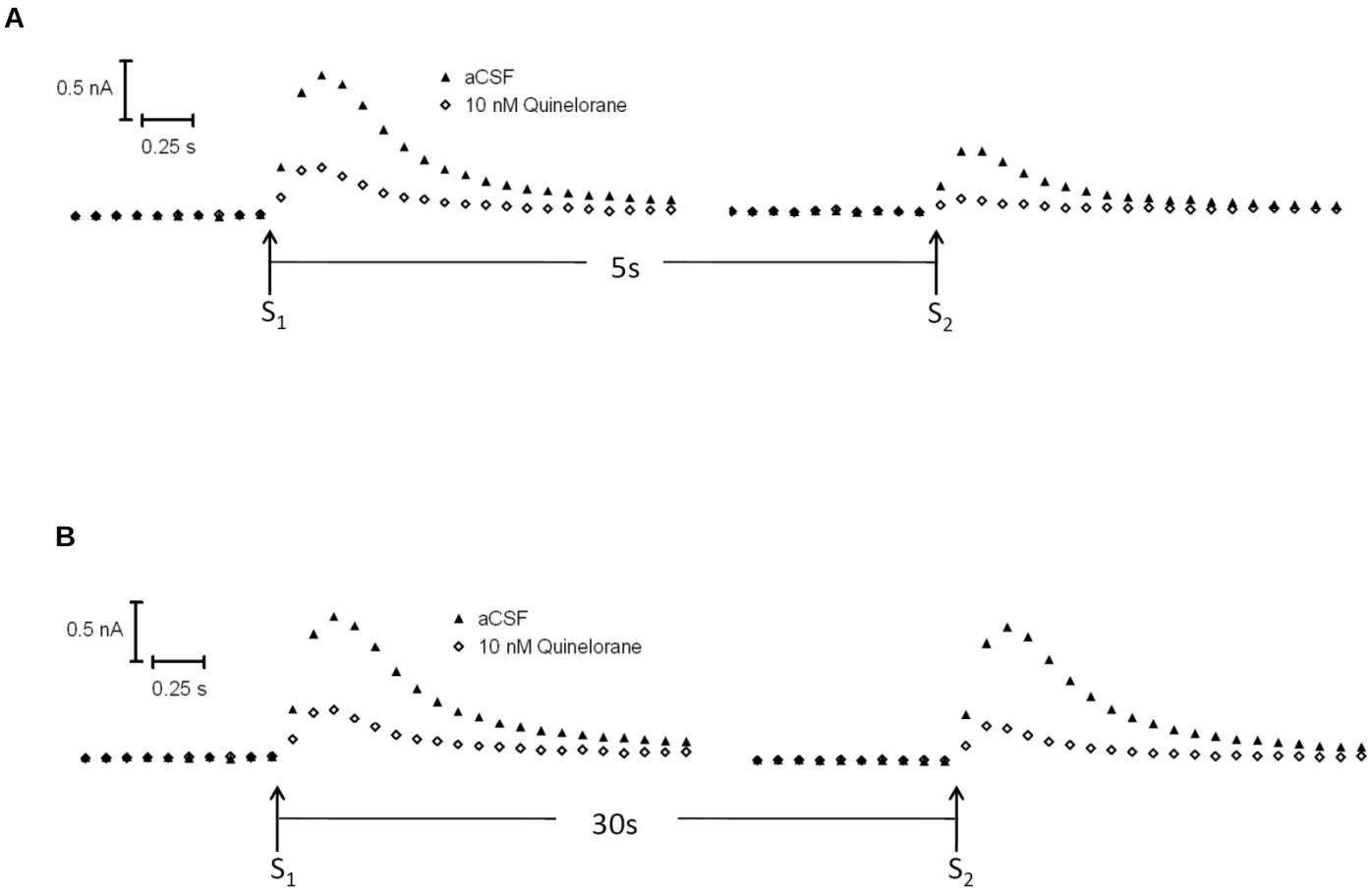

Figure 2.1. Short-term inhibition of dopamine release. Representative traces of the brain slice response to paired-pulse stimulations in the dorsal striatum at short and long pulse separations are shown with the change in magnitude upon addition of quinelorane. Stimulations are indicated by the arrows and separated by the time noted between the arrows. A) The ratio of dopamine release elicited by a second stimulation pulse relative to the release elicited by the first stimulation pulse (S_2/S_1) is 0.42 for a 5s pulse separation and is further reduced by 40% with the addition of 10 nM quinelorane. B) The S_2/S_1 ratio is 0.94 under control conditions with a 30s pulse separation and is further reduced by 23% with the addition of 10 nM quinelorane.

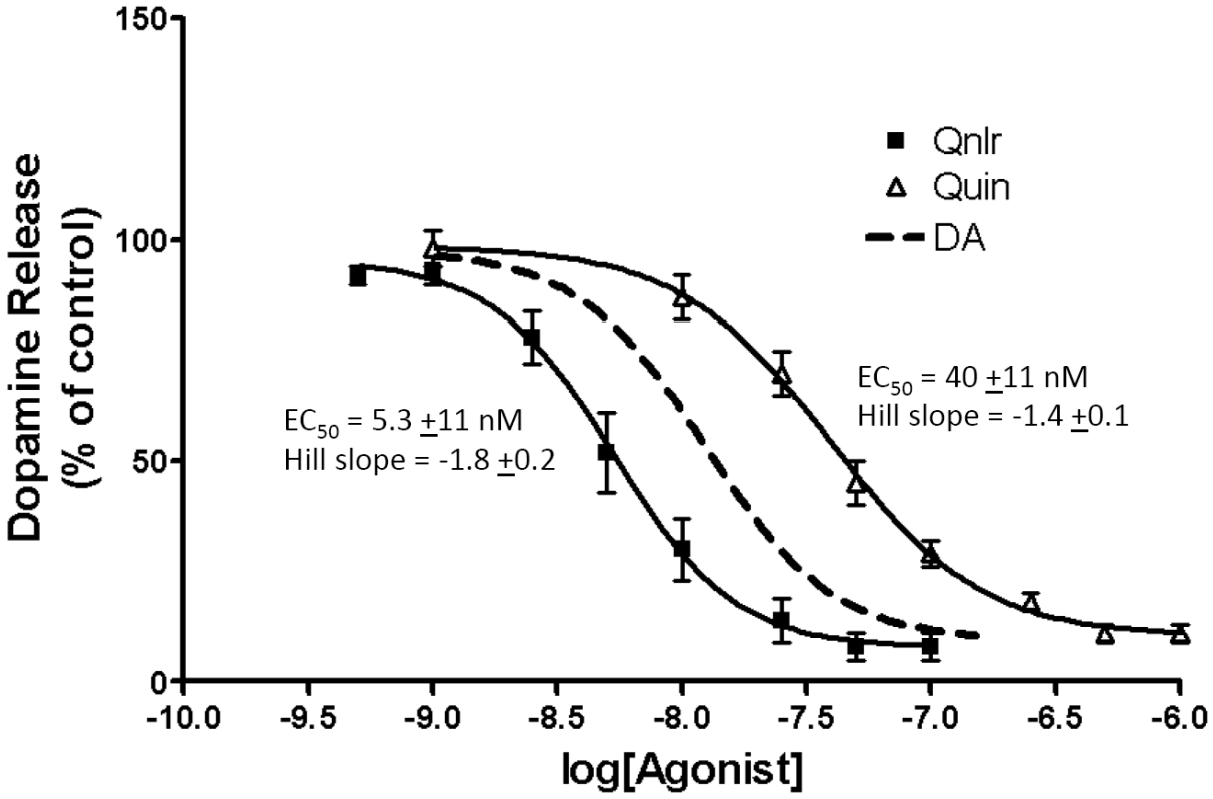

Figure 2.2. D_2-autoreceptor mediated inhibition of release. The peak current response for a single-pulse stimulation was measured as a function of D_2-autoreceptor agonist concentration and normalized to the average response pre-drug. Sigmoidal dose response curve fits are statistically similar for all parameters except the EC_{50}. Therefore, a hypothetical dopamine response curve was built using an EC_{50} of 12 $\pm$12 nM and a Hill slope of -1.7 $\pm$0.2.

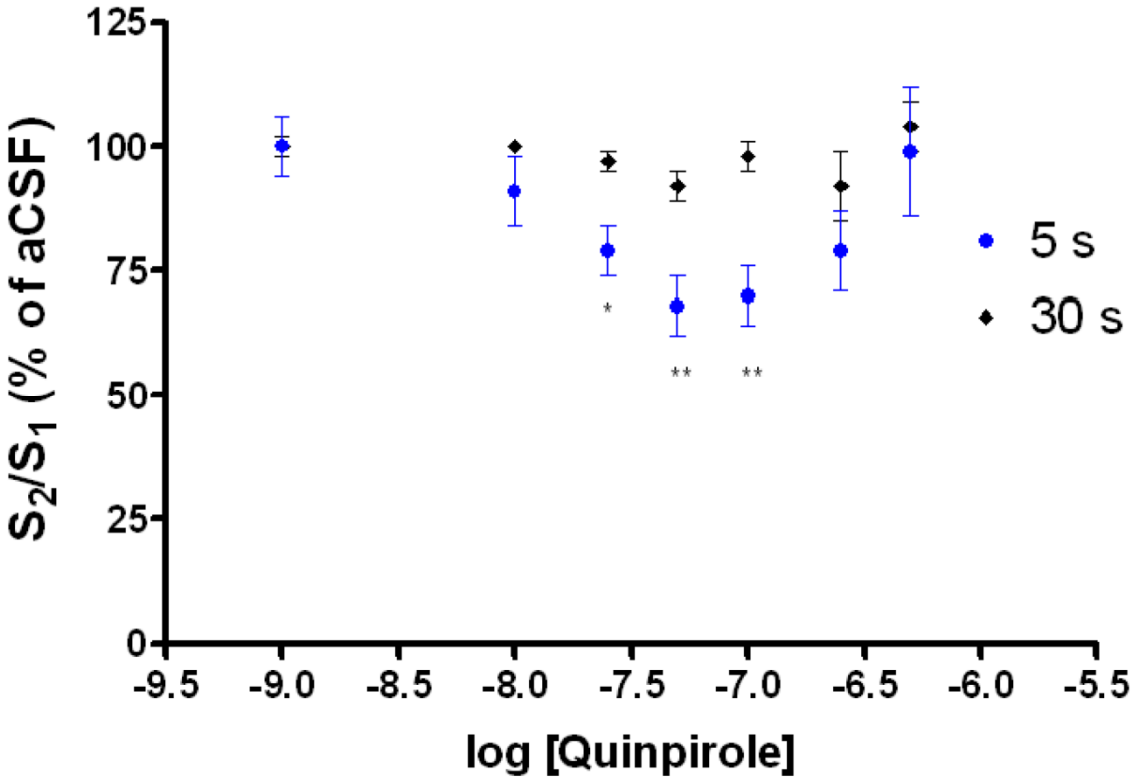

Figure 2.3. Quinpirole short-term inhibition dose response. The change in the S_2/S_1 ratio with the cummative dosing of quinpirole is expressed relative to the pre-drug value. There is no change in this ratio when using a 30 s pulse separation. The change in response when using a 5 s pulse separation diverges from the 30 s response significantly at 25 nM (* $p < 0.01$), 50 nM and 100nM (** $p < 0.005$).

The percent changes for a 5 s pulse interval are similar in pattern between the two agonists (Figure 2.4). However, for quinelorane there is less difference between the percent changes with a short and long pulse interval. This is due to the modest decrease in S_2/S_1 ratio for the 30 s pulse interval. In fact, there is a significant difference ($p < 0.001$) at 10 nM between quinelorane (87 $\pm$3%) and quinpirole (100 $\pm$1%).

Dependence on Receptor Availability

Injection of EEDQ (6 mg/kg, i.p.) 24 hours before a brain slice experiment reduces available D_2 receptors by about 44% (Saller et al., 1989). The result of reducing the fraction of available receptors is an increased lower plateau ($p < 0.0001$, Figure 2.5). The changes in the S_2/S_1 ratio with increasing concentrations of quinpirole are similar with vehicle (1:2:1 ratio of propylene glycol:water:ethanol) treatment as seen previously (Figure 2.6). EEDQ treatment prevents the return of S_2/S_1 ratios to pre-drug levels (at 1 μM, $p < 0.02$). The divergence in S_2/S_1 ratio between vehicle-treated mice and EEDQ-treated mice occurs at quinpirole concentrations above 500 nM, concentrations at which the bottom plateaus diverge.

Discussion

Short-term inhibition, expressed as an S_2/S_1 ratio, changes with D_2-autoreceptor activation. This is true for two different agonists of differing potency and is likely true for dopamine. Although dopamine could not be used in these experiments, its potency has been reported in transfected cells (4-14 nM) and is between the potency of quinpirole and quinelorane (Bates et al., 1991; Mercier et al., 2001). Therefore a dose-response curve for dopamine

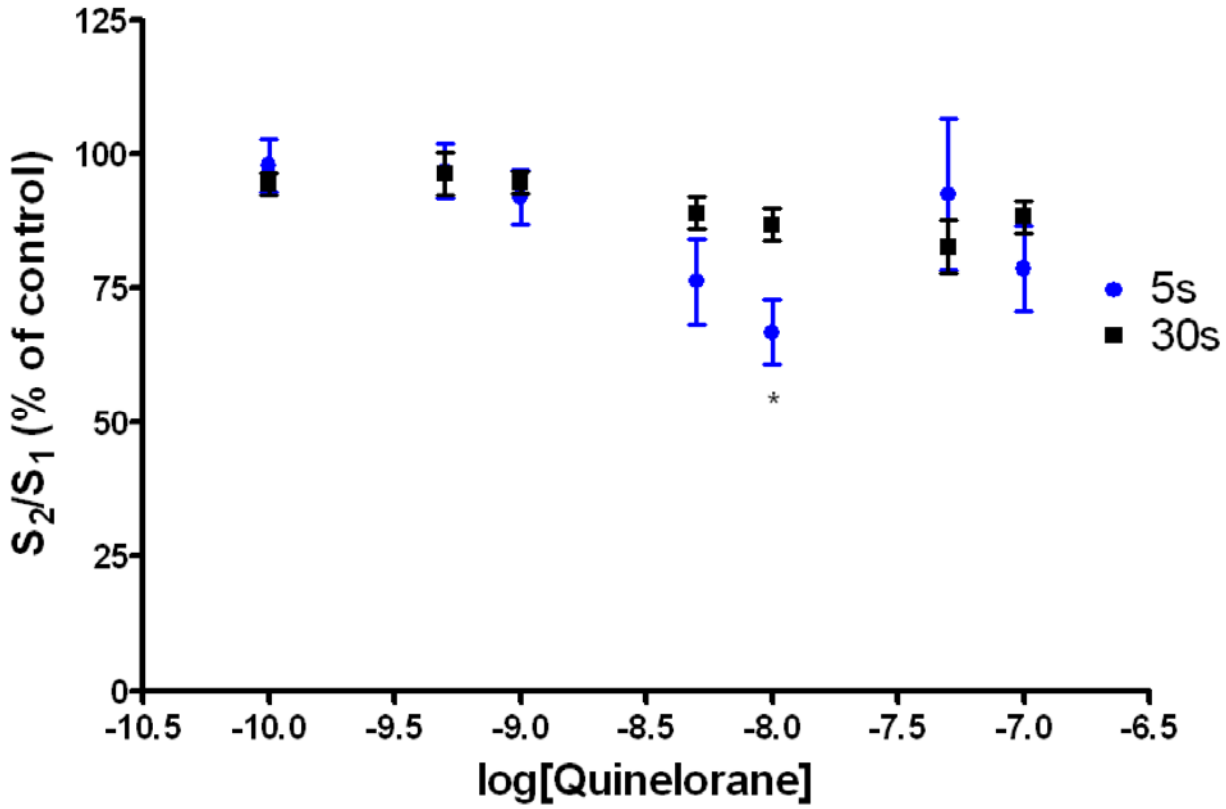

Figure 2.4. Quinelorane short-term inhibition dose response. The change in the S_2/S_1 ratio with the cummative dosing of quinlorane is expressed relative to the pre-drug value. The change in S_2/S_1 ratio when using a 5 s pulse separation diverges from the 30 s response significantly at 10 nM (*$p < 0.01$).

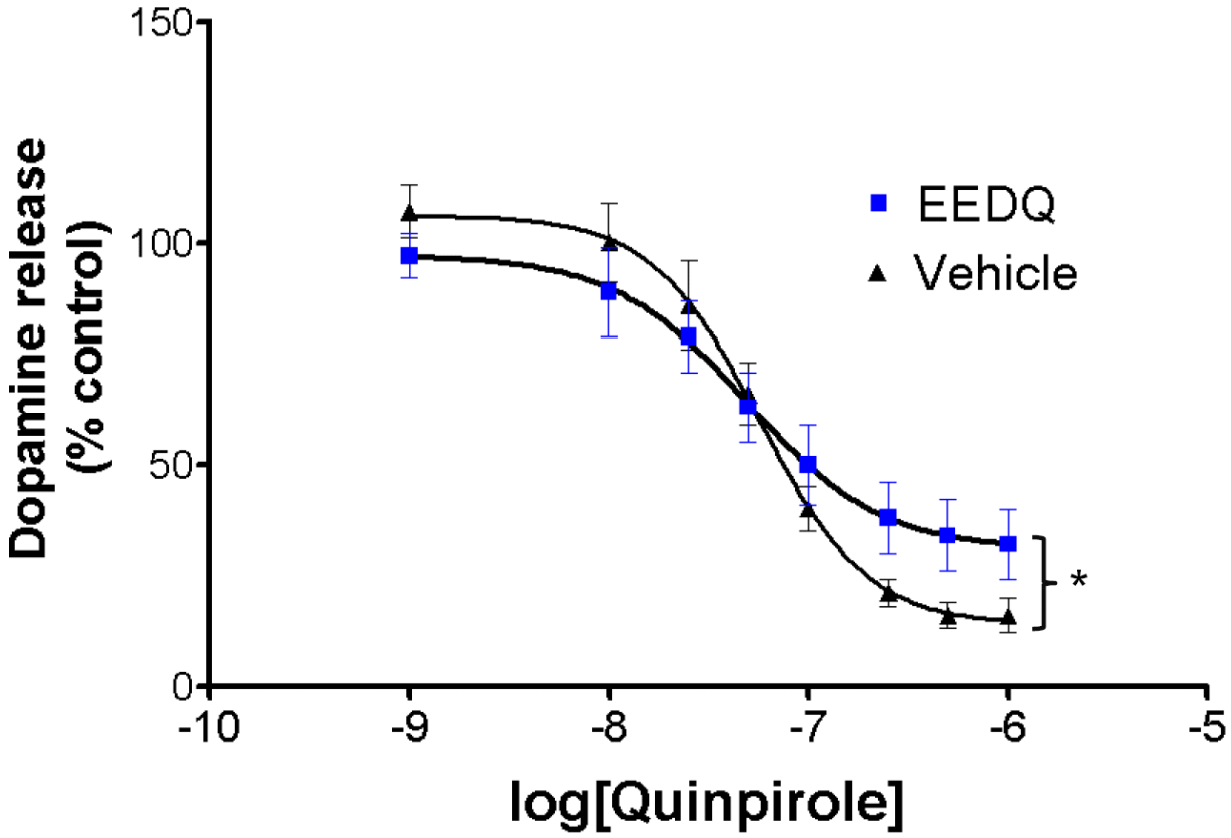

Figure 2.5. EEDQ effect on quinpirole dose response. The quinpirole dose response was evaluated in the dorsal striatum of mice injected with either vehicle or EEDQ (6 mg/kg, i.p.) 24 hours prior to the experiment. The bottom plateau is significantly increased in the EEDQ-treated animal (* $p < 0.0001$). The other paramers of the dose response to quinpirole are similar in vehicle-treated mice (EC_{50} = 57 $\pm$11 nM, Hill slope = -1.6 $\pm$0.1) and EEDQ-treated mice (EC_{50} = 48 $\pm$11 nM, Hill slope = -1.3 $\pm$0.1).

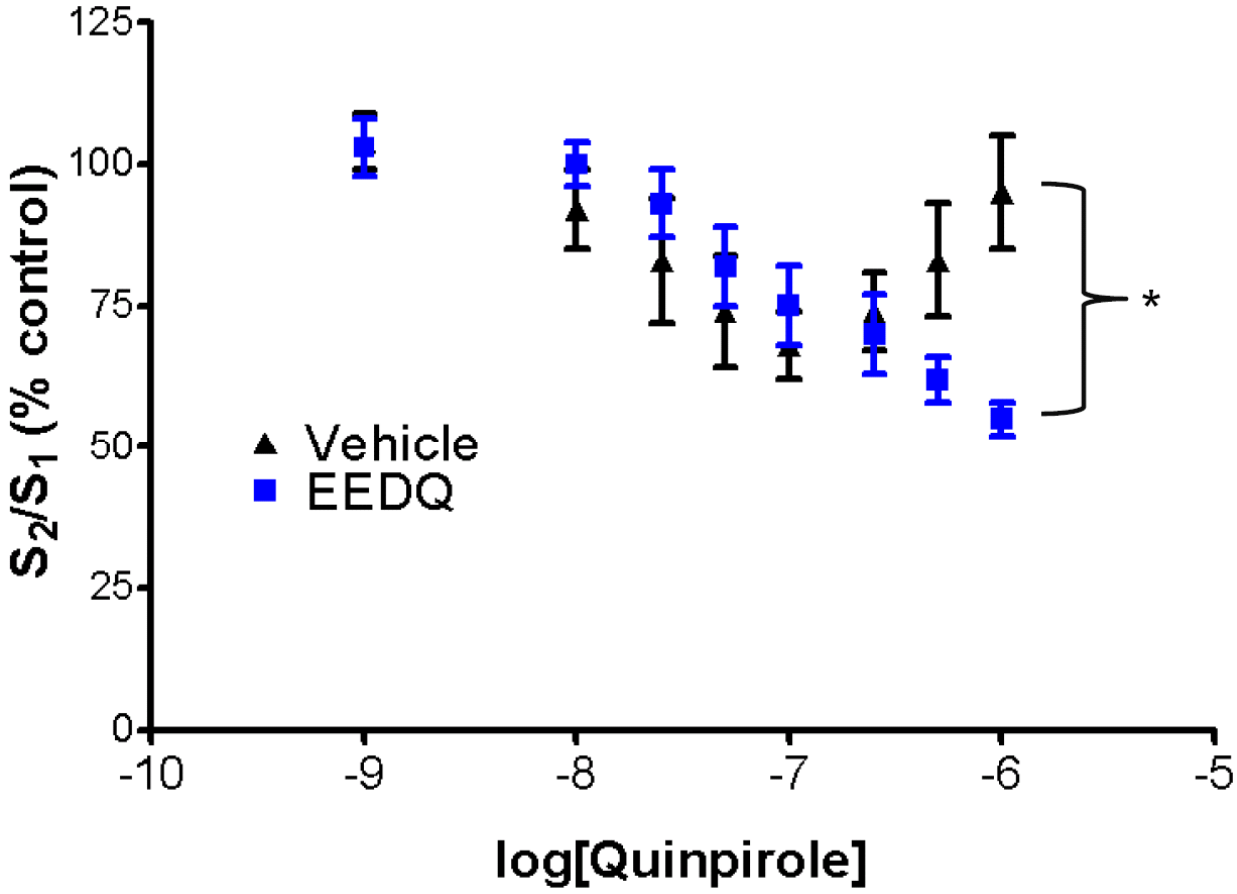

Figure 2.6. EEDQ effect on quinpirole short-term inhibition dose response. The change in S_2/S_1 ratio diverges between vehicle-treated mice and EEDQ-treated mice above 500 nM quinpirole. The S_2/S_1 ratio is significantly different at 1 μM (* $p < 0.02$).

would lie between the dose-response curves for those two agonists, displayed as a dash line in Figure 2.2. Furthermore, the changes in short-term inhibition measured can be assumed to occur for dopamine at concentrations intermediate to those measured for these agonists.

Using a short pulse interval, the change in the S_2/S_1 ratio with agonist concentration is biphasic, a falling portion with an inflection about the EC_{50} of the agonist followed by a rising portion. For a longer pulse interval, where short-term inhibition is much weaker, the agonists have much less effect on the S_2/S_1 ratio. Although there appears to be very little short-term inhibition with a 30 s pulse interval under control conditions or in the presence of quinpirole, quinelorane increases the short-term inhibition at this long pulse interval. This may be due to quinelorane's greater potency. Persistent activation of D_2 receptors can lead to sensitization (Vortherms et al., 2006). Sensitization would make the autoreceptor more responsive to the dopamine released upon the second stimulation thereby increasing short-term inhibition.

The initial decrease of short-term inhibition with a 5 s pulse interval can be understood as an additive effect of the dopamine released for S_1 and the inhibitory action of the agonist. It may also include some degree of sensitization. There are three factors that may contribute to the return of the S_2/S_1 ratio to baseline. First, S_1 is growing smaller and therefore is having less of an inhibitory effect. Second, the receptor occupancy is higher with an increasing quinpirole background, so the addition of a small amount of dopamine from S_1 may not contribute significantly to the autoreceptor response. Third, the autoreceptors are possibly being desensitized due to the high level of activation inherent to this experiment. The first two factors can be addressed by reducing the receptor reserve with EEDQ.

EEDQ chemically modifies the dopamine receptor irreversibly such that in can no longer bind either agonists or antagonists but without changing the dissociation constant (K_d) of the remaining receptors (Belleau et al., 1969; Kalsner, 1970). Due to the reduction in available D_2-autoreceptors, the maximal inhibition is less with EEDQ treatment than with vehicle. The greater magnitude of S_1 relative to vehicle at these high concentrations of quinpirole keeps the S_2/S_1 ratio low despite the increased receptor occupancy. A rightward shift in the dose-response curve has been reported as an effect of EEDQ administration. This effect is found when measuring inhibition of forskolin-stimulated cAMP accumulation (Burris et al., 2002) and inhibition of forskolin-induced activation of tyrosine hydroxylase (Bohmaker et al., 1989). Measuring changes in second messenger levels may be more sensitive to these perturbations than the cummulative cellular output of how much dopamine is released. This shift has also been reported in the rat striatum by measuring the inhibition of tritiated dopamine release with apomorphine (Yokoo et al., 1988). The release was elicited by 2 min, 1 Hz, unipolar (20 mA, 2 ms) electrical stimulations. These stimulations are much more intense than the single-pulse stimulations used here. The rightward shift may become apparent with greater dopamine release. Since the EC_{50} did not change in our preparation, it indicates that there is a sufficient receptor reserve to respond to modest concentrations of agonist but at higher concentrations the receptors become saturated.

These results indicate that changes in tonic activation of D_2-autoreceptors causes changes in the strength of short-term inhibition. The concentrations over which these changes occur shift with the potency of the agonist, but the range remains about an order of magnitude. Therefore a similar pattern would presumably emerge for dopamine, with a decrease followed by an increase in the S_2/S_1 ratio about its EC_{50}. Therefore, the dopamine concentrations enveloping the dynamic range in short-term inhibition would be between 2.4 nM and 60 nM.

There are many differences remaining between *in vivo* and brain slice preparations beyond autoreceptor tone that could impact the extension of these results to the intact animal. For example, in the brain slice stimulation is local to the measurement which can cause the release of other substances that could interact with the dopamine terminal. The concentration of dopamine release is much higher under control conditions in a brain slice than spontaneous release events in the intact animal. The dopamine concentration of spontaneous release events in the caudate putamen are reported to be about 200nM (Robinson et al., 2002), yet the pre-drug concentrations of dopamine release in brain slices are about 1.5 μM. With the appropriate caveats, these results show that changes in the tonic activation of autoreceptors are relevant to short-term dynamics of dopamine release.

References

Bates MD, Senogles SE, Bunzow JR, Liggett SB, Civelli O, Caron MG (1991) Regulation of responsiveness at D2 dopamine receptors by receptor desensitization and adenylyl cyclase sensitization. Mol Pharmacol 39:55-63.

Belleau B, DiTullio V, Godin D (1969) The mechanism of irreversible adrenergic blockade by N-carbethoxydihydroquinolines--model studies with typical serine hydrolases. Biochem Pharmacol 18:1039-1044.

Bohmaker K, Puza T, Goldstein M, Meller E (1989) Absence of spare autoreceptors regulating dopamine agonist inhibition of tyrosine hydroxylation in slices of rat striatum. J Pharmacol Exp Ther 248:97-103.

Burris KD, Molski TF, Xu C, Ryan E, Tottori K, Kikuchi T, Yocca FD, Molinoff PB (2002) Aripiprazole, a novel antipsychotic, is a high-affinity partial agonist at human dopamine D2 receptors. J Pharmacol Exp Ther 302:381-389.

Grace AA (1991) Phasic versus tonic dopamine release and the modulation of dopamine system responsivity: a hypothesis for the etiology of schizophrenia. Neuroscience 41:1-24.

Kalsner S (1970) Enhancement of the alpha receptor blocking action of N-ethoxycarbonyl-2--ethoxy-1,2-dihydroquinoline (EEDQ) by amines. Life Sci I 9:961-974.

Kawagoe KT, Zimmerman JB, Wightman RM (1993) Principles of voltammetry and microelectrode surface states. J Neurosci Methods 48:225-240.

Kennedy RT, Jones SR, Wightman RM (1992) Dynamic observation of dopamine autoreceptor effects in rat striatal slices. J Neurochem 59:449-455.

Kita JM, Parker LE, Phillips PE, Garris PA, Wightman RM (2007) Paradoxical modulation of short-term facilitation of dopamine release by dopamine autoreceptors. J Neurochem 102:1115-1124.

May LJ, Kuhr WG, Wightman RM (1988) Differentiation of dopamine overflow and uptake processes in the extracellular fluid of the rat caudate nucleus with fast-scan in vivo voltammetry. J Neurochem 51:1060-1069.

Mercier D, Falardeau P, Levesque D (2001) Autoreceptor preference of dopamine D2 receptor agonists correlates with preferential coupling to cyclic AMP. Neuroreport 12:1473-1479.

Montague PR, McClure SM, Baldwin PR, Phillips PE, Budygin EA, Stuber GD, Kilpatrick MR, Wightman RM (2004) Dynamic gain control of dopamine delivery in freely moving animals. J Neurosci 24:1754-1759.

Phillips PE, Hancock PJ, Stamford JA (2002) Time window of autoreceptor-mediated inhibition of limbic and striatal dopamine release. Synapse 44:15-22.

Robinson DL, Heien ML, Wightman RM (2002) Frequency of dopamine concentration transients increases in dorsal and ventral striatum of male rats during introduction of conspecifics. J Neurosci 22:10477-10486.

Saller CF, Kreamer LD, Adamovage LA, Salama AI (1989) Dopamine receptor occupancy in vivo: measurement using N-ethoxycarbonyl-2-ethoxy-1,2-dihydroquinoline (EEDQ). Life Sci 45:917-929.

Venton BJ, Zhang H, Garris PA, Phillips PE, Sulzer D, Wightman RM (2003) Real-time decoding of dopamine concentration changes in the caudate-putamen during tonic and phasic firing. J Neurochem 87:1284-1295.

Vortherms TA, Nguyen CH, Bastepe M, Juppner H, Watts VJ (2006) D2 dopamine receptor-induced sensitization of adenylyl cyclase type 1 is G alpha(s) independent. Neuropharmacology 50:576-584.

Yokoo H, Goldstein M, Meller E (1988) Receptor reserve at striatal dopamine receptors modulating the release of [3H]dopamine. Eur J Pharmacol 155:323-327.

Chapter 3

Visualizing Dopaminergic Neurons in Transgenic Mice

Introduction

The mammalian brain is sufficiently complex and heterogeneous that placement of chemical sensors must be precise and specific so that appropriate interpretation of the measured responses can be made. The identification of specific cell types within a brain slice would aid the placement of chemical sensors, such as microelectrodes. For example, dopaminergic terminals are sparse in some regions of the brain including the prefrontal cortex, amygdala, and hippocampus. Measuring dopamine release in these regions can be challenging due to the difficulty in placing microelectrodes sufficiently close to release sites. The localization of a fluorescent signal to a particular cell type would provide a target for sensor placement. Traditional histological techniques are generally not useful in this application because they employ fixation or permeabilization of the tissue which sacrifices the viability of the sample.

To aid in the visualization of dopaminergic neurons in mouse brain slices, two approaches have been investigated, both with transgenic mice. The first involves labeling live tissue with fluorescently tagged antibodies to a transgenic marker that is expressed in specific cells. The second approach involves the targeted expression of a fluorescent protein. Cell specificity is accomplished the same way in each mouse type; the expression of the transgene is driven by the tyrosine hydroxylase (TH) promoter. TH is specifically

expressed in catecholaminergic cells, so the transgenes will be expressed specifically as well.

A line of transgenic mice were generated which express human placental alkaline phosphatase (PLAP) on the outer surface of the cell membrane of catecholaminergic cells (Gustincich et al., 1997). An antibody specific to PLAP conjugated to a fluorescent dye has been used to localize a fluorescent signal to PLAP expressing cells in culture (Hochstetler et al., 2000). In this chapter, the efficacy of using these mice and the antibody-dye conjugate for visualizing dopaminergic neurons in brain slices is explored.

Another line of transgenic mice have since been generated that express enhanced green fluorescent protein (GFP) in catecholaminergic neurons (Kessler et al., 2003). Brain slices from these animals require no antibody labeling since they intrinsically fluoresce. The use of these mice in identifying release sites in the central amygdaloid nucleus and ventral temental area (VTA) is explored.

Materials and Methods

Animals

Animals were handled in accordance with protocols approved by the Institutional Animal Care and Use Committee of the University of North Carolina. A transgenic mouse line was used that express human placental alkaline phosphatase in catecholaminergic cells (Gustincich et al., 1997). A transgenic mouse line in which catecholamine containing cells express the gene for the enhanced green fluorescent protein was used (Kessler et al., 2003). Upon receipt, mice were housed at the University of North Carolina Animal

Husbandry Facility in Kerr Hall. Mice were provided food and water ad libitum and were kept under conditions of controlled temperature, humidity, and a 12-h light/dark cycle.

Brain slices

Mice were deeply anesthetized by ether inhalation and decapitated. The brain was immediately removed and placed in ice-cold aCSF. The aCSF solution consisted of (in mM): NaCl 126, KCl 2.5, NaH_2PO_4 1.2, $CaCl_2$ 2.4, $MgCl_2$ 1.2, $NaHCO_3$ 25, HEPES 20, D-glucose 11. The pH was adjusted to 7.4 with 5 M NaOH and the buffer was continuously saturated with 95% O_2/5% CO_2. The cerebellum was sliced off with a razor blade and the brain was mounted on a Teflon block using Krazy Glue ®. Brain slices were made using an NVSL vibratome (World Precision Instruments, Sarasota, FL, USA). Coronal slices containing the striatum were made 300-μm thick, obtained at +0.5 to +1.0 mm from bregma. Coronal slices containing the substantia nigra and ventral tegmental area were obtained at -2.8 to -3.3 mm from bregma. For immunohistochemistry, the brain slices were made 200-μm thick. Brain slices were stored in ice-cold aCSF. A single slice was submerged under aCSF maintained at 34°C and continuously flowing (2 mL/min) through a superfusion chamber (Warner Instruments, Hamden, CT, USA). Each brain slice was equilibrated for 30 min prior to obtaining measurements.

Labeling with PLAP Antibody

The monoclonal PLAP antibody, E6, (De Waele et al., 1982) was conjugated to the Alexa Fluor ® 555 dye (Invitrogen, Carlsbad, CA) as previously described (Gustincich et al., 1997). The slices were incubated in a 35-mm culture plate with the antibody-dye conjugate (3 μg/1mL of aCSF) for 15 minutes at 37° C in an incubator. Then, the slice was placed in the tissue superfusion chamber, where the slice is rinsed with aCSF buffer and recovers for 30 minutes before stimulating release.

Epifluorescent Microscopy

To visualize the fluorescence in brain slices, an upright microscope (Nikon Eclipse E600FN, Melville, NY) was used with a xenon lamp source to excite fluorescence. a Nikon G-2E/C bandpass filter set (filter 540/25 for excitation, 620/60 for emission, and a 565 LP dichroic mirror) was employed when viewing samples from PLAP mice,, and a Nikon endow GFP bandpass filter set (filter 470 CWL for excitation, 525 CWL for emission, and a 495 LP dichroic mirror) was employed when viewing samples from GFP mice. A CCD camera (Photometrics Sensys, Tucson, Arizona) was used to capture images. Photoshop was used to determine the relative fluorescence within a slice.

Electrochemistry

Carbon-fiber cylinder microelectrodes were made as previously described (Kawagoe et al., 1993) using T650 carbon fibers (Amoco, Greenville, SC, USA) cut to a length of 25 μm. Electrodes were epoxied (Miller-Stevenson, Danbury, CT, USA) to ensure a good seal, and dipped immediately in acetone for a few seconds to remove residual epoxy from the carbon fiber. A triangular waveform, starting at -0.4 V, increasing to 1.0 V, and scanning back to -0.4 V, was applied to the carbon-fiber working electrode, versus a Ag/AgCl reference electrode, at a scan rate of 600 V/s. An update rate of 10 Hz was used for all experiments.

The carbon fiber was inserted until the tip was 60-70 μm below the surface of the brain slice between the prongs of a bipolar stimulating electrode (FHC, Bowdoinham, ME, USA), situated 200 μm apart. To evoke dopamine release, a single biphasic stimulating current pulse (2 ms each phase, 350 μA in amplitude) was applied to the stimulating electrode. The current arising from dopamine or serotonin oxidation (at about 0.6 V) in successive voltammograms was measured and plotted versus time.

Immunohistochemistry

Slices were fixed in 2% formaldehyde in Sorenson's buffer (0.15 m Na_2HPO_4/KH_2PO_4 at pH 7.4) for 4 h. The slices were rinsed three times with 1X PBS (Tissue Culture Facility, Chapel Hill, NC, USA). Then, normal goat serum (NGS, Life Technologies, Rockville, MD, USA) was combined with 0.2% BSA/PBS solution (1 : 10, NGS : BSA/ PBS) containing 0.3% Triton-100X. The slices were incubated in this blocking solution for 2 h. The Primary antibody solutions were incubated for overnight (15hours) at 4°C with slow agitation and rinsed with PBS. For double labeling, secondary antibody was diluted 1:1000 and incubated overnight with the slices. For PLAP/DAT or PLAP/TH double labeling experiments, the PLAP primary antibody-dye conjugate was simultaneously incubated with either the DAT or TH unconjugated primary antibody (Rabbit, Invitrogen). Primary antibodies were diluted into 0.5 mL of PBS and then 5 mL of blocking solution to final dilutions as follows: anti-DAT, 1:100; anti-TH, 1:100. The secondary antibodies used wasAlexa Fluor ® 488 conjugated goat anti-rabbit. Then, the slices were rinsed with PBS, placed on slides, and examined by confocal microscopy.

Confocal microscopy

Throughout this work, anatomical locations were determined by comparison with a mouse brain atlas (Paxinos and Franklin, 2004). The brain slices containing the desired regions were placed onto microscope slides with glass wells to maintain their structural integrity. Into these wells, Aqua-Poly/Mount (Polysciences, Inc., Warrington, PA) was added. After the slices were placed in mounting medium, they were coverslipped, and sealed with clear nail varnish. The confocal images were collected on a Leica SP2 Laser Scanning Confocal Microscope (Leica Microsystems, Confocal Microscopy, Germany) in the Michael Hooker Microscopy Facility at the University of North Carolina at Chapel Hill. Photomultiplier tubes

were used to detect the fluorescence from the fluorochromes in the multiple-labeling experiments.

Results

Dopamine Release and Fluorescence in PLAP mice

In brain slices fluorescently labeled with an antibody to PLAP, nerve terminal regions with high fluorescent intensity are expected to release more dopamine than areas of lower fluorescent intensity because the fluorescent intensity should be a direct index of terminal density. This hypothesis was tested in the dorsal lateral caudate putamen of the PLAP mice. The epifluorescent image shows the quality of labeling with this protocol (Figure 3.1a). It appears that there is some non-specific adsorption on the surface of the slice that becomes clearer when the epifluorescent image is compared to a confocal image of conventional immunohistochemical labeling with TH. Confocal microscopy is widely used to allow one to focus below this top layer and capture images of specific labeling. Epifluorescence captures light from the entire specimen, including the surface of the slice. The rectangles indicate where the electrode was placed while stimulated release was measured. The average current traces are shown for each position. The magnitude of release was determined by the peak current in the cyclic voltammogram taken at the time when dopamine release has reached a maximal level following stimulation. When the relative fluorescent intensity is compared to the oxidation current of dopamine, there is a weak linear relationship ($r^2 = 0.23$, Figure 3.1c). To determine why this might be true, the expression of PLAP and the efficacy of this labeling protocol were tested, as discussed below. The mice were known to have the gene for PLAP from genotyping results (data not shown).

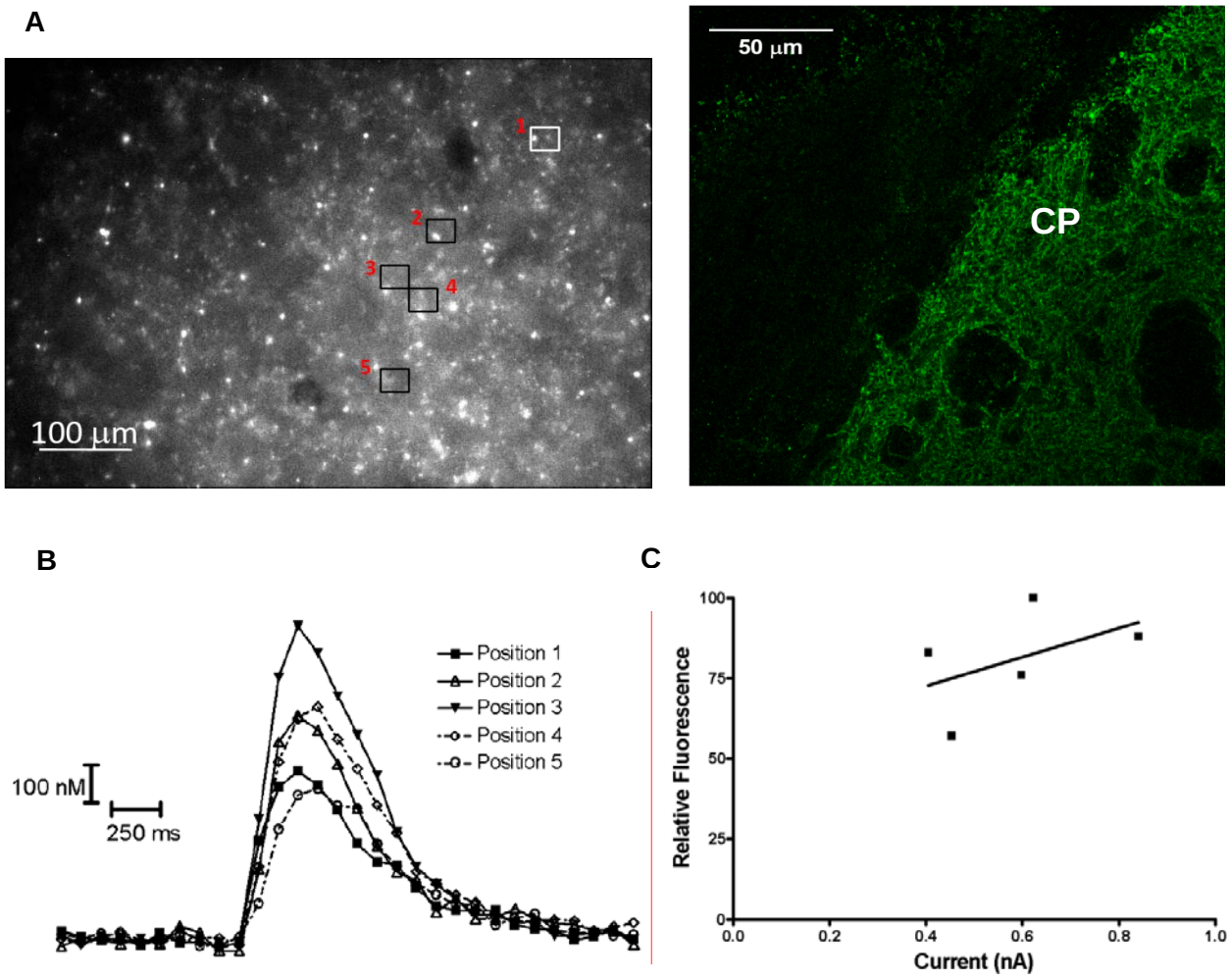

Figure 3.1. Relationship between fluorescent intensity of PLAP labeling and dopamine release. A) PLAP labeling of a live mouse brain slice containing the caudate putamen (CP). Squares indicate electrode location for the corresponding traces. TH labeling of fixed tissue imaged by confocal microscopy to the right. B) Single-pulse stimulated release at the positions indicated in the squares. C) Linear regression of the relative fluorescence in the squares compared to the release at those positions ($r^2 = 0.23$).

PLAP Labeling

To test the spatial specificity of PLAP expression, co-localization experiments were conducted with a membrane bound marker, the dopamine transporter (DAT), and a cystolic marker, tyrosine hydroxylase (TH). As shown in Figure 3.2a the plasma membrane is clearly visualized by the fluorescence arising from the DAT antibody. There is high co-localization of TH and PLAP labeling in the same cell (Figure 3.2b). However, the PLAP labeling does not overlay DAT labeling, but instead is found within the membrane.

PLAP labeling of fixed, permeabilized tissue was conducted in horizontal brain slices to determine the depth at which a slice could be prepared that contains a lengthy projection of axons to facilitate remote stimulation. Figure 3.3 shows the labeling of an axon that arborizes in a terminal field of the nucleus accumbens. One could place the working electrode among the terminals and the stimulating electrode along the axons. The stimulating electrode would be placed some distance sufficient to elicit dopamine release but not stimulate the other cells local to those releasing terminals. This slice was obtained by gluing the brain to the slicing block upside down, such that the dorsal surface is contacting the glue.

PLAP Antibody Permeation

For slices in which measuring release is a goal, incubation times with the antibody must be short to retain cell function. To determine whether a tissue labeling protocol is viable with the short-time incubations, the depth of penetration of the antibody into the slice was examined after a 15 minute incubation. Images of brain slices labeled with the PLAP antibody conjugate were taken with a confocal microscope and a side view was obtained.

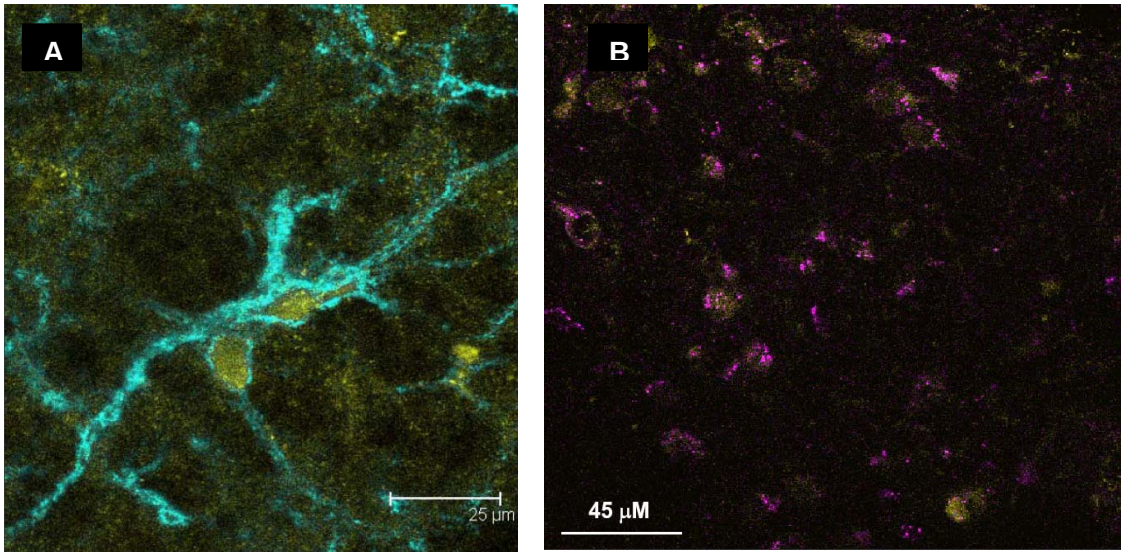

Figure 3.2. Cytoplasmic expression of PLAP. A) DAT (cyan) and PLAP (yellow) labeling of the VTA, B) TH (magenta) and PLAP (yellow) labeling of the VTA.

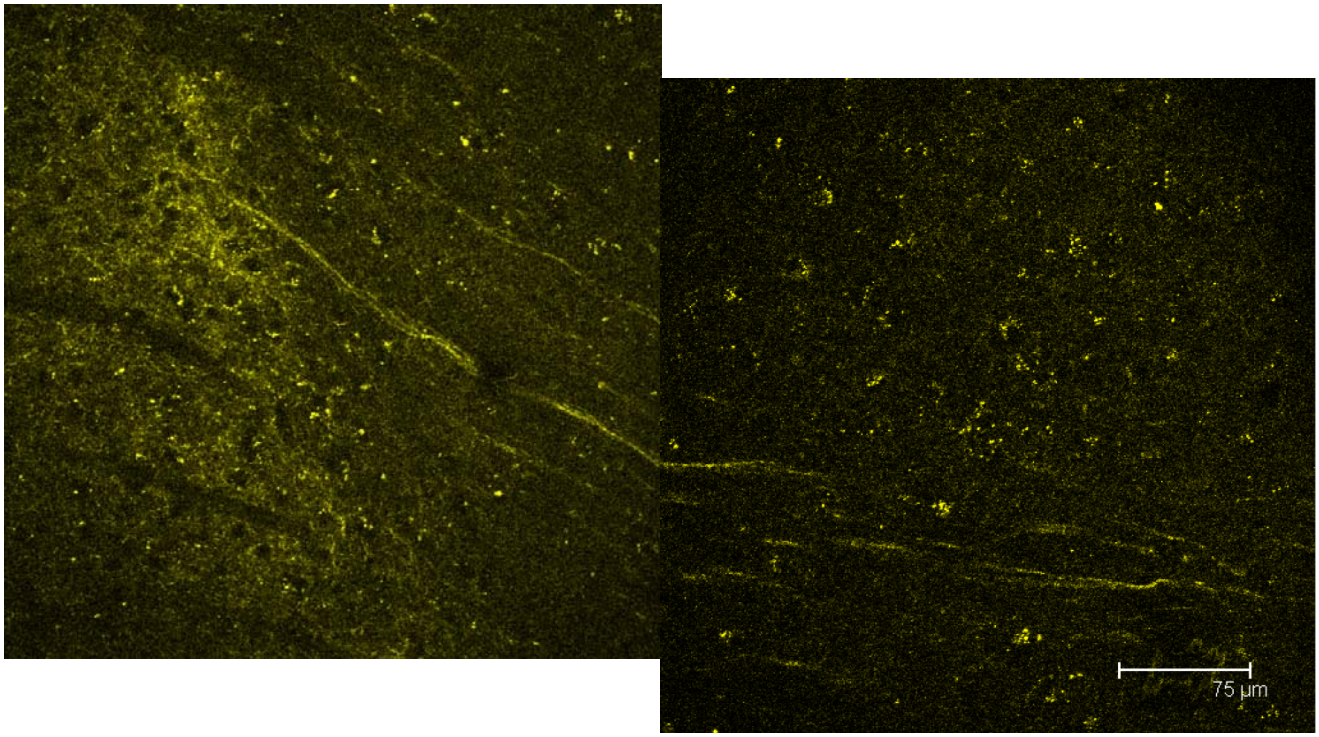

Figure 3.3. PLAP labeling of a horizontal slice containing the mesolimbic pathway. Axons from the medial forebrain bundle can be seen to arborize in the terminal field of the nucleus accumbens.

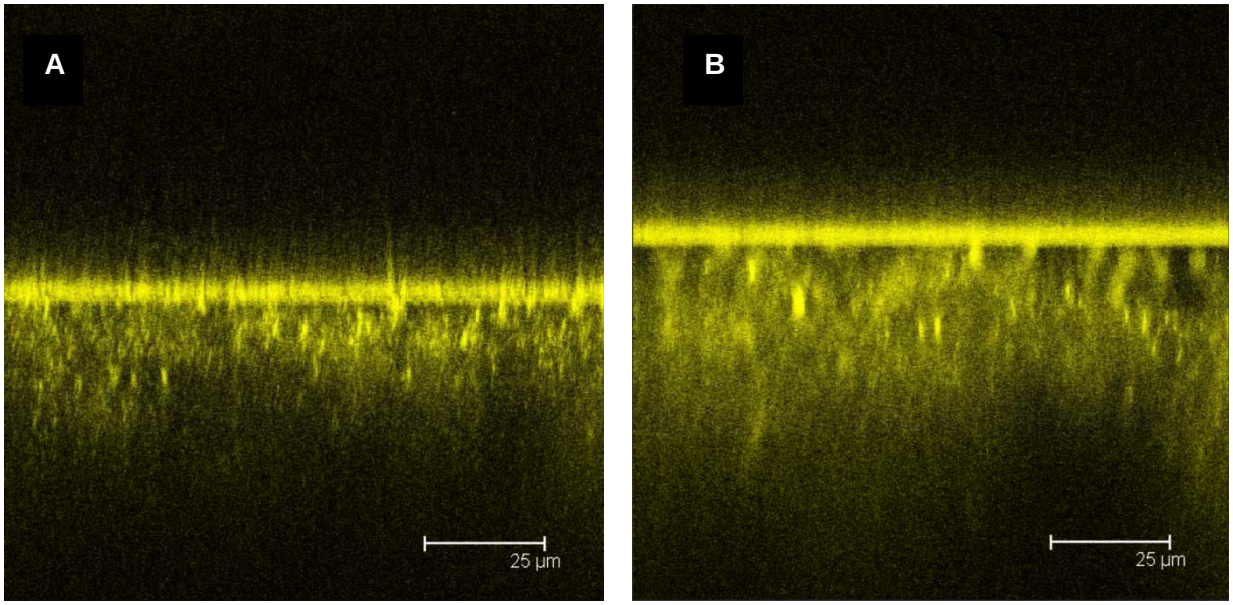

Figure 3.4. An confocal images of xz profiles after a 15 min incubation of the brain slice in a solution containing the PLAP antibody. The slice is not fixed or permeabilized. A) Striatum, B) VTA.

The resulting images were taken from a terminal rich region and a cell body region with similar results (Figure 3.4). The bright thick line at the top indicates the surface of the slice and the degree of non-specific adsorption that occurs. This presents a problem for epifluorescence as the surface obfuscates the view of the more specific labeling deeper in the slice. In both brain regions, the fluorescence reaches a depth of approximately 50 μm. That may be the depth the antibody conjugate has diffused and labeled or it could be a limit on sampling depth due to scattering and absorption of light by the tissue. In either case, the light used to direct electrode placement is coming from a depth shallower than the 60-70 μm that the electrodes are normally placed.

Dopamine Release and Fluorescence in GFP mice

Since visualizing dopaminergic cells in GFP mouse brain slices does not require a labeling step, there should be a stronger correlation between dopamine release and fluorescence. A brain region of sparse dopaminergic innervation, the amygdala, was used to more sharply resolve release sites (Figure 3.5a). The relationship between relative fluorescent intensity and current due to dopamine oxidation is linear (r^2 = 0.999, Figure 3.5c).

Somatodendritic release was tested in the VTA. Cells were easily identified due to their intense fluorescence; however, release was a similar magnitude throughout the VTA (Figure 3.6). The most intense fluorescence and weakest release were measured at the cell bodies in the VTA. The linear regression reveals little relationship between fluorescence and release (Figure 3.6c).

Discussion

The weak relationship of dopamine release and fluorescent intensity suggest that the PLAP labeling was not completely specific. A fundamental assumption of the live tissue labeling approach is that the PLAP protein is being expressed on the surface of the cell where it is

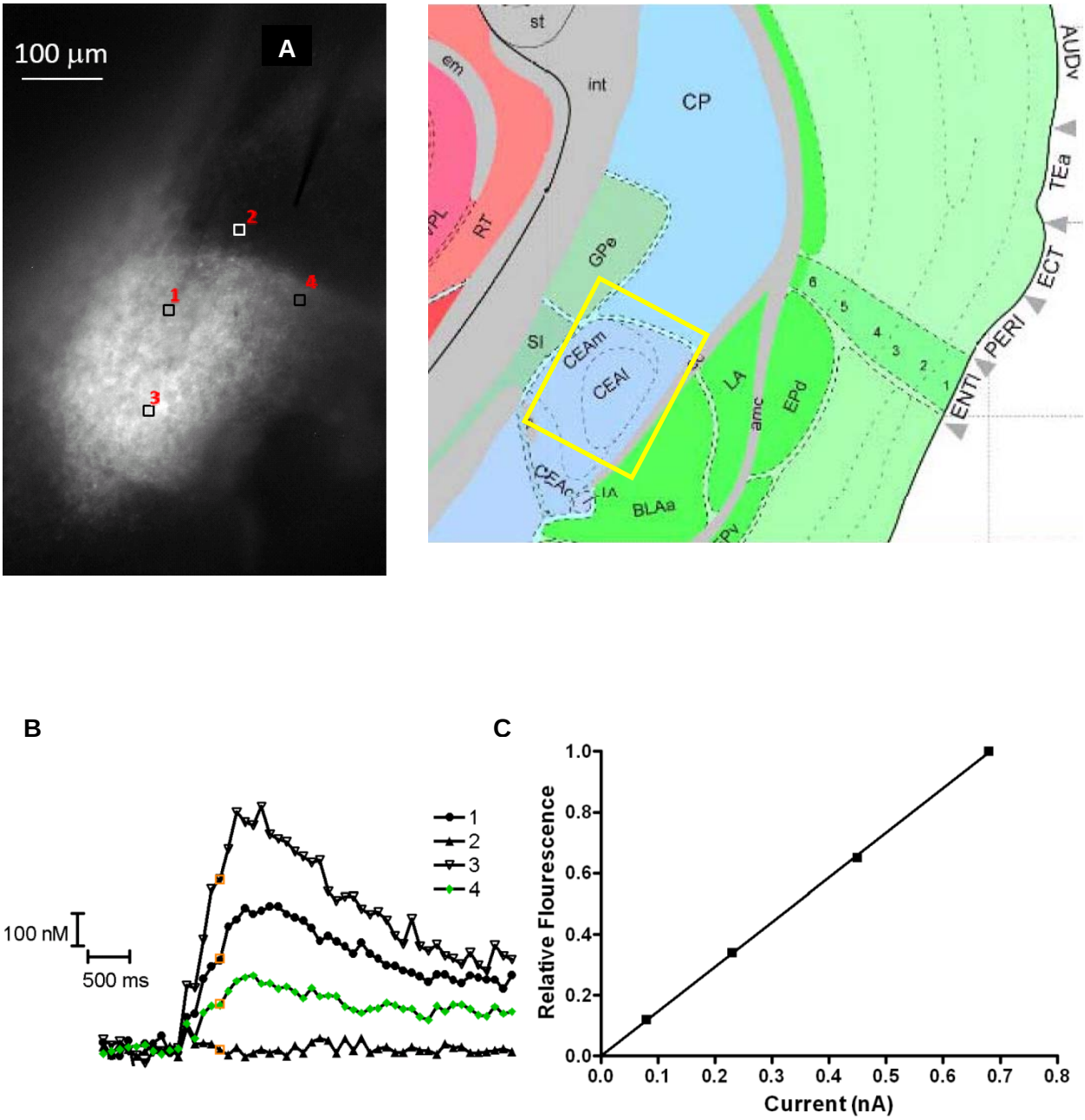

Figure 3.5. Relationship between fluorescent intensity and dopamine release in the central amygdaloid nucleus. A) Epifluorescent image of a GFP mouse brain slice containing the central amygdala. To the right is a mouse brain atlas (braininfo.rprc.washington.edu), the yellow box indicates corresponding region. Squares indicate electrode location for the corresponding traces. B) Stimulated release (24-pulse, 60 Hz) at the corresponding positions. The orange squares indicate the end of the stimulation. C) Linear regression of the relative fluorescence in the squares compared to the release at those positions (r^2 = 0.999).

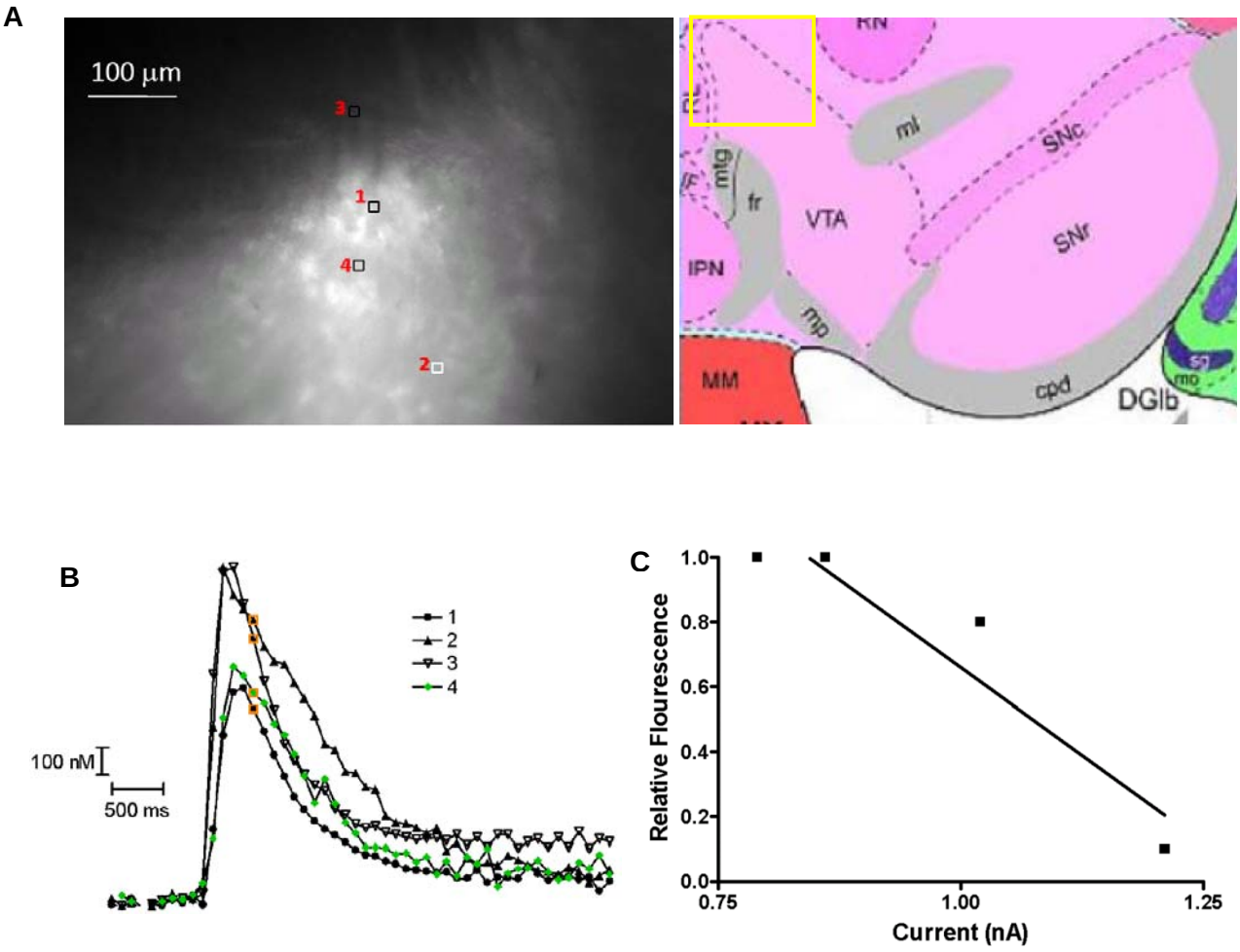

Figure 3.6. VTA Relationship between fluorescent intensity and dopamine release. A) Epifluorescent image of a GFP mouse brain slice containing the VTA. Squares indicate electrode location for the corresponding traces. To the right is a mouse brain atlas(braininfo.rprc.washington.edu), the yellow box indicates corresponding region. B) Stimulated release (10-pulse, 60 Hz) at the corresponding positions. The orange squares indicate the end of the stimulation. C) The relative fluorescence in the squares compared to the release at those positions (r^2 = 0.89).

accessible to the antibody. If it were expressed within the cell, the antibody would be prevented from interacting with its target, unless the tissue is permeabilized as in Figure 3.3. However, permeabilized cell membranes prevent the study of release since the cells are no longer functionally viable. If PLAP was being expressed on the surface as desired, then the labeling for PLAP and DAT, a surface protein, should overlay. This is not the case but rather TH, a cytoplasmic protein, and PLAP labeling are co-localized. These findings indicate that PLAP is not being expressed properly on the cell surface and would thus not be available for live tissue labeling. This change in expression from early reports may be due to genetic drift. Genetic drift is a stochastic process of change in allele frequencies. Given sufficient breeding cycles, the expression of a non-native protein can be altered and even silenced (Hickman-Davis and Davis, 2006).

A lack of sufficient tissue permeation by the labeled antibody was found with short incubation times. When one conducts immunohistochemistry with fixed tissue, antibody incubation is performed on the order of hours. The short incubation time is used here in the interest of keeping the tissue live and viable. Longer incubation times were attempted, but the brain slice did not recover. There may be ways to improve tissue survivability for longer incubations. However, this is unnecessary thanks to the development of a mouse that makes visualization much less labor intensive.

PLAP mice require the antibody to be harvested from hybridoma cells, then purified, conjugated to the dye, purified again, and screened for proper dye-to-protein ratio. To visualize dopamine neurons in GFP mice requires only an excitation source and the proper filters. The linear regression of dopamine release and GFP fluorescent intensity is very high at neuron terminals in the amygdala due to the specificity of gene expression. This means the fluorescent signal in these mice can be reliably used to guide electrode placement in regions of low terminal density.

The visualization of cell bodies in the VTA provides the means to test the nature of somatodendritic release in dopamine neurons. Release of a similar magnitude in all recording areas could be due to two possible explanations. First, uptake may be sufficiently slow that dopamine diffuses from release sites and creates a uniform concentration throughout the recording area. Second, most release may originate from the diffuse network of dendrites instead of the cell bodies. In fact, the less intensely fluorescent areas adjacent to the cells in the VTA consist of a dense network of dendrites that do not fluoresce brightly due to their small diameter. Since these less fluorescent regions is where release was the highest, it seems that release primarily occurs at the dendrites not the cell bodies

The facile identification of dopamine neurons within brain slice preparations provides the opportunity to perform novel experiments. One such experiment involves remote stimulation of release. The working electrode is placed among nerve terminals to measure dopamine release in the standard fashion. The stimulating electrode is placed some distance away along axons that project to the terminals from which release will be measured. By arranging electrodes in this manner, one will specifically stimulate the dopamine neurons and not the other neighboring cell types. This type of experiment is explored more fully in Chapter 5. By extension, one could move the working electrode to the cell bodies in the VTA from which these axons project. By stimulating the axons and measuring release at the cell bodies, one can study antidromic stimulation. This will provide similar benefits of specificity over the VTA experiment in Figure 6. Release from midbrain dopamine cells, using both local and antidromic stimulation, is explored more fully in Chapter 6. In conclusion, GFP mice allow rapid identification of dopaminergic neurons and aid proper electrode placement. This facilitates making measurements in otherwise challenging regions of the brain, such as the amygdala, and in novel contexts, such as with remote stimulation.

References

Bunin MA, Prioleau C, Mailman RB, Wightman RM (1998) Release and uptake rates of 5-hydroxytryptamine in the dorsal raphe and substantia nigra reticulata of the rat brain. J Neurochem 70:1077-1087.

De Waele P, De Groote G, Vand De Voorde A, Fiers W, Franssen J, Jerlon P, Urbain J (1982) Isolation and identification of nomoclonal-antibodies directed against human placental alkaline phosphatase. Arch Int Physiol Biochim Biophys 90:b21.

Gustincich S, Feigenspan A, Wu DK, Koopman LJ, Raviola E (1997) Control of dopamine release in the retina: a transgenic approach to neural networks. Neuron 18:723-736.

Hickman-Davis JM, Davis IC (2006) Transgenic mice. Paediatr Respir Rev 7:49-53.

Hochstetler SE, Puopolo M, Gustincich S, Raviola E, Wightman RM (2000) Real-time amperometric measurements of zeptomole quantities of dopamine released from neurons. Anal Chem 72:489-496.

Kawagoe KT, Zimmerman JB, Wightman RM (1993) Principles of voltammetry and microelectrode surface states. J Neurosci Methods 48:225-240.

Kessler MA, Yang M, Gollomp KL, Jin H, Iacovitti L (2003) The human tyrosine hydroxylase gene promoter. Brain Res Mol Brain Res 112:8-23.

Paxinos G, Franklin KBJ (2004) The mouse brain in stereotaxic coordinates, Compact 2nd Edition. Amsterdam ; Boston: Elsevier Academic Press.

Zheng J, Wu J, Sun Z (2003) An approach to identify over-represented cis-elements in related sequences. Nucleic Acids Res 31:1995-2005.

Chapter 4

Comparison of eGFP Transgenic Mice and their WT Background Strain

Introduction

The dopaminergic system within the mammalian brain has been widely studied due to its central role in a number of brain functions and disorders. The mesocorticolimbic pathway includes cells of the ventral tegmental area (VTA) that project to the nucleus accumbens (NAc), amygdala, and frontal cortex. This pathway is involved in emotion, reward, and memory processing (Jackson and Westlind-Danielsson, 1994; Schultz et al., 1997; Phillips et al., 2004) and plays a role in disorders such as schizophrenia and drug addiction (Di Chiara and Imperato, 1988; Goldstein and Deutch, 1992). The nigrostriatal pathway includes cells of the substantia nigra compacta (SNc) that project to the dorsal striatum. This pathway is involved in motor control (Bradbury et al., 1985; Missale et al., 1998; Sealfon, 2000) and plays a role in diseases such as Parkinson's and Huntington's disease (Bjorklund and Lindvall, 1984; Jakel and Maragos, 2000; Johnson et al., 2006). The tuberoinfundibular pathway refers to dopamine neurons in the hypothalamus that project to the pituatary gland to regulate levels of prolactin in blood (Picetti et al., 1997) and plays a role in lactation and fertility (Civelli et al., 1993).

The development of transgenic mice that express green fluorescent protein (GFP) in catecholaminergic cells has provided a new tool for studying these dopamine systems. Mice that express GFP under the regulation of the tyrosine hydroxylase (TH) promoter have been used to study TH regulation through development (Matsushita et al., 2002).

Fluorescent cells facilitate enrichment strategies prior to implantation, which is used as a strategy to alleviate disorders such as Parkinson's disease (Sawamoto et al., 2001; Donaldson et al., 2005). Cells can now be tracked during development and differentiation to provide more information on factors determining cell fate (Zhao et al., 2004). We use the fluorescence of dopaminergic neurons within brain slices from GFP transgenic mice to aid electrode placement for the electrochemical monitoring of extracellular dopamine concentrations. This is especially useful in sparsely innervated areas where release sites can be difficult to find. Additionally, visualizing the neurons of the mesolimbic pathway within horizontal brain slices allows a stimulating electrode to be placed along the axons of cells that release dopamine measured in the NAc. The working electrode can also be placed in the VTA to look at antidromic release.

However these are transgenic mice expressing a non-native protein, so it cannot be assumed that cell function is identical to wild-type mice. Some transgene products interact with numerous processes that can cause pleiotropic effects on phenotype (Giddings, 2002). GFP mice generated by Sawamoto and co-workers were evaluated in neuronal postnatal cell culture and were found to reliably identify dopaminergic neurons expressing expected characteristics (Jomphe et al., 2005). The mice used in that study were heterozygous because the homozygotes had low survivability. As mentioned by the authors, this could be due to random insertion of the transgene in the coding region or promoter of an important gene. The mice used in this study were generated independently in the Iacovitti lab and have the advantage of being homozygous. Therefore, a systematic comparison of GFP mice and C57 mice, their wild-type background strain, has been conducted to assess parameters important to brain slice experiments.

Materials and methods

Chemicals

Cocaine hydrochloride was obtained from Sigma-Aldrich (St Louis, MO, USA). For administration of cocaine to brain slices, 10 mM stock solutions were prepared by dissolving the appropriate weight of cocaine hydrochloride into a known volume of deionized water.

Animals

Animals were handled in accordance with protocols approved by the Institutional Animal Care and Use Committee of the University of North Carolina. A transgenic mouse line in which dopamine neurons express the gene for the enhanced green fluorescent protein was used (Kessler et al., 2003). C57/BL6 (wild-type) mice were obtained from The Jackson Laboratory (Bar Harbor,ME, USA) at 5–6 weeks of age. Upon receipt, mice were housed at the University of North Carolina Animal Husbandry Facility in Kerr Hall. Mice were provided food and water ad libitum and were kept under conditions of controlled temperature, humidity, and a 12-h light/dark cycle.

Brain slices

Mice were deeply anesthetized by ether inhalation and decapitated. The brain was immediately removed and placed in ice-cold aCSF. The aCSF solution consisted of (in mM): NaCl 126, KCl 2.5, NaH_2PO_4 1.2, $CaCl_2$ 2.4, $MgCl_2$ 1.2, $NaHCO_3$ 25, HEPES 20, D-glucose 11. The pH was adjusted to 7.4 with 5 M NaOH and the buffer was continuously saturated with 95% O_2/5% CO_2. The cerebellum was sliced off with a razor blade and the brain was mounted on a Teflon block using Krazy Glue ®. Brain slices were made using an NVSL vibratome (World Precision Instruments, Sarasota, FL, USA). Coronal slices containing the striatum were made 300-μm thick, obtained at +0.5 to +1.0 mm from bregma. Coronal slices containing the substantia nigra and ventral tegmental area were obtained at -2.8 to -3.3 mm from bregma. Brain slices were stored in ice-cold aCSF. A single slice was

submerged under aCSF maintained at 34°C and continuously flowing (2 mL/min) through a superfusion chamber (Warner Instruments, Hamden, CT, USA). Each brain slice was equilibrated for 30 min prior to obtaining measurements. To expose the brain slice to a given drug or calcium concentration, the appropriate volume of drug or calcium stock solution was added to the buffer reserve and introduced by a peristaltic pump to the slice through a threeway valve. A cumulative dosing regimen was used to collect concentration-response data. Brain slices were allowed to equilibrate for 30 min at a given drug or calcium concentration prior to exposing the slice to the next higher concentration.

Electrochemistry

Carbon-fiber, cylindrical microelectrodes were made as previously described (Kawagoe et al., 1993) using T650 carbon fibers (Amoco, Greenville, SC, USA) cut to a length of 25 μm. Electrodes were epoxied (Miller-Stevenson, Danbury, CT, USA) to ensure a good seal, and dipped immediately in acetone for a few seconds to remove residual epoxy from the carbon fiber. A triangular waveform, starting at -0.4 V, increasing to 1.0 V, and scanning back to -0.4 V, was applied to the carbon-fiber working electrode, versus a Ag/AgCl reference electrode, at a scan rate of 600 V/s. An update rate of 10 Hz was used for all experiments except for those used to obtain uptake kinetics, for which an update rate of 60 Hz was used.

The carbon fiber was inserted until the tip was 60-70 μm below the surface of the brain slice in the dorsolateral caudate region of the striatum between the prongs of a bipolar stimulating electrode (FHC, Bowdoinham, ME, USA), situated 200 μm apart. To evoke dopamine release, a single biphasic stimulating current pulse (2 ms each phase, 350 μA in amplitude) was applied to the stimulating electrode. The current arising from dopamine oxidation (at about 0.6 V) in successive voltammograms was measured and plotted versus

time. Electrodes were calibrated against dopamine standards of known concentrations in a flow cell after each brain slice experiment.

High Performance Liquid Chromatography

Tissue samples were punched from slices (500 μm thickness) with a 2.5 mm diameter cork borer. The tissue was blotted dry with a Kimwipe,weighed dry, and homogenized with a sonic dismembrator (Fisher Sci., Model 60, Pittsburgh, PA, USA) in 200 μL of 0.1 N $HClO_4$ spiked with 1 μM hydroquinone. The homogenized tissue was centrifuged at 6000 rpm for 10 min, and the supernatant was removed and filtered using a 0.2-μm syringe microfilter (Millex-LG). Injections (10 μL) were made onto a reverse phase column (C-18, 5 μm, 4.8 x 250 mm, Waters symmetry 300). The mobile phase (prepared in HPLC grade water) contained 0.1 M citric acid, 1 mM hexyl sodium sulfate, 0.1 mm EDTA, and 10% methanol (pH 3.5) at a flow rate of 1 mL/min. Catecholamines were detected with a thin-layer radial electrochemical flowcell (BASi, West Lafayette, IN, USA) at a potential of 700 mV versus a Ag/AgCl reference electrode. Catecholamine standards were prepared from 10 mM stock solutions in 0.1 N perchloric acid.

Dopamine Release and Calcium Dependence

For each phenotype, dopamine release was recorded at four different locations in the caudate. At each location, measurements were taken every five minutes for five trials. The resulting data was averaged and counted as a single reading. To determine the dependence of dopamine release on the extracellular concentration of calcium, dopamine release at a single site in the dorsolateral caudate was confirmed at a calcium concentration of 2.4 mM and then replaced with calcium-free buffer. Once release was extinguished, increasing concentrations of calcium were introduced as described above.

Kinetic analysis

Dopamine uptake follows Michaelis–Menten kinetics (Wightman et al., 1988; Kawagoe et al., 1992; Jones et al., 1995). Thus, the presumed scheme is (Matthews and Holde, 1996):

$$(DA)_o + T \leftrightarrow (DA)T \rightarrow (DA)_I + T$$

where $(DA)_o$ is extracellular dopamine, $(DA)_i$ is intracellular dopamine, and T is the dopamine transporter. The Michaelis–Menten rate equation for dopamine uptake may be written as:

$$d[DA]/dt = [DA]_p - V_{max}/(K_M/[DA] + 1)$$

where [DA] is the brain extracellular concentration of dopamine, $[DA]_p$ is the change in concentration of dopamine at the electrode produced by each stimulus pulse, and V_{max} and K_M are Michaelis–Menten rate constants which describe dopamine uptake DAT. In the absence of added drugs, K_M was fixed at 0.2 μM and the values for $[DA]_p$ and V_{max} were adjusted to obtain a best fit. The rate equation was numerically integrated and compared with the experimental data using locally written software (Wu et al., 2001). Since the K_M of DAT in eGFP mice may not be 0.2 μM, the resulting V_{max} may be in error. To determine a more accurate K_M, a competitive inhibitor analysis was used.

In the presence of a competitive inhibitor (I), the additional equilibrium must be considered:

$$I + T \leftrightarrow IT$$

Under this paradigm $(K_M)_{app}$ is defined as $K_M(1 + [I]/K_i)$, where K_i is the dissociation constant for the above reaction, and is defined as $K_i = [I][T]/[IT]$. Thus, a plot of $(K_M)_{app}$ versus [I] should be linear with a slope of K_M/K_i and a y-intercept of K_M (Matthews and Holde, 1996). A linear regression was used to determine a value of K_M from each set of cumulative doses of cocaine for a given slice. This new K_M value was then used to determine V_{max} in the absence of drug. The changes in the apparent K_M were determined again using this more accurate V_{max} value. By holding the y-intercept of the linear regression at the value of K_M, a K_i value was calculated. The V_{max}, K_M, and K_i, values for each mouse genotype were pooled to obtain average values and standard error.

Statistics

Phenotypical differences were evaluated statistically using paired t-tests in GraphPad Prism software (GraphPad Software Inc., San Diego, CA, USA). Data were considered significant at the 95% confidence level and are reported as the mean ± SEM for n animals.

Results

Tissue Content

Tissue punches of the caudate were used to determine dopamine tissue content at dopaminergic terminals, and tissue punches of the midbrain were used to determine dopamine tissue content at dopaminergic cell bodies. Midbrain punches were taken to encompass the ventral tegmental area (VTA) but may also include some parts of the adjacent dopaminergic structure, the SNc. There are no significant differences between

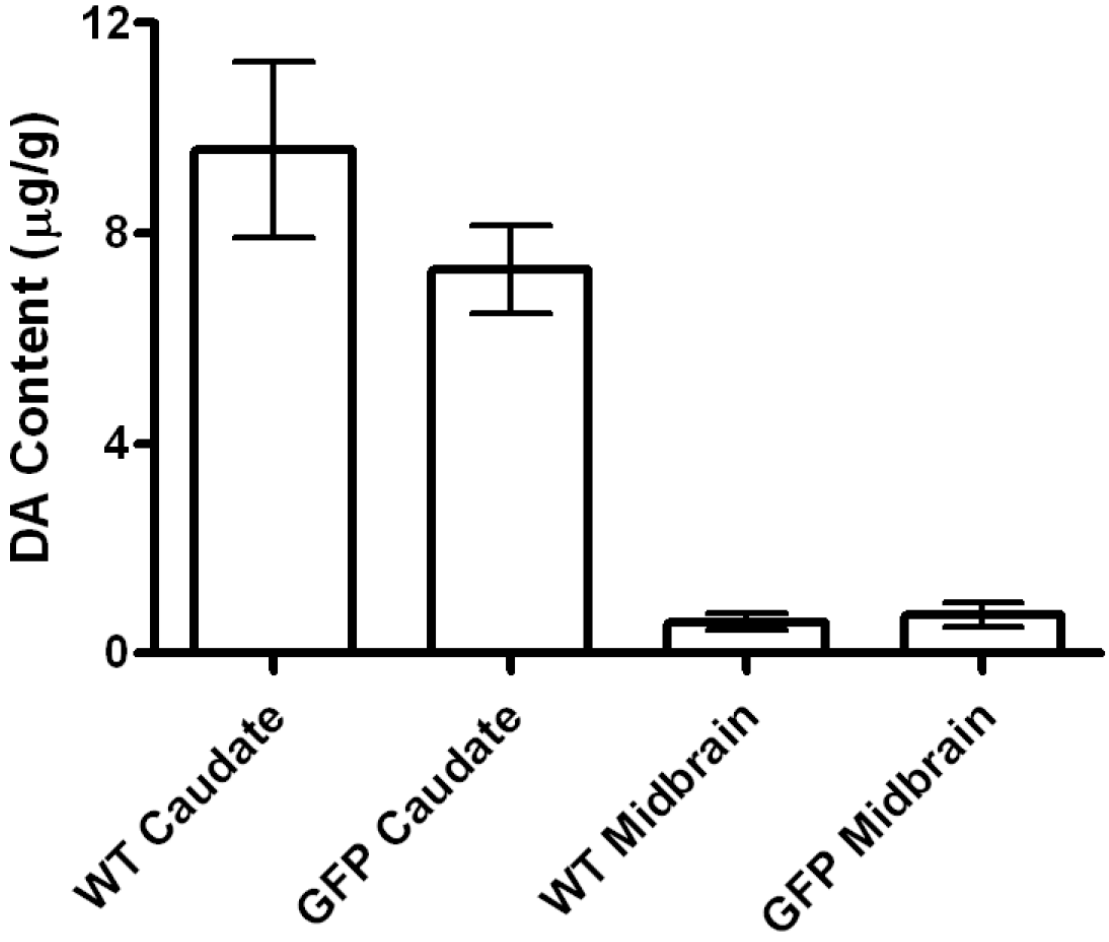

Figure 4.1. Dopamine tissue content. HPLC analysis of tissue punches from brain slices containing the regions referenced in the column titles. Recovery of dopamine is determined from an internal standard, hydroquinone. Dopamine tissue content is normalized to the mass of the tissue sample. The dopamine tissue content of WT and GFP mice are not significantly different when compared by region ($p > 0.05$, $n = 4$).

GFP and WT mice in either region ($p > 0.05$, between mice in each region, Figure 4.1). There is much greater dopamine content in the caudate than in the midbrain for both phenotypes. The WT caudate contains 9.6 ± 1.7 μg DA/g tissue and the GFP caudate contains 7.3 ± 0.8 μg DA/g tissue. These values are slightly less than those reported for striatal dopamine content in C57 black mice (Gao et al., 1998). They used dry weights, and wet weights were used in this work, which will cause actual dopamine content to be underrepresented.

Dopamine Release and Calcium Dependence

Dopamine release due to single pulse stimulation in the caudate of GFP mice, as measured by FSCV, is not significantly different than wild-type mice ($p > 0.05$, Figure 4.2). Representative traces of stimulated release for a one-pulse stimulation form a WT mouse and a GFP mouse are shown in Figure 4.2. The rising portion of the signal is the increase in extracellular following stimulation. A cyclic voltammogram at the time the release event is at its maximum identifies the released substance as dopamine. The falling portion of the signal is due to uptake by DAT. The linear portion near the maximum is a V_{max} dominated region. As the extracellular concentrations falls, uptake rates become exponential in a K_M dominated region. Moreover, the calcium dependence of dopamine release in the two animal types overlay (Figure 4.3). Dopamine release is normalized to the release measured at 3.0 mM calcium to remove the variability of release between slices.

Uptake Kinetics

The validity of using the competitive inhibitor analysis was established by analyzing wild-type mice and comparing to reported values. The V_{max} (5.0 $\pm$0.3 μM/s), K_M (0.25 $\pm$0.03 μM),

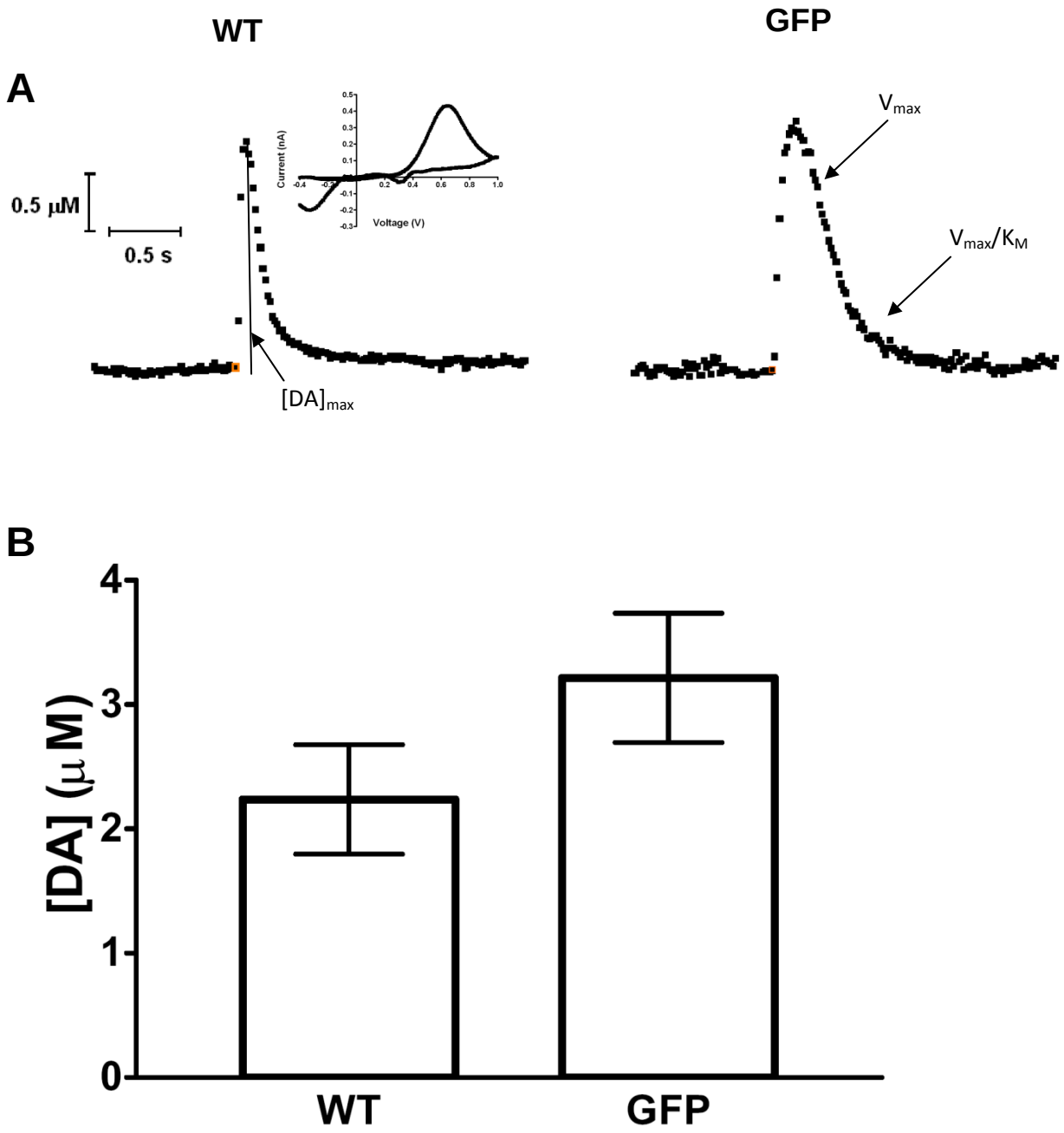

Figure 4.2. Stimulated dopamine release. A) Representative traces from a WT and GFP mouse following a single-pulse stimulation, as indicated by the orange square. The CV identifies dopamine at the peak of the signal. V_{max} dominates uptake during the linear portion at the top of the curve and K_M dominates uptake at low concentrations where the trace curves toward baseline. B)The peak concentration of dopamine released following a one-pulse stimulation as measured by FSCV. Five traces were averaged at each of four locations within one slice per animal were averaged to represent one data point. The concentration of dopamine released upon stimulation in WT and GFP mice are not significantly different ($p > 0.05$, $n = 6$).

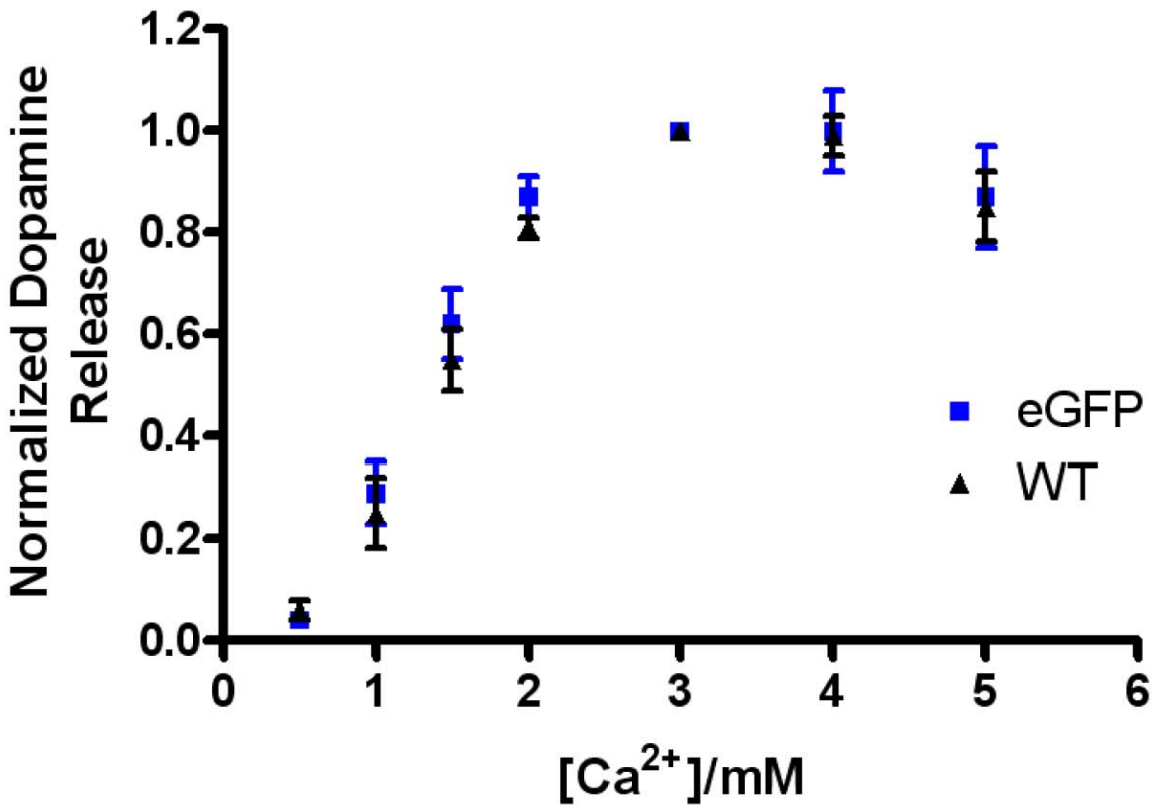

Figure 4.3. Calcium dependence of dopamine release. The amount of dopamine release in each brain slice was normalized to the release measured at 3 mM calcium to take out the variability of release from one slice to another. There is no significant difference between the values at each concentration ($p > 0.05$, $n = 5$).

(n=5)	**WT**	**GFP**
$\mathbf{K_M}$ (μM)	0.25 ±0.03	0.25 ±0.02
$\mathbf{V_{MAX}}$ (μM/s)	5.0 ± 0.3	2.8 ±0.4
$\mathbf{K_I}$ (μM)	0.26 ±0.05	0.49 ±0.13

Table 1. Uptake parameters of WT and GFP mice. The parameters describing uptake in these brain slices are the result of a competitive inhibitor analysis using a simplex modeling program. A post-experiment calibration provided the sensitivity and time constant of each electrode used. The values shown are mean ± s.e.m. of the values obtained in each slice.

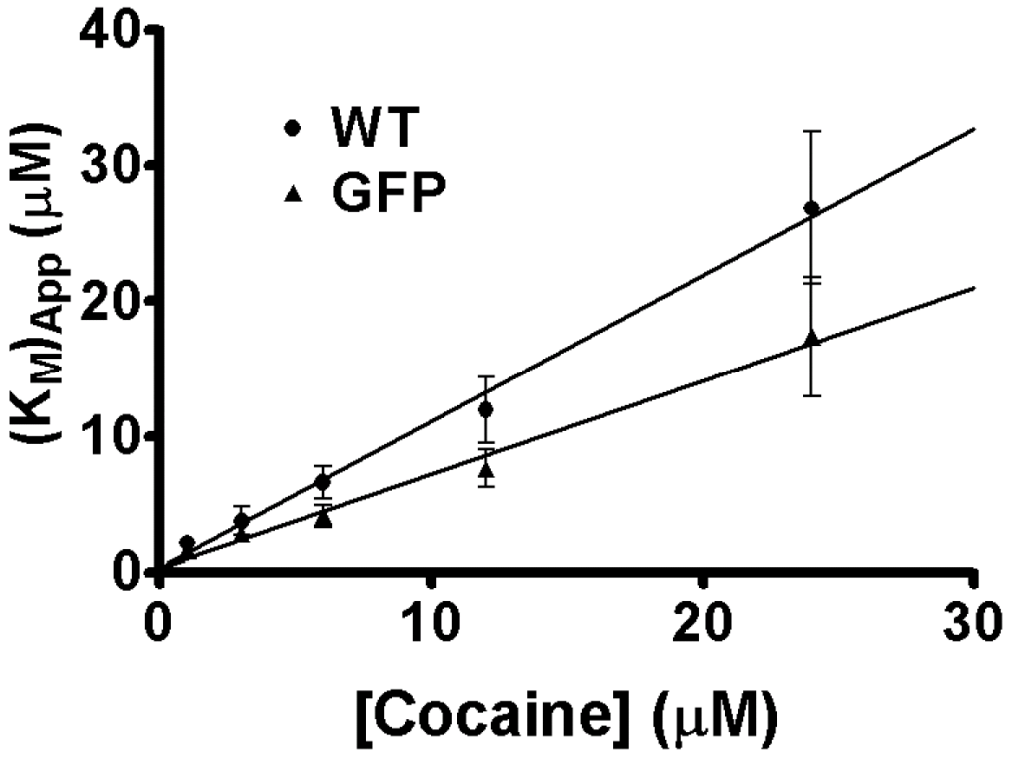

Figure 4.4. Uptake inhibition of DAT by cocaine. The y-intercept is held at the value determined for K_M. The K_M value at each cocaine concentration was determined by holding constant the V_{MAX} value determined form the pre-drug file, which is an average of five traces. Each point is the average and the error bars represent s.e.m. for n = 5.

and K_i for cocaine (0.26 $\pm$0.05 μM) values reported in Table 1 for the WT mouse are similar to, although slightly higher than, values reported elsewhere. Uptake in GFP mice were compared to WT mice using this analysis. While the K_M (0.25 $\pm$0.02 μM) for the GFP mouse is not significantly different than the WT ($p > 0.05$, $n = 5$), the V_{max} (2.8 $\pm$0.4 μM/s) is lower ($p < 0.002$, $n = 5$). Figure 4.4 shows the change in $(K_M)_{app}$ with cocaine concentration and the linear regression used to find K_i. The K_i for the GFP mouse and WT mouse is not significantly different ($p < 0.002$, $n = 5$).

Discussion

Generally, these GFP mice are in all measured ways similar to WT C57/BL6 mice except that a lower V_{MAX} was found in the GFP mice. Since the GFP transgene is coupled to the promoter for TH one would expect that if there were some difference in the mice it would be related to synthesis or tissue content of dopamine. However, the random nature of transgene insertion into chromosomes can bring about unforeseen differences whether pleiotropic or compensatory. Although behavior was not directly tested, anecdotally the mice do not appear to exhibit a phenotypic difference.

The similarity in tissue dopamine content and stimulated release indicates that the terminal density of the dorsal striatum is similar between the mice. Taken together with the difference in V_{MAX} there may be fewer transporters per terminal in GFP mice. Although the rate of synthesis was not tested directly, the global assessment of content and release shows that the overall volume of synthesis does not appear impaired.

The similar sensitivities to extracellular concentrations of calcium indicate that the calcium channels, calcium buffering and vesicular-fusion mechanisms are unaffected. Tissue content of dopamine and calcium response being similar between WT and GFP further buttresses the assertion that release is the same.

The use of a competitive inhibitor analysis is an approach to determine uptake parameters in a sample of unknown kinetics. To validate this approach the analysis was first carried out on WT mice. Values of K_M in the absence of uptake inhibitors have been determined in synaptosomal preparations to be approximately 0.2 μM (Horn, 1990). This was taken as a starting value from which to derive a V_{max} that could be used to assess shifts in K_M in the presence of cocaine. During the first iteration, for which K_M was held at 0.2 μM, the V_{max} value (4.8 ± 0.2 μM/s) closely matches the previously reported value of 4.3 ±0.5μM/s (Jones et al., 1999). Allowing the y-intercept to float during the linear regression yielded a slightly higher K_M which in turn yielded a slightly, but not significantly, higher V_{max}. Using this V_{max} in a second assessment of shifts in K_M produced K_I values similar to values reported from synaptosomal preparations in the rat (Richelson and Pfenning, 1984). These results are sufficiently accurate as to validate a comparison between mouse types. All values were found to be similar except a lower V_{MAX} was found in the GFP mice. V_{max} is proportional to dopamine transporter concentration, so a lower V_{max} implies a lower DAT expression level. It is not clear at this time why DAT expression should be different. Additionally, other uptake inhibitors could be used to verify this difference in V_{MAX}. In addition, different regions of the brain could be tested for differences in V_{MAX} to determine if this difference only exists in the dorsal striatum. Although the expression level of DAT may have been altered in GFP mice, the transporters take up dopamine with similar kinetics as in WT mice and are similarly inhibited by cocaine.

Given the similarities in release in the striatum, it would be interesting to probe release in other regions more difficult to study, such as the hypothalamus and limbic cortex. With the visualization of neurons being possible, release in horizontal or sagittal slices can be exploited. There are other properties of these mice that could be investigated as well, such as assessing D_2-autoreceptors and V_{MAT} activity. One can pursue experiments with

these mice expecting release parameters to be similar to WT's and expecting cocaine inhibit uptake with a similar efficiency with the caveat that the actual rates of uptake may be different.

References

Bjorklund A, Lindvall O (1984) Dopamine-containing systems in the CNS. Handbook Chem Neuroanat 2:55-113.

Bradbury AJ, Costall B, Kelly ME, Naylor RJ, Smith JA (1985) Biochemical correlates of motor changes caused by the manipulation of dopamine function in the substantia nigra of the mouse. Neuropharmacology 24:1155-1161.

Civelli O, Bunzow JR, Grandy DK (1993) Molecular diversity of the dopamine receptors. Annu Rev Pharmacol Toxicol 33:281-307.

Di Chiara G, Imperato A (1988) Drugs abused by humans preferentially increase synaptic dopamine concentrations in the mesolimbic system of freely moving rats. Proc Natl Acad Sci U S A 85:5274-5278.

Donaldson AE, Marshall CE, Yang M, Suon S, Iacovitti L (2005) Purified mouse dopamine neurons thrive and function after transplantation into brain but require novel glial factors for survival in culture. Mol Cell Neurosci 30:601-610.

Gao ZG, Cui WY, Zhang HT, Liu CG (1998) Effects of nicotine on 1-methyl-4-phenyl-1,2,5,6-tetrahydropyridine-induced depression of striatal dopamine content and spontaneous locomotor activity in C57 black mice. Pharmacol Res 38:101-106.

Giddings G (2002) Multigenes and multipurpose genes. Curr Opin Biotechnol 13:133-135.

Goldstein M, Deutch AY (1992) Dopaminergic mechanisms in the pathogenesis of schizophrenia. Faseb J 6:2413-2421.

Horn AS (1990) Dopamine uptake: a review of progress in the last decade. Prog Neurobiol 34:387-400.

Jackson DM, Westlind-Danielsson A (1994) Dopamine receptors: molecular biology, biochemistry and behavioural aspects. Pharmacol Ther 64:291-370.

Jakel RJ, Maragos WF (2000) Neuronal cell death in Huntington's disease: a potential role for dopamine. Trends Neurosci 23:239-245.

Johnson MA, Rajan V, Miller CE, Wightman RM (2006) Dopamine release is severely compromised in the R6/2 mouse model of Huntington's disease. J Neurochem 97:737-746.

Jomphe C, Bourque MJ, Fortin GD, St-Gelais F, Okano H, Kobayashi K, Trudeau LE (2005) Use of TH-EGFP transgenic mice as a source of identified dopaminergic neurons for physiological studies in postnatal cell culture. J Neurosci Methods 146:1-12.

Jones SR, Garris PA, Kilts CD, Wightman RM (1995) Comparison of dopamine uptake in the basolateral amygdaloid nucleus, caudate-putamen, and nucleus accumbens of the rat. J Neurochem 64:2581-2589.

Jones SR, Joseph JD, Barak LS, Caron MG, Wightman RM (1999) Dopamine neuronal transport kinetics and effects of amphetamine. J Neurochem 73:2406-2414.

Kawagoe KT, Zimmerman JB, Wightman RM (1993) Principles of voltammetry and microelectrode surface states. J Neurosci Methods 48:225-240.

Kawagoe KT, Garris PA, Wiedemann DJ, Wightman RM (1992) Regulation of transient dopamine concentration gradients in the microenvironment surrounding nerve terminals in the rat striatum. Neuroscience 51:55-64.

Kessler MA, Yang M, Gollomp KL, Jin H, Iacovitti L (2003) The human tyrosine hydroxylase gene promoter. Brain Res Mol Brain Res 112:8-23.

Matsushita N, Okada H, Yasoshima Y, Takahashi K, Kiuchi K, Kobayashi K (2002) Dynamics of tyrosine hydroxylase promoter activity during midbrain dopaminergic neuron development. J Neurochem 82:295-304.

Matthews C, Holde Kv (1996) In: Biochemistry, 2nd Edition (Benjamin/Cummings, ed), p 1158. Menlo Park, CA: .

Missale C, Nash SR, Robinson SW, Jaber M, Caron MG (1998) Dopamine receptors: from structure to function. Physiol Rev 78:189-225.

Phillips AG, Ahn S, Floresco SB (2004) Magnitude of dopamine release in medial prefrontal cortex predicts accuracy of memory on a delayed response task. J Neurosci 24:547-553.

Picetti R, Saiardi A, Abdel Samad T, Bozzi Y, Baik JH, Borrelli E (1997) Dopamine D2 receptors in signal transduction and behavior. Crit Rev Neurobiol 11:121-142.

Richelson E, Pfenning M (1984) Blockade by antidepressants and related compounds of biogenic amine uptake into rat brain synaptosomes: most antidepressants selectively block norepinephrine uptake. Eur J Pharmacol 104:277-286.

Sawamoto K, Nakao N, Kobayashi K, Matsushita N, Takahashi H, Kakishita K, Yamamoto A, Yoshizaki T, Terashima T, Murakami F, Itakura T, Okano H (2001) Visualization, direct isolation, and transplantation of midbrain dopaminergic neurons. Proc Natl Acad Sci U S A 98:6423-6428.

Schultz W, Dayan P, Montague PR (1997) A neural substrate of prediction and reward. Science 275:1593-1599.

Sealfon SC (2000) Dopamine receptors and locomotor responses: molecular aspects. Ann Neurol 47:S12-19; discussion S19-21.

Wightman RM, Amatore C, Engstrom RC, Hale PD, Kristensen EW, Kuhr WG, May LJ (1988) Real-time characterization of dopamine overflow and uptake in the rat striatum. Neuroscience 25:513-523.

Wu Q, Reith ME, Wightman RM, Kawagoe KT, Garris PA (2001) Determination of release and uptake parameters from electrically evoked dopamine dynamics measured by real-time voltammetry. J Neurosci Methods 112:119-133.

Zhao S, Maxwell S, Jimenez-Beristain A, Vives J, Keuhner E, Zhao J, O'Brien C, de Felipe C, Semina E, Li M (2004) Generation of embryonic stem cells and transgenic mice expressing green fluorescent protein in midbrain dopaminergic neurons. European Journal of Neuroscience 19.

Chapter 5

Development of a Remote Stimulation Protocol

Introduction

The importance of the mesolimbic dopamine system to behavior has been widely studied. Mesolimbic dopamine neurons encode stimulus-reward associations (Schultz et al., 1997), subserve the alerting aspects of reward circuitry (Wightman and Robinson, 2002), and relay a reward prediction error signal (Mirenowicz and Schultz, 1996). Increases in dopamine transmission underlie the reinforcing properties of many drugs of abuse (Di Chiara and Imperato, 1988; Wise, 2004). The mesolimbic pathway includes dopaminergic cells of the ventral tegmental area (VTA) that project axons through the medial forebrain bundle (MFB) to the nucleus accumbens (Acb). This pathway can now be visualized in transgenic mice that express green fluorescent protein (GFP) in dopaminergic neurons (Figure 1). However, since dopamine neurons are part of a complex circuit of cells, it is difficult through *in vivo* experiments to determine the specific properties of the dopamine neuron that contribute to the function of the system.

Brain slice experiments are conducted to understand the activity of dopamine neurons independently of the brain system with which they are a part. By taking a brain slice the region of interest is isolated from many of the inputs from other regions of the brain. Additionally, pharmacological agents can be added to the buffer supporting the brain slice. This is a more spatially constrained application than the global effects that may arise from systemic injection of drugs in the whole animal. Finally, brain slice experiments allow the

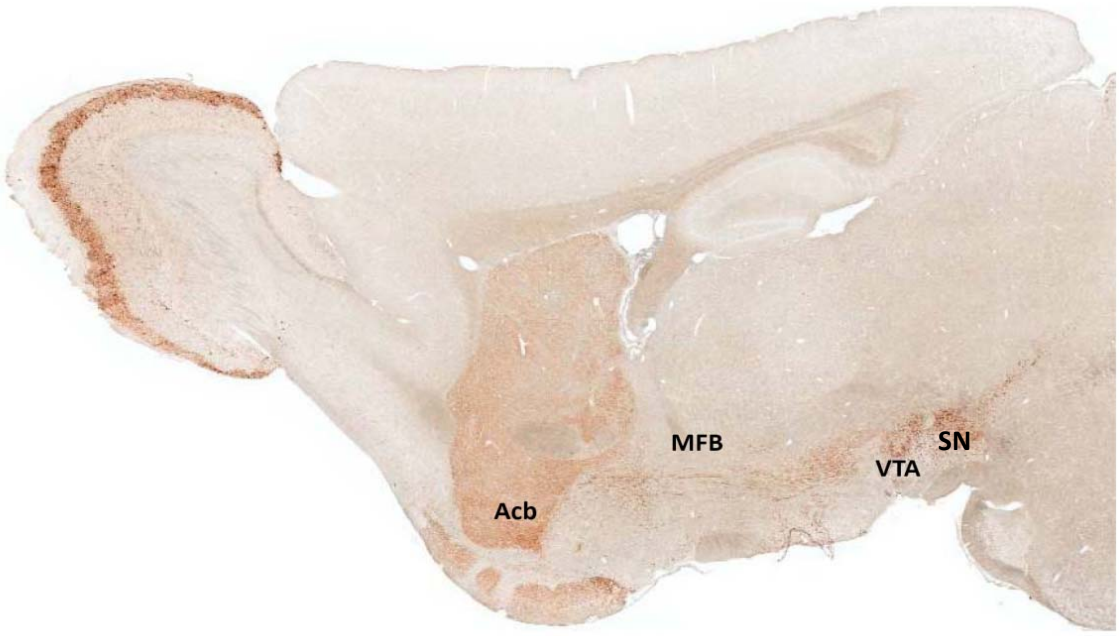

Figure 5.1. A sagittal brain slice of a TH-GFP mouse stained with an antibody to GFP (gensat.org). Components of the mesolimbic pathway are labeled and include the cell body region (VTA), axonal region (MFB), and terminal region (Acb). Also labeled are components of the nigrostriatal pathway which includes the cell body region (SN), axonal region (MFB), and terminal region (CP).

precise placement of electrodes with the aid of microscopy. This facilitates the use of fluorescent techniques to aid in identification of specific cell types.

Traditional brain slice protocols for study of the mesolimbic system utilize local stimulation of dopamine terminals within coronal slices of the Acb. Since coronal slices sever the nerve terminals from the rest of the cell, the stimulation to elicit dopamine release must be delivered near the recording location. This local stimulation also causes other cell types near the dopamine terminals to release their contents, such as γ-aminobutyric acid (GABA), glutamate, and acetylcholine. These substances can effect the function of the dopamine terminal.

An alternate approach is to take horizontal slices that encompass neurons of the mesolimbic pathway. Axons or cell bodies can be stimulated in order to elicit dopamine release at the terminals some distance away without stimulating other adjacent cell types to release their contents. This approach is possible because of the availability of GFP transgenic mice. This allows the mesolimbic dopamine neurons to be identified by their fluorescence, which will direct electrode placement. First, the stimulating electrode must be placed a sufficient distance from the working electrode to avoid stimulating other cell types. Second, the working electrode must be placed to avoid measuring norepinephrine release, which is electrochemically indistinguishable. In this work horizontal brain slices of GFP transgenic mice containing mesolimbic dopamine neurons are used to perform remote stimulation, establish criterion for electrode placement, and investigate dopamine release dynamics with this novel approach.

Materials and Methods

Chemicals

Desipramine hydrochloride and GBR-12909 dihydrochloride were obtained from Sigma-Aldrich (St Louis, MO, USA). For administration on brain slices, 10 mM stock solutions were prepared by dissolving the appropriate weight of drug into a known volume of deionized water.

Animals

Animals were handled in accordance with protocols approved by the Institutional Animal Care and Use Committee of the University of North Carolina. A transgenic mouse line in which catecholamine containing cells express the gene for the enhanced green fluorescent protein was used (Kessler et al., 2003). The mice are homozygous for GFP, making genotyping unnecessary. During the initial breeding to build the colony, genotyping was used to confirm that all mice carry the gene (data not shown). Upon receipt, mice were housed at the University of North Carolina Animal Husbandry Facility in Kerr Hall. Mice were provided food and water ad libitum and were kept under conditions of controlled temperature, humidity, and a 12-h light/dark cycle.

Brain slices

Mice were deeply anesthetized by ether inhalation and decapitated. The brain was immediately removed and placed in ice-cold aCSF. The aCSF solution consisted of (in mM): NaCl 126, KCl 2.5, NaH_2PO_4 1.2, $CaCl_2$ 2.4, $MgCl_2$ 1.2, $NaHCO_3$ 25, HEPES 20, D-glucose 11. The pH was adjusted to 7.4 with 5 M NaOH and the buffer was continuously saturated with 95% O_2/5% CO_2. The cerebellum was sliced off with a razor blade and the brain was mounted on a Teflon block using Krazy Glue ®. Brain slices were made using an NVSL vibratome (World Precision Instruments, Sarasota, FL, USA). Coronal slices containing the striatum were made 300-μm thick, obtained at +0.5 to +1.0 mm from bregma. For immunohistochemistry, the brain slices were made 200-μm thick. Brain slices were stored in ice-cold aCSF. A single slice was submerged under aCSF maintained at 34°C and

continuously flowing (2 mL/min) through a superfusion chamber (Warner Instruments, Hamden, CT, USA). Each brain slice was equilibrated for 30 min prior to obtaining measurements. When pharmacological agents were used, they were added to the buffer to a known concentration and superfused for 30 min prior to measuring their effect.

Epifluorescent Microscopy

To visualize the fluorescence in brain slices, an upright microscope (Nikon Eclipse E600FN, Melville, NY) was used with a xenon lamp source to excite fluorescence. A Nikon endow GFP bandpass filter set (filter 470 CWL for excitation, 525 CWL for emission, and a 495 LP dichroic mirror) was employed when viewing samples from GFP mice. A CCD camera (Photometrics Sensys, Tucson, Arizona) was used to capture images.

Electrochemistry

Carbon-fiber cylinder microelectrodes were made as previously described (Kawagoe et al., 1993) using T650 carbon fibers (Amoco, Greenville, SC, USA) cut to a length of 25 μm. Electrodes were epoxied (Miller-Stevenson, Danbury, CT, USA) to ensure a good seal, and dipped immediately in acetone for a few seconds to remove residual epoxy from the carbon fiber. A triangular waveform, starting at -0.4 V, increasing to 1.0 V, and scanning back to -0.4 V, was applied to the carbon-fiber working electrode, versus a Ag/AgCl reference electrode, at a scan rate of 600 V/s. An update rate of 10 Hz was used for all experiments.

The carbon fiber was inserted until the tip was 60-70 μm below the surface of the brain slice between the prongs of a bipolar stimulating electrode (FHC, Bowdoinham, ME, USA), situated 200 μm apart. To evoke dopamine release, a single biphasic stimulating current pulse (2 ms each phase, 350 μA in amplitude) was applied to the stimulating electrode. The current arising from dopamine oxidation (at about 0.6 V) in successive voltammograms was measured and plotted versus time.

Kinetic analysis

Dopamine uptake follows Michaelis–Menten kinetics (Wightman et al., 1988; Kawagoe et al., 1992; Jones et al., 1995). Thus, the presumed scheme is (Matthews and Holde, 1996):

$$(DA)_o + T \leftrightarrow (DA)T \rightarrow (DA)_I + T$$

where $(DA)_o$ is extracellular dopamine, $(DA)_i$ is intracellular dopamine, and T is the dopamine transporter. The Michaelis–Menten rate equation for dopamine uptake may be written as:

$$d[DA]/dt = [DA]_p - V_{max}/(K_M/[DA] + 1)$$

where [DA] is the brain extracellular concentration of dopamine, $[DA]_p$ is the change in concentration of dopamine at the electrode produced by each stimulus pulse, and V_{max} and K_M are Michaelis–Menten rate constants which describe dopamine uptake DAT. These same processes can be used to describe uptake by the norepinephrine transporter (NET). In the absence of uptake inhibitors, K_M was fixed at 0.2 μM and the values for $[DA]_p$ and V_{max} were adjusted to obtain a best fit. In the presence of uptake inhibitors, the change in uptake kinetics should appear as a change in K_M (Jones et al., 1995). Therefore, V_{max} was held constant at pre-drug values and K_M was adjusted to obtain a best fit. The rate equation was numerically integrated and compared with the experimental data using locally written software (Wu et al., 2001).

Immunohistochemical Labeling

Slices were fixed in 2% formaldehyde in Sorenson's buffer (0.15 m Na_2HPO_4/KH_2PO_4 at pH 7.4) for 4 h. The slices were rinsed three times with 1X PBS (Tissue Culture Facility, Chapel Hill, NC, USA). Then, normal goat serum (NGS, Life Technologies, Rockville, MD, USA) was combined with 0.2% BSA/PBS solution (1 : 10, NGS : BSA/ PBS) containing 0.3% Triton-

100X. The slices were incubated in this blocking solution for 2 h. The Primary antibody solutions were incubated for overnight (15hours) at 4°C with slow agitation and rinsed with PBS. For double labeling, secondary antibody was diluted 1:1000 and incubated overnight with the slices. For DβH/GFP double labeling experiments, the primary antibody for GFP (Rabbit, Invitrogen) is conjugated to Alexa Fluor ® 488, and the primary antibody for DβH is unconjugated (Sheep, Invitrogen). Primary antibodies were diluted into 0.5 mL of PBS and then 5 mL of blocking solution to final dilutions as follows: anti-GFP, 1:400; anti-DβH, 1:500. The secondary antibodies used were Alexa Fluor ® 555 conjugated goat anti-rabbit. Then, the slices were rinsed with PBS, placed on slides, and examined by confocal microscopy.

Confocal microscopy

Throughout this work, anatomical locations were determined by comparison with a mouse brain atlas (Paxinos and Franklin, 2004). The brain slices containing the desired regions were placed onto microscope slides with glass wells to maintain their structural integrity. Into these wells, Aqua-Poly/Mount (Polysciences, Inc., Warrington, PA) was added. After the slices were placed in mounting medium, they were coverslipped, and sealed with clear nail varnish. The confocal images were collected on a Leica SP2 Laser Scanning Confocal Microscope (Leica Microsystems, Confocal Microscopy, Germany) in the Michael Hooker Microscopy Facility at the University of North Carolina at Chapel Hill. Photomultiplier tubes were used to detect the fluorescence from the fluorochromes in the multiple-labeling experiments.

Results

Epifluorescence and Stimulation of Mesolimbic Dopamine Pathway

One can imagine passing a horizontal plane through the mesolimbic pathway in Figure 5.1 oriented to be coming out of the page. If a slice was taken through the rodent brain at this orientation at a sufficient depth and thickness to encompass a segment of those dopamine neurons, one would have the slice shown in Figure 5.2, an epifluorescent image of a horizontal GFP mouse brain slice containing the mesolimbic pathway. A black line near the number 1 is a shadow of the carbon-fiber microelectrode among the nerve terminals where release is measured. The cell bodies are sufficiently bright to make visualizing the axons difficult and are thus placed out of view on the right. The axons are the thin, filamentous structures that project from the cell bodies to the terminals on the left. The numbers indicate the placement of the stimulating electrode. The corresponding cyclic voltammograms below the image were measured at the peak of release upon stimulation. A single-pulse stimulation was used at position 1. A 24-pulse, 60 Hz stimulation was used at positions 2 and 3 because a single-pulse stimulation did not elicit a detectable signal. Even with this more intense stimulation, less release is observed as the stimulating electrode is moved posterior towards the cell bodies. This can be explained if some axons are severed in the slicing process. The more posterior, the less axons are available that make connections to the terminals, thus less release upon stimulation of the axons. The CV's indicate that the released substance is a catecholamine, due to the oxidation potential at 0.6 V and the reduction potential at -0.2 V.

Defining Remote Stimulation

The release observed in the previous experiment could be due to the stimulation of axons, or the stimulating current may have been sufficient to directly elicit a response from the terminals about the working electrode. In slices containing no axons, only stimulating terminals can elicit release, so the separation distance between stimulating electrode and

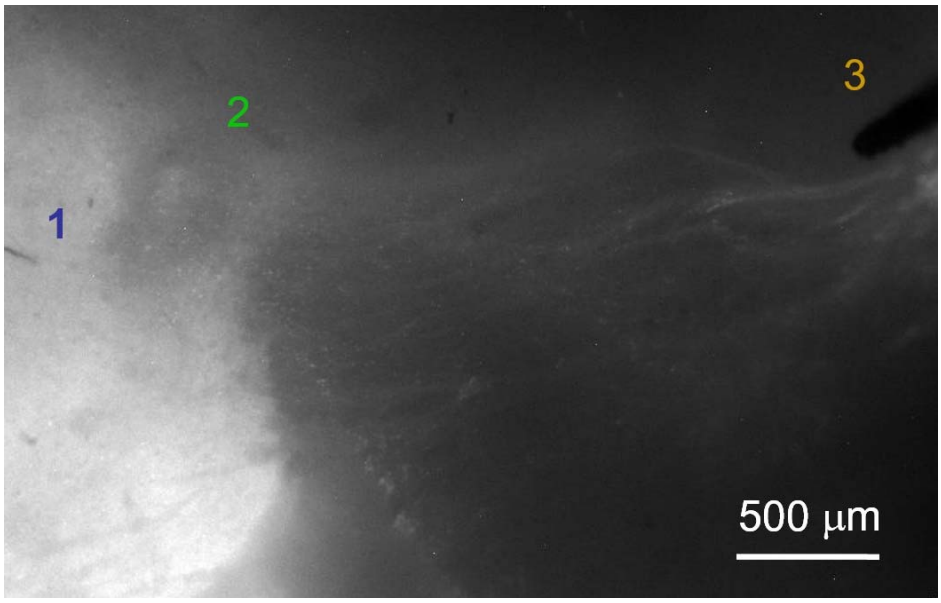

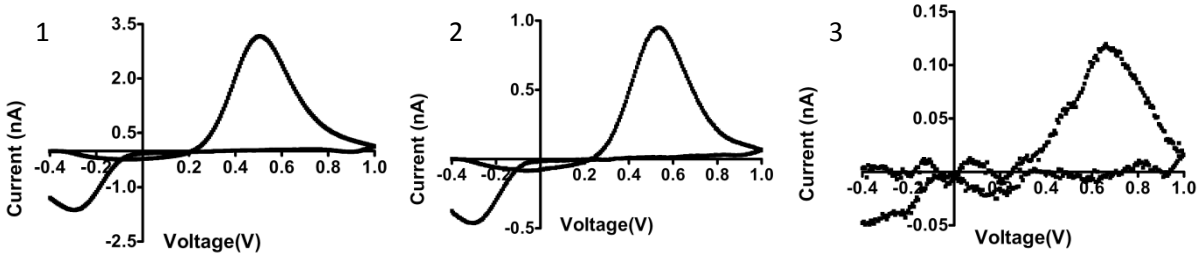

Figure 5.2. Remote stimulation of mesolimbic dopamine neurons. At the top is an epifluorescent image from a horizontal brain slice of a GFP mouse containing the mesolimbic pathway. The numbers indicate the placement of the stimulating electrode and the corresponding cyclic voltammagram measured by the working electrode upon stimulation. A single-pulse stimulation was used at position 1. A 24-pulse 60 Hz stimulation was used at positions 2 and 3 because a single-pulse stimulation did not elicit a detectable signal.

working electrode at which release ceases to be observed would define the outer limits of local stimulation. Coronal slices of the nucleus accumbens (Acb) were used. These slices contain dopamine terminals severed from the rest of the cell. The stimulating electrode is then stepped toward the working electrode at distances determined from CCD images of the slice. The magnitude of stimulated release at each distance is compared in Figure 5.3. Regardless of which stimulation intensity was used, release was not detected when the stimulating electrode was separated from the working electrode by more than 600 μm. All experiments referred to as using remote stimulation utilized an electrode separation greater than 600 μm, usually 800-1000μm.

DβH Distribution Relative to GFP

The relative level of GFP expression throughout many brain regions has been reported previously (Kessler et al., 2003). However, the distribution of interferants is also relevant. Norepinephrine is electrochemically indistinguishable from dopamine, and the microelectrode sensitivity differs between them. Proper electrode placement is important to avoiding a mixed signal. Here, the distribution of dopamine neurons and noradrenergic terminals in coronal and horizontal slices are investigated. Dopamine-β-hydroxylase (DβH) is the enzyme that converts dopamine into norepinephrine. Therefore DβH was used as a marker for noradrenergic neurons. It was previously shown that noradrenergic neurons express very little if any GFP, so GFP is a marker for dopaminergic neurons (Kessler et al., 2003). The anatomical distribution of GFP and DβH were determined immuno-histochemically.

Coronal slices from +1.5 mm to 0.0 mm from bregma were tested. Brain atlas images are shown to the right of the confocal images (Paxinos and Watson, 2007). In the nucleus accumbens (Acb) a DβH signal emerges at approximately 0.70 mm from Bregma

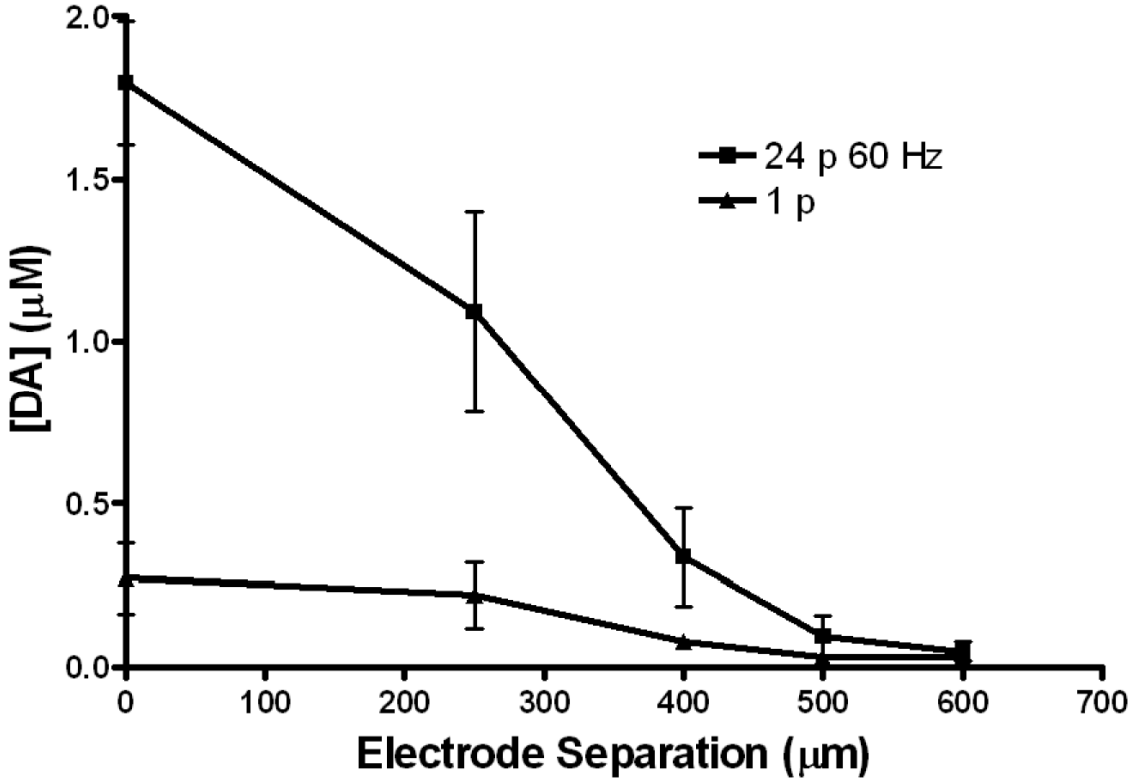

Figure 5.3. Release and Electrode Separation. The peak concentration of dopamine release upon stimulation is measured as a function of the separation between the microelectrode and the stimulating electrode. The measurements are taken in a coronal slice of the Acb. The stimulating electrode was moved as the microelectrode remained stationary. Greater stimulation pulses elicit measurable release from a greater distance, but release drops to zero at an electrode separation of 600 μm.

about the anterior commissure (ac) (Figure 5.4), which is consistent with the known distribution in wild-type mice. The confocal images reveal little overlap in labeling, supporting the conclusion that GFP is not expressed in noradrenergic neurons. Since the signal anterior to 0.70 mm Bregma consists of only GFP labeling the electrochemical signal at these locations should be due to dopamine and not norepinephrine.

Horizontal slices from -6.8 mm to -8.0 mm from dura, a membrane surrounding the brain, were evaluated for the presence of GFP and DβH. The image in Figure 5.5A depicts a horizontal slice containing the mesolimbic pathway (Paxinos and Watson, 2007). The squares indicate the location from which the confocal images were taken. In panel 5.5B, images on the left are taken at a location indicated by box 1 and the images on the right are taken at a location indicated by box 2, which is posterior to box 1. GFP labeling indicates dense GFP expression in the dorsal portions of the slice in the Acb at all depths tested. These images also confirm the presence of axons in these slices, which facilitate remote stimulation. As with the coronal labeling, the DβH signal emerges posterior to a GFP only signal. There is also DβH labeling along the midline of the slice. Therefore, a voltammetric measurement should avoid norepinephrine detection by placing the microelectrode within the anterior Acb and away from the midline. There appears to be greater DβH labeling in the most ventral slices. Therefore, slices used in the subsequent experiments were taken from approximately -6.8 mm to -7.2 mm from dura.

Pharmacology

Placing the microelectrode within the anterior Acb and away from the midline, remotely stimulated catecholamine release is measured. To determine if the release is from dopaminergic neurons, noradrenergic neurons, or both, selective uptake inhibitors desipramine (desi) and GBR-12909 (GBR) were used. If the released substance is

+1.4 mm from bregma

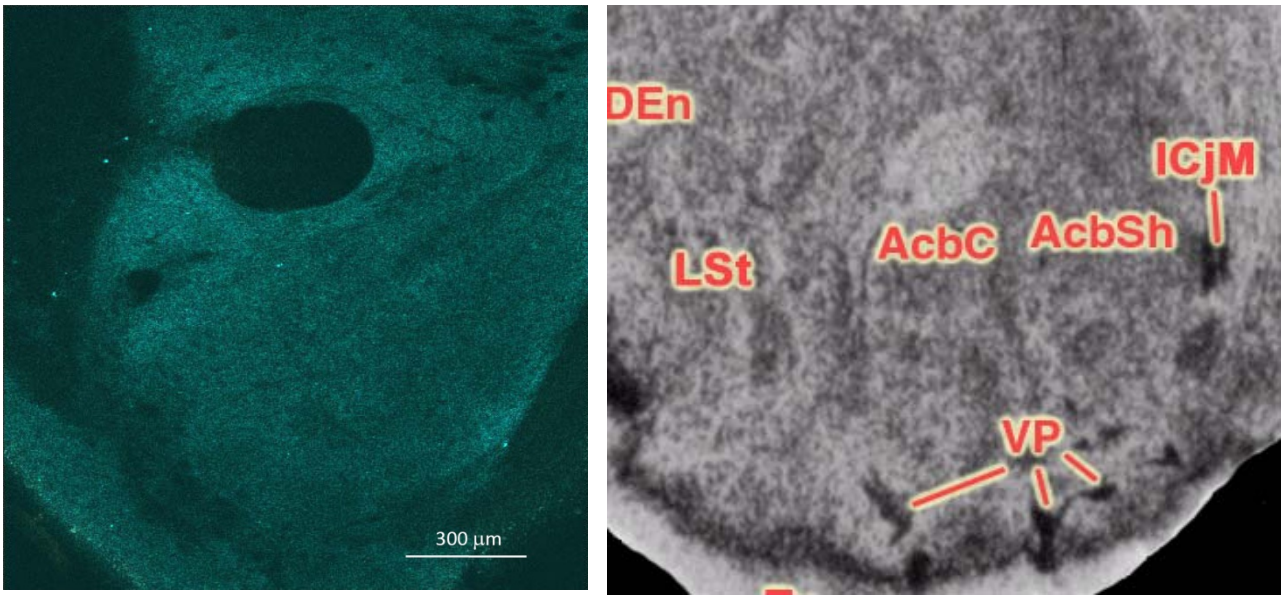

+0.7 mm from bregma

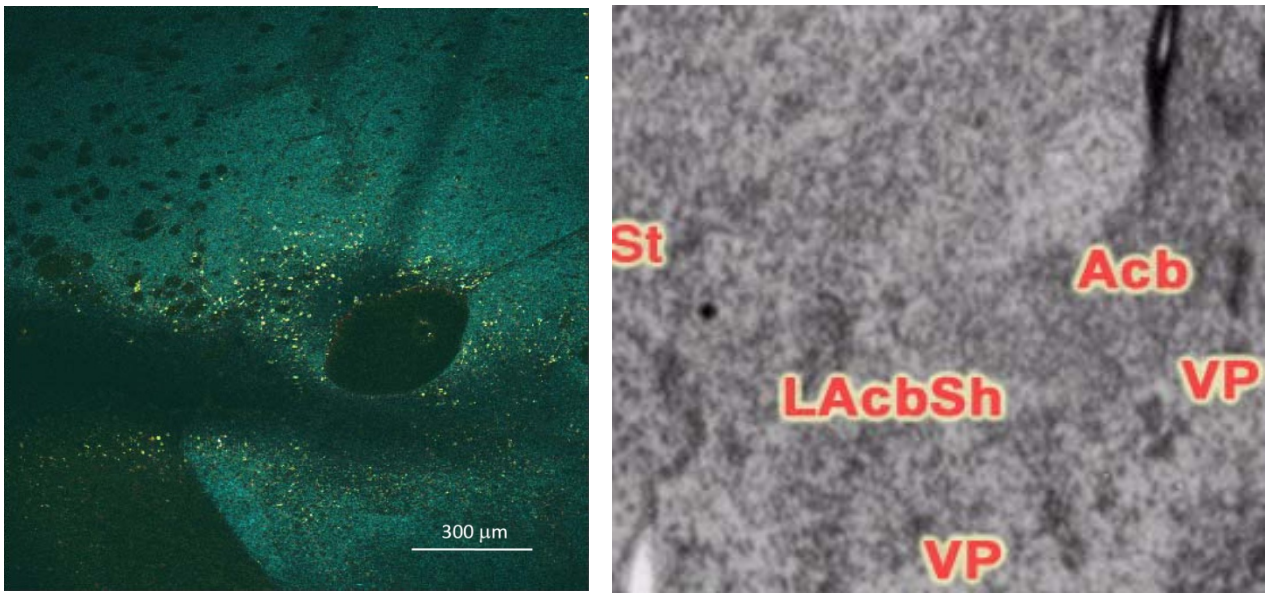

Figure 5.4. Immunohistochemical co-localization of GFP (cyan) and DβH (yellow) in coronal slices of the GFP mouse striatum. The ventral striatum (Acb) is shown at two locations. The NAc labels solely for GFP until about 0.7 mm from bregma. Then the signals are both present from 0.7 mm to 0.0 mm from bregma, the most anterior slice tested. To the right of each image is a representation of the region from the mouse brain atlas (mbl.org).

A

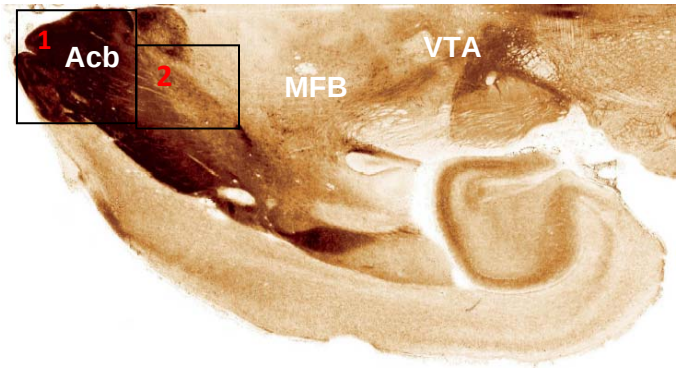

B

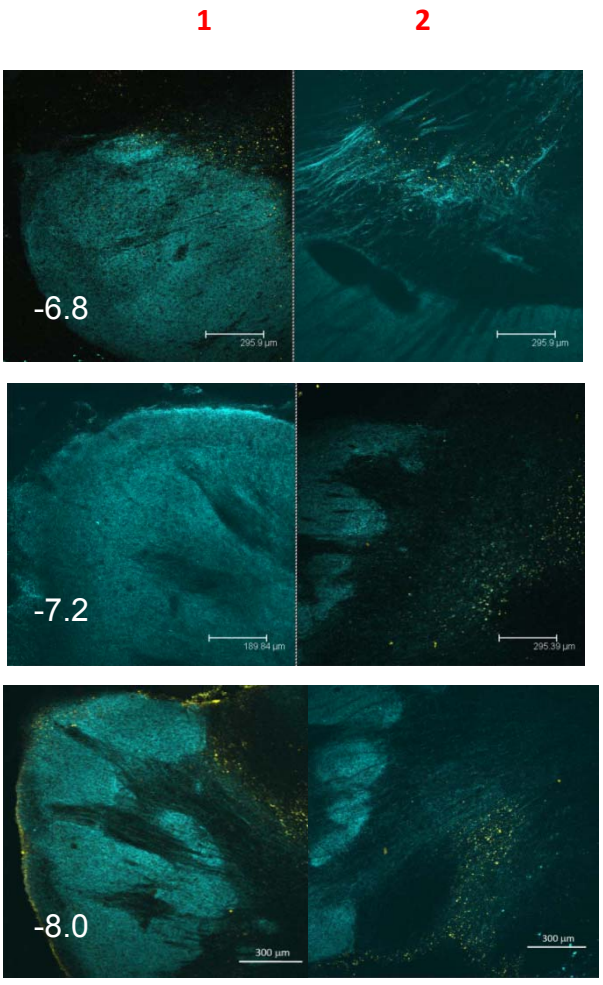

Figure 5.5. Immunohistochemical co-localization of GFP (cyan) and DβH (yellow) in horizontal slices of the GFP mouse striatum. A.) Representative slice taken from the rat brain (Paxinos and Watson, 2007). The two squares indicate the location the confocal images were collected. B.) The images to the left are horizontal slices from square 1 and the images on the right are from square 2. The images in a row are from the same slice of a depth indicated in mm from dura by the white numbers.

norepinephrine, then uptake is controlled by the norepinephrine transporter (NET). If the released substance is dopamine, then uptake is controlled by the dopamine transporter (DAT). Desipramine is a selective uptake inhibitor of NET, and GBR-12909 is a selective uptake inhibitor of DAT. The order these drugs were introduced to the slice was randomized. A 300 nM solution of one of the drugs was added, and after 30 min incubation, two files were collected. Then a 300 nM solution of both drugs was added, and after 30 min incubation, two more files were collected. The change in K_M with the addition of each solution was used to determine the presence of either transporter.

Representative traces are shown in Figure 5.6A where desipramine is added first, then GBR-1209 is added in the presence of desipramine. The rate of uptake is unaffected by desipramine but slowed by GBR-12909. In all slices examined (n = 5), desipramine did not increase K_M (93 $\pm$10% of pre-desipramine files), and GBR-12909 caused a large change in K_M (405 $\pm$108% of pre-GBR files). The change in K_M caused by GBR-12909 is significant relative to change in K_M caused by desipramine ($p > 0.05$). The much greater effect of GBR-12909 indicates that uptake is regulated by DAT in this location in the Acb.

Heterogeneity

Figure 5.7a shows release profiles recorded at different depths above and below the surface of a horizontal slice elicited by single-pulse local stimulation while the stimulating electrode was stationary at the surface of the slice. The surface of the slice was determined visually by lowering the electrode until it appeared to make contact with the slice. This process has about a 10 μm error. The distance the electrode was moved in the z-axis was determined with piezoelectric manipulators with an error of 0.1 μm. Dopamine could be detected from 50 μm above the slice to 200 μm below the surface of the slice where the experiment was

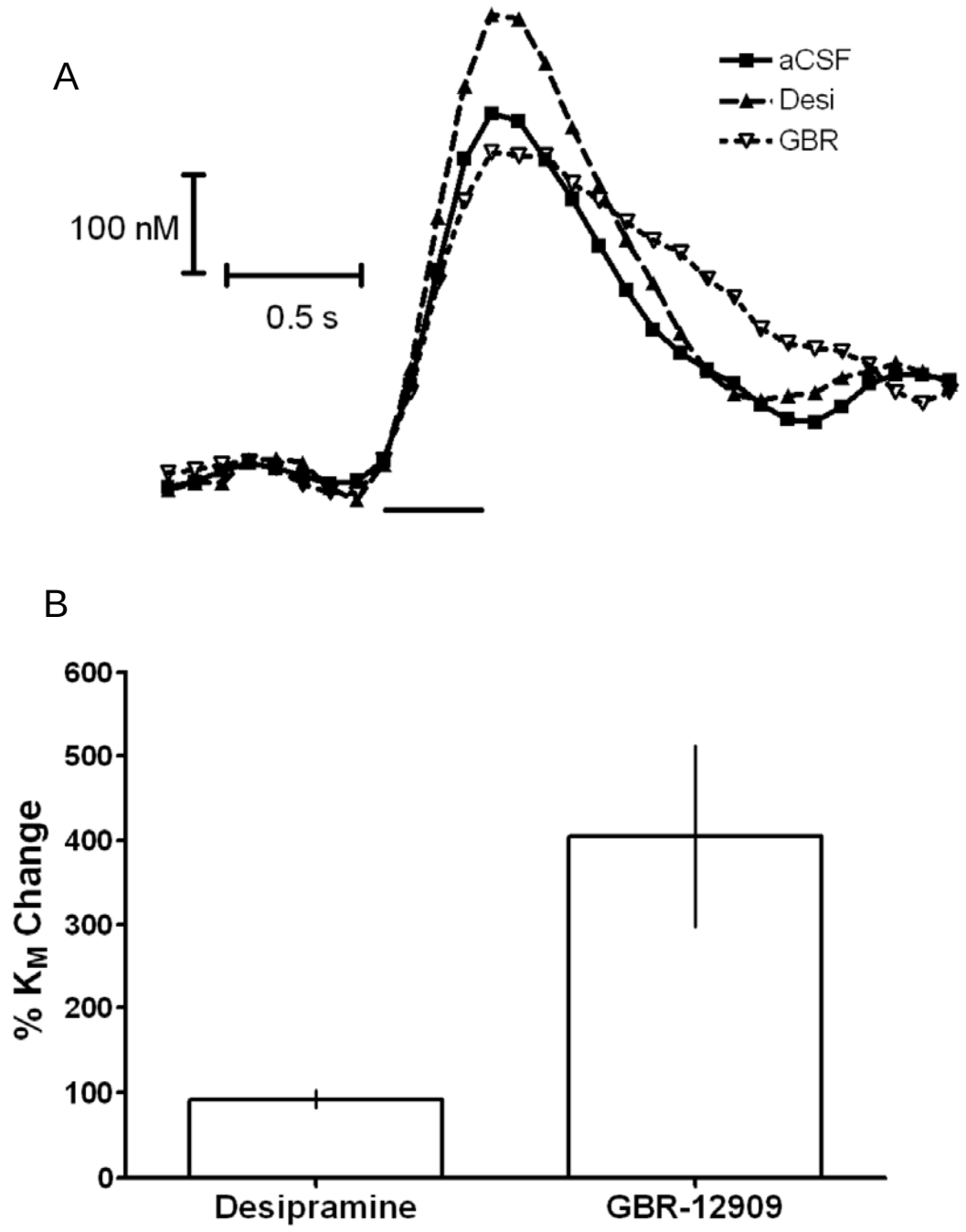

Figure 5.6. Uptake inhibited by GBR-12909(GBR) but not by desipramine (Desi). A.) Representative traces of remotely stimulated release. The bar indicates the duration of stimulation (24-pulse, 60 Hz). Uptake in the control trace (aCSF) and with Desi on board are similar, but uptake is slowed noticeably with the addition of GBR. B.) Uptake was modeled with Michaelis-Menton kinetics. Desi did not cause a significant change (93 $\pm$10% of pre-desipramine) in uptake, but GBR-12909 caused a large shift (405 $\pm$108 % of pre-GBR). The difference in K_M shift due to drug is significantly different between desi and gbr ($p < 0.05$, $n = 5$).

terminated. The concentration of dopamine release increases with the lowering of the electrode until a depth of 50 μm. The latency between the stimulation and the peak of release is an indication of the average distance from the release sites to the surface of the electrode (Venton et al., 2003). This latency is much longer above the slice where dopamine is diffusing from release sites in the slice. The latency decreases as the electrode is lowered into the slice. The latency increases again starting at a depth around 150 μm, indicating the release sites are increasingly further from the electrode.

Unlike local stimulation, remote stimulation elicits little to no dopamine release at or above the surface of the slice. The example traces shown in Figure 5.7b reveal a small range of depths where dopamine release is detected in this slice and the concentration is dramatically higher at a 150 μm depth than any other. While local stimulation presumably excites most of the terminals near the stimulating electrode, remote stimulation should only excite the terminals connected to axons near the stimulating electrode, thus confining the volume in which release can be measured.

Four slices from four different animals were used to probe the heterogeneity of dopamine release at different sampling depths (Figure 5.8). The separate samples are shown to avoid masking the heterogeneity by averaging. Release increases then decreases with sampling depth for samples 1 and 4. In samples 2 and 3, release increases with depth. A depth may have not been reached where the release would decrease again as with the other samples.

Lateral heterogeneity was also investigated with remote stimulation. The working electrode is moved along the medial-lateral axis relative to a starting location where remotely stimulated release is observed. Again, release was sampled at a depth of 60-70

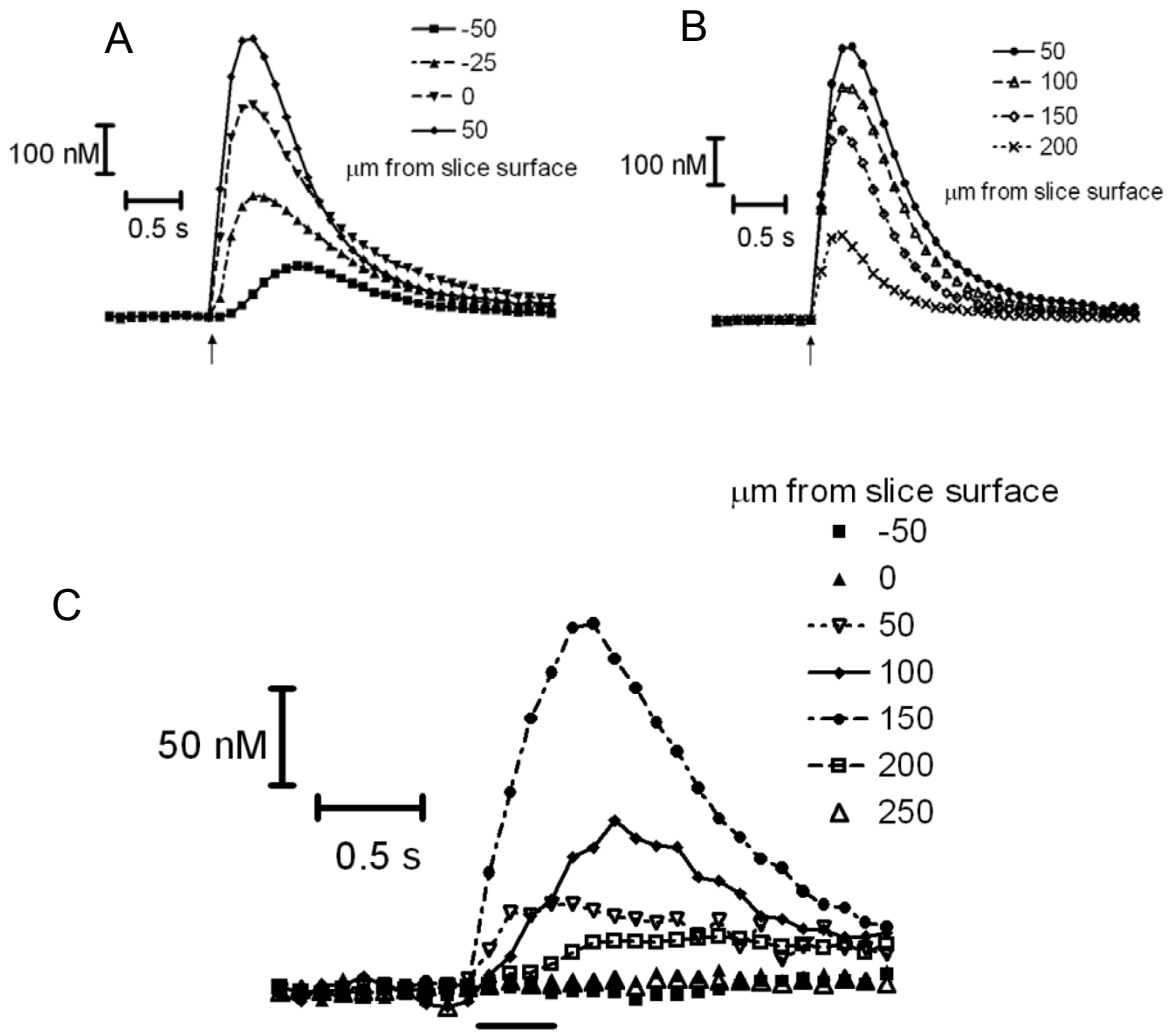

Figure 5.7. Depth profile with local and remote stimulation. Recordings of dopamine release at different depths above (negative values) and within (positive values) a coronal slice of the Acb. A.) Release elicited by single-pulse local stimulation, delivered at the arrow. B.) Release elicited by a 24-pulse, 60 Hz stimulation occurring over the time indicated by the line under the trace. Release occurs over a narrow depth window well below the depths where the maximal release is measured with local stimulation.

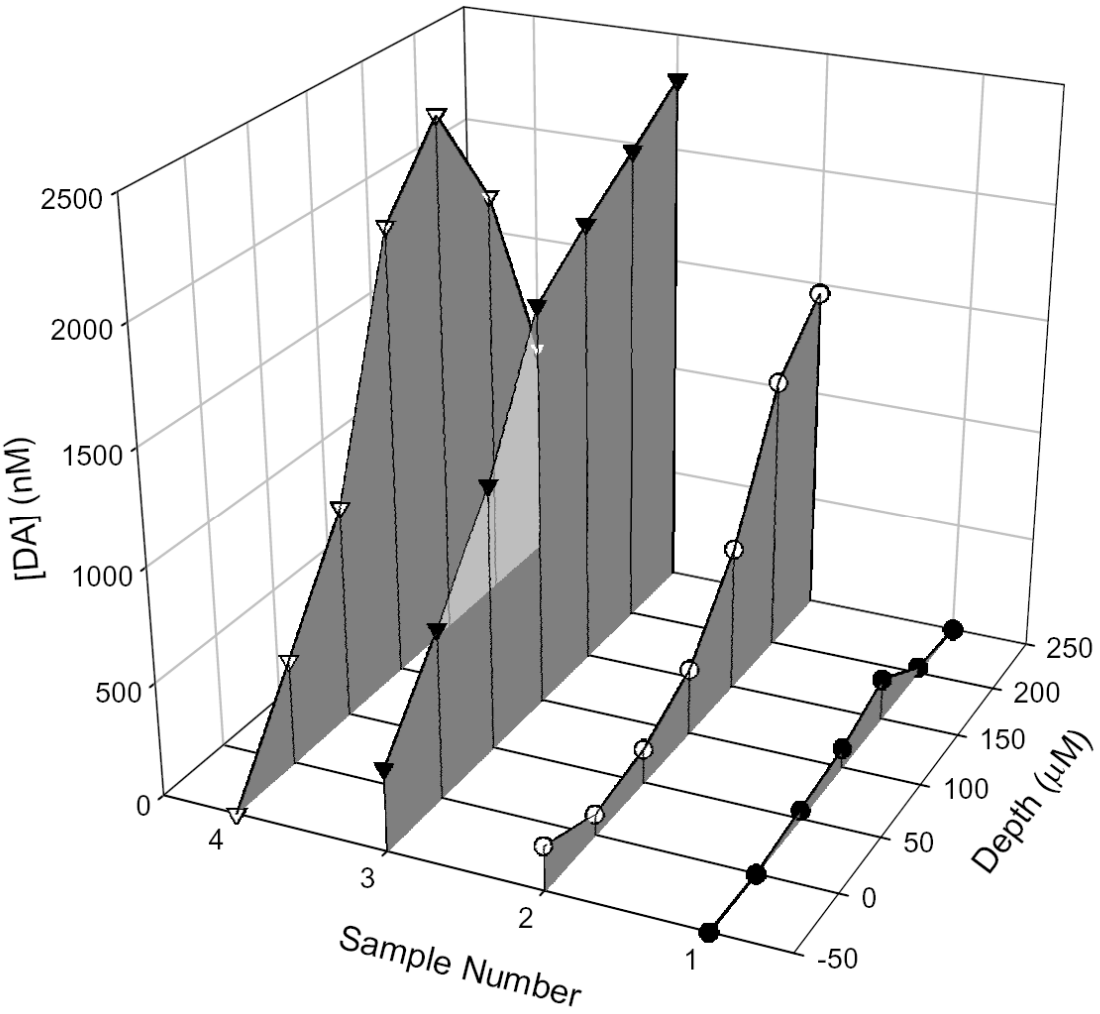

Figure 5.8. Release depth profile with remote stimulation. The extracellular concentration of dopamine release elicited by a 24-pulse, 60 Hz remote stimulation at different depths within four different brain slices from four animals. The depth is relative to the surface of the slice (0 μm). The negative depth is above the slice. The electrode is traversing ventral to dorsal as it is lowered through the tissue. Release is heterogeneous within the Acb. This provides additional evidence that the release is indeed due to remote stimulation since the greatest release is measured at greater than 100 μm below the surface of the slice.

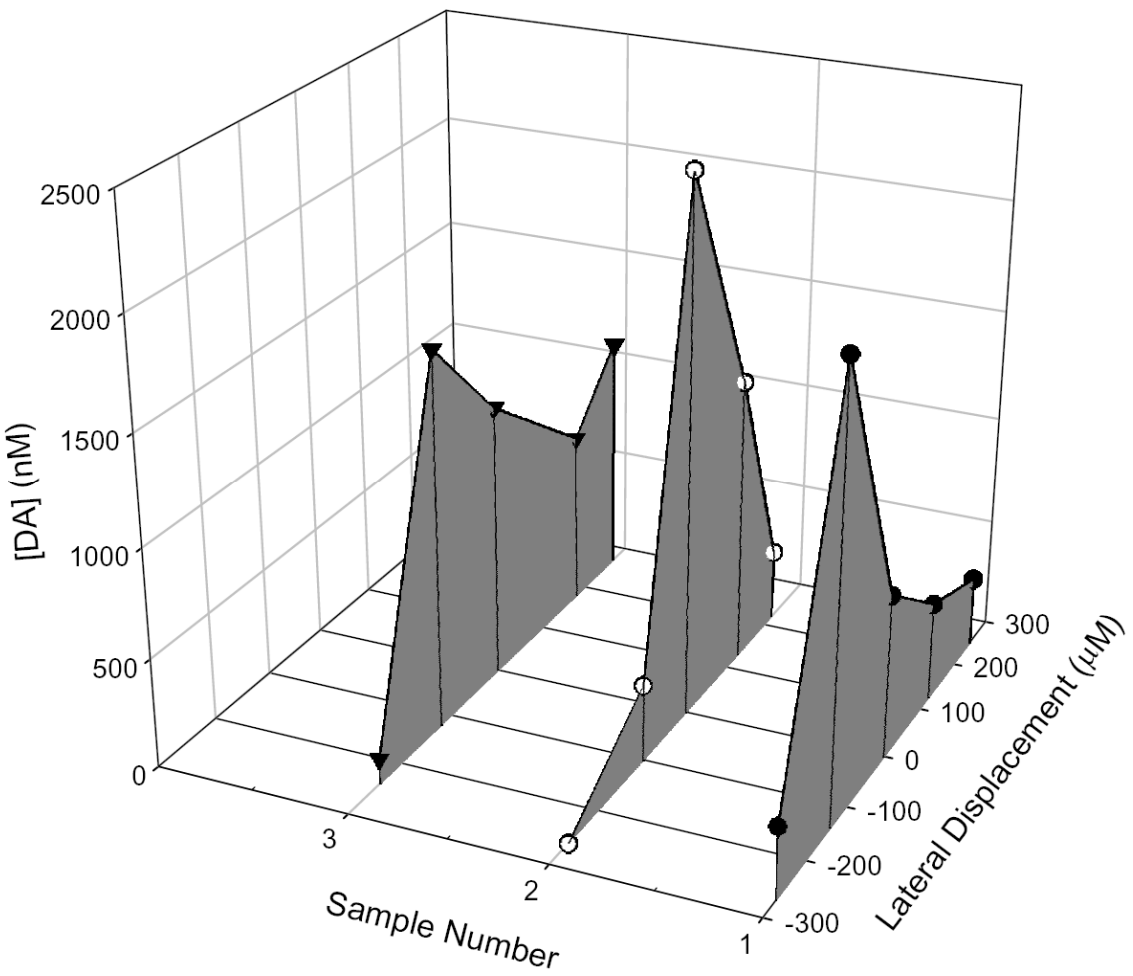

Figure 5.9. Lateral heterogeneity of release with remote stimulation. The extracellular concentration of dopamine release elicited by a 24-pulse, 60 Hz remote stimulation at different recording locations along a medial-lateral axis at a depth of 60-70 μm within three different brain slices from three animals. Lateral displacement is relative to consistent starting location about the center of the Acb (0 μm). Displacement is measured lateral (negative) to medial (positive) from CCD images of the slice. Release is heterogeneous within the Acb, and the distribution is skewed medial, similar to the direction of the pathway.

stimulating electrode. However, with remote stimulation the differences in release are due to differences in the terminal density of neurons whose axons are being stimulated. Figure 5.9 displays the measured release in three samples as the electrode surveys release sites μm below the surface of the brain slice. With local stimulation, release varies with distance from the medial (towards the midline) and lateral (away from midline) from a starting site. Efforts were made to start the survey in a similar location between brain slices. In all samples there appears to be an optimal location where the greatest release can be measured.

Stimulation Parameters

Figure 5.10A includes representative traces of release due to remote stimulation using a 10 Hz, 20-pulse stimulation and a 30 Hz, 20-pulse stimulation. Figure 5.10B includes representative traces of release due to local stimulation using the same parameters. There is a much greater difference in release magnitude between the two stimulation frequencies in the case of remote stimulation. In fact, there is little change in release with stimulation frequency across animals when using local stimulation (Figure 5.10C, slope = 0.009 $\pm$0.002) indicating that release is maximal even with a 10 Hz stimulation. The change in release with stimulation frequency is significantly different between local and remote stimulation ($p > 0.002$, $n = 4$). The relationship between stimulation frequency and dopamine release is linear *in vivo* (Wightman et al., 1988) and with remote stimulation (Figure 5.10C, $r^2 = 0.967$).

The change in release with pulse number is significantly less with local stimulation than remote stimulation ($p > 0.01$, $n = 5$). Figure 5.11A and 5.11B displays representative traces of release due to remote stimulation and local stimulation, respectively, using 60 Hz stimulations of the pulse numbers indicated. The change in

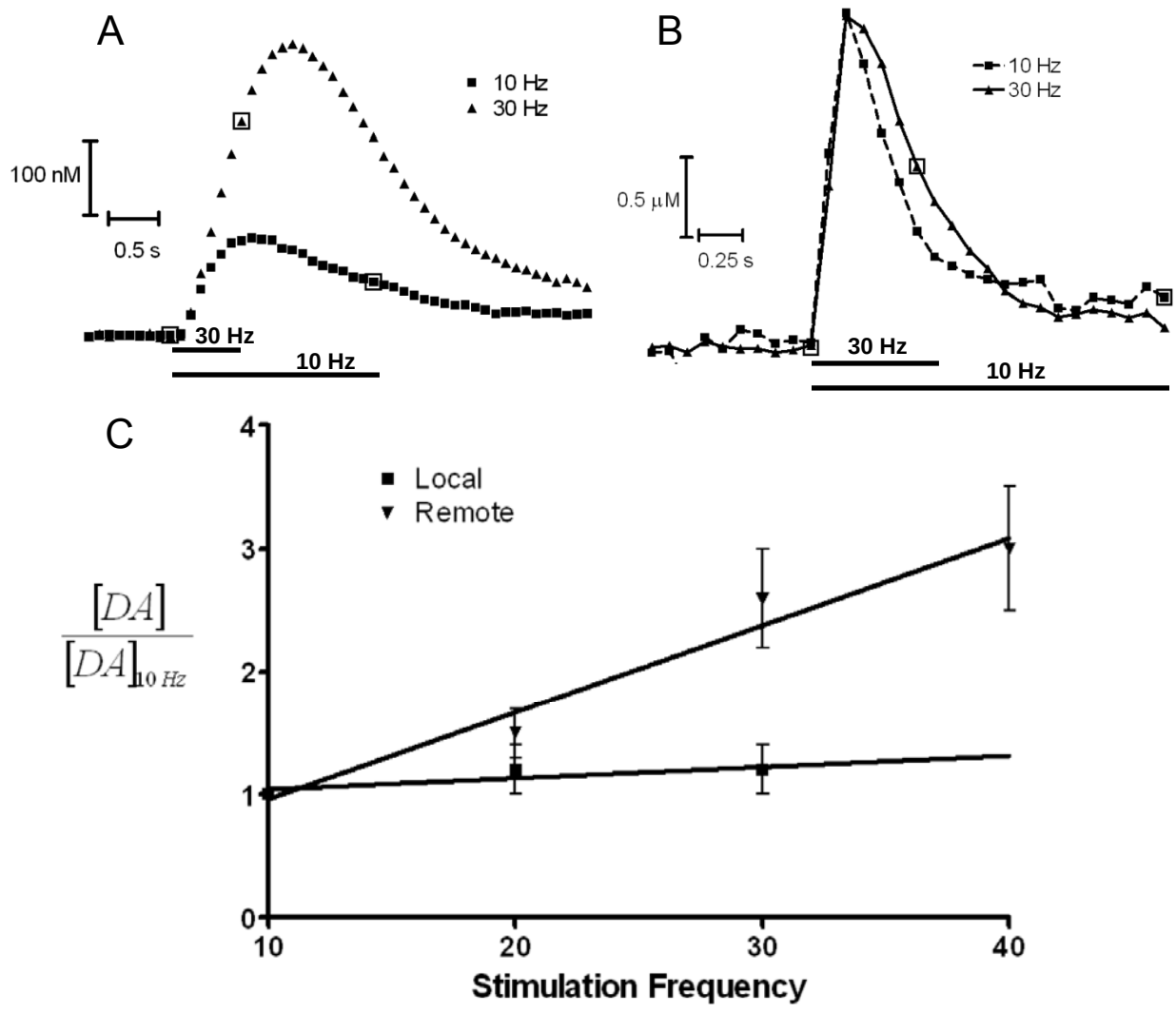

Figure 5.10. The effect of stimulation frequency on dopamine release. A.) Remotely stimulated dopamine release at 10 Hz and 30 Hz. The stimulation duration is indicated by the empty squares and the bar below the traces. B.) Local stimulation of dopamine release at the same frequencies, indicated by the empty squares. Stimulation frequency has little effect with local stimulation. C.) The peak concentration of dopamine release relative to that released with a 10 Hz stimulation. All stimulations are 20-pulse. The slope of the linear regressions are as follows: Local stimulation (0.009 $\pm$0.002), Remote stimulation (0.071 $\pm$0.009). The statistical difference is significant, as determined by an ANCOVA ($p > 0.002$).

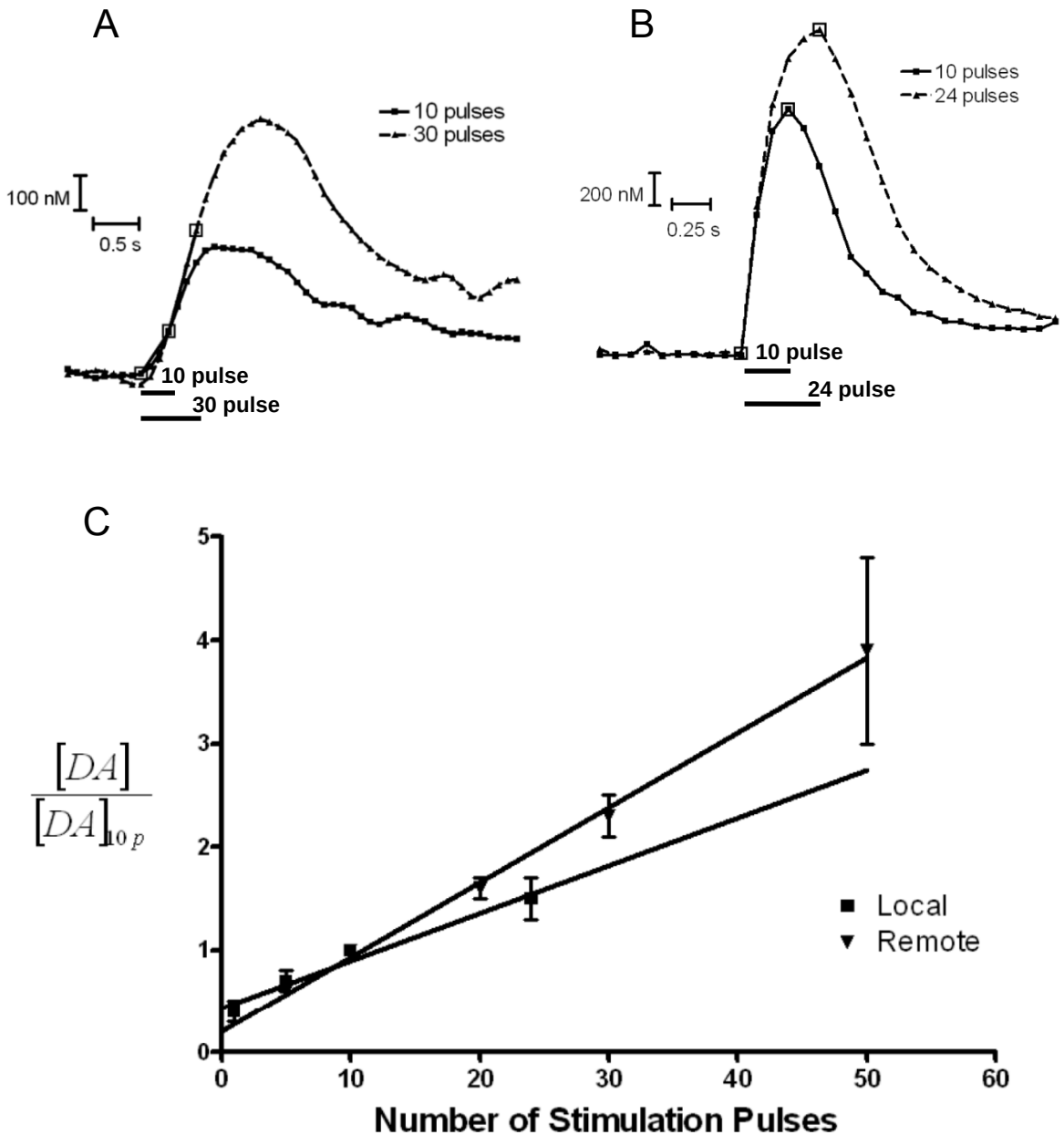

Figure 5.11. The effect of stimulation pulse number on dopamine release. A.) Remotely stimulated dopamine release with 10-pulses and 30-pulses. The stimulation duration is indicated by the empty squares and the bar below the traces. B.) Local stimulation of dopamine release at the same pulse numbers, indicated by the empty squares. Stimulation pulse number as less effect with local stimulation. C.) The peak concentration of dopamine release relative to that released with a 10-pulse stimulation. All stimulations are at 60 Hz. The slope of the linear regressions are as follows: Local stimulation (0.046 $\pm$0.006), Remote stimulation (0.073 $\pm$0.002). The statistical difference is significant, as determined by an ANCOVA ($p > 0.01$).

dopamine release with stimulation pulse number is greater with remote stimulation (Figure 5.11C, slope = 0.073 ±0.002) than with local stimulation (Figure 5.11C, slope = 0.046 ±0.006).

Dopamine Release Dynamics

A stimulation protocol of a 24-pulse, 60 Hz stimulation delivered every two seconds for five stimulation events was used to probe short-term dopamine release dynamics. When this stimulation protocol is used *in vivo*, facilitation of release is observed (Montague et al., 2004). Facilitation of release is an increase in dopamine release with subsequent stimulations thought to be due to desensitization of D_2-autoreceptors (Kita et al., 2007). Under normal buffer conditions, including 2.4 mM calcium, a constant decrease in release is observed with each stimulation in the brain slice (Figure 5.12A). Providing tonic D_2-autoreceptor activation with 25 nM quinpirole attenuates how rapidly dopamine release decreases. When the concentration of calcium in the buffer is reduced to 1.2 mM, the concentration of dopamine release decreases and the size of the peaks are more similar (as measured from valley to peak about the stimulation, Figure 5.12B). When 25 nM quinpirole is added to this low calcium buffer, the peak concentration of dopamine release increases with each stimulation event until the fourth and fifth stimulation. Therefore, a reduction in the buffer calcium concentration and the addition of quinpirole are necessary to achieve facilitation with remote stimulation in this horizontal brain slice. Although obtained only once, this illustrates that changes in traditional brain slice methods are necessary for dopamine release dynamics to be studied in a physiologically relevant manner.

Discussion

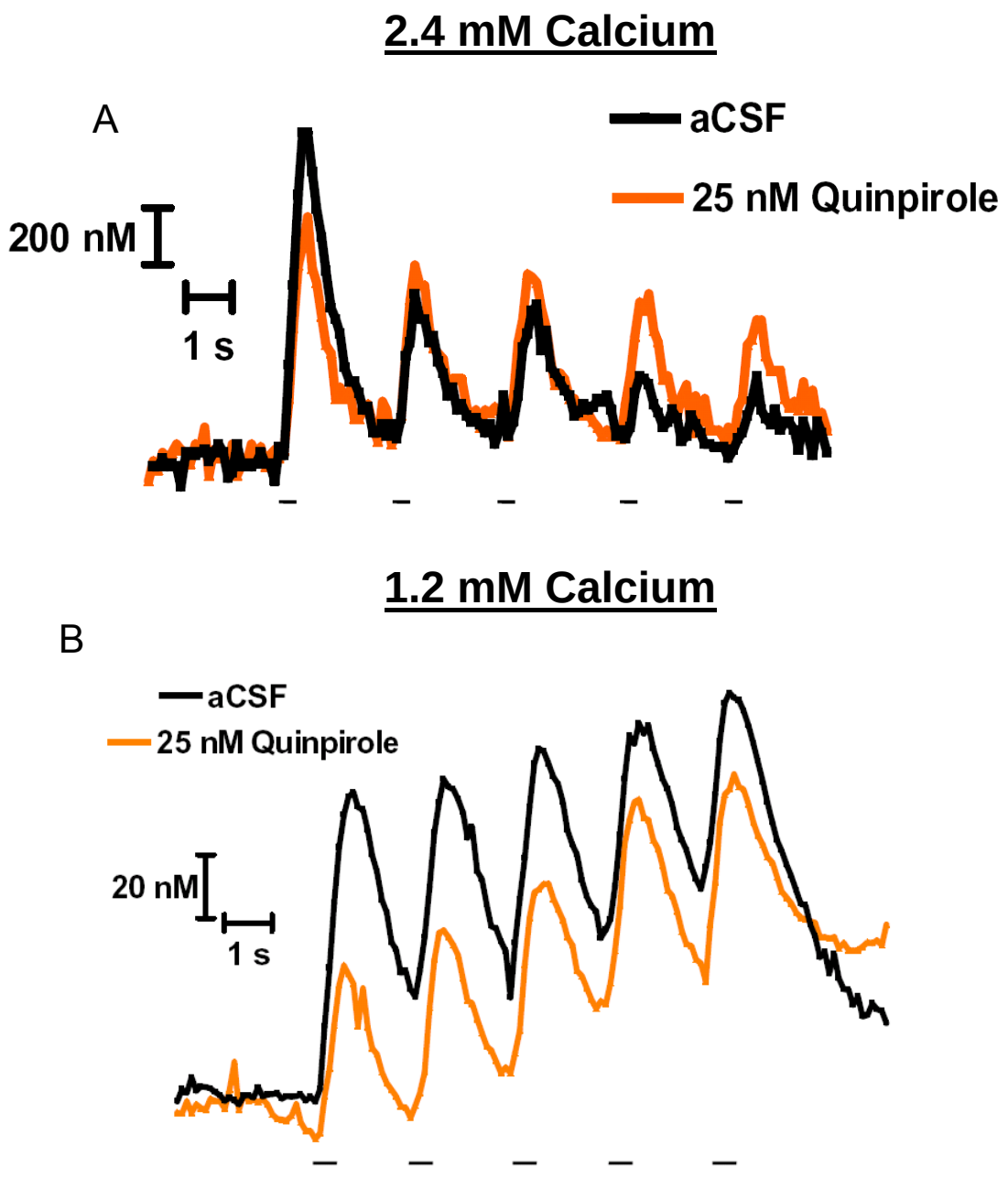

Figure 5.12. Short-term dopamine release dynamics with remote stimulation in different calcium conditions. 24-pulse, 60 Hz stimulations delivered every 2 s as indicated by the bars under the traces. A.) Recording of dopamine release due to stimulation protocol under standard buffer conditions (2.4 mM calcium) and with the addition of 25 nM quinpirole. B.) Recording from the same slice with the same stimulations, now under a low calcium conditions (1.2 mM) and with the addition of 25 nM quinpirole. Not only do these release profiles change dramatically with differenct calcium conditions, but also the facilitated release in B resembles the release profile *in vivo* under the same stimulation conditions.

The intrinsic fluorescence of dopaminergic neurons in GFP transgenic mice facilitates the placement of electrodes in brain slices. This feature makes it possible to use remote stimulation in horizontal brain slices. The use of remote stimulation to selectively excite dopamine neurons overcomes limitations in traditional brain slice experiments and expands the available experimental options. Among these options is the ability to examine dopamine release dynamics in a manner consistent with *in vivo* protocols.

While electrodes can simply be placed on fluorescent objects in the slice to elicit measurable catecholamine release, several criterion must be satisfied to ensure the selective stimulation of dopaminergic neurons. The first criterion is to ensure that release is elicited by stimulating axons and not terminals local to the microelectrode. To avoid the release of neuroactive substances from cells adjacent to dopamine terminals, the stimulating electrode must be separated a sufficient distance from the microelectrode to eliminate a stimulated response from the terminals. An electrode separation of at least 600 μm is sufficient to avoid stimulating dopamine terminals local to the microelectrode and by extension avoids the stimulation of other terminals and cell bodies in close proximity. A second criterion is to measure release selectively from dopaminergic neurons and not other neurons that release electroactive substances. Many cell types have projections that traverse the MFB. Therefore, stimulating axons in the MFB provides little selectively. Selectivity is provided by placing the microelectrode in locations where dopamine neurons terminate and other cell types projecting from the MFB do not. The primary interferent from neurons known to traverse the MFB is norepinephrine. Noradrenergic neurons might be expected to express GFP since TH is expressed in those cells; however noradrenergic cells simply do not fluoresce or fluoresce so weakly as to be undetectable (Kessler et al., 2003). This was confirmed by the immunohistochemical results of this work. The lack of GFP expression in noradrenergic neurons may be due to where the transgene was inserted in the

chromosome. For example, the transgene could be in the proximity of a cis regulatory unit, a segment of DNA that plays a role in determining the temporal and spatial domains of gene expression (Zheng et al., 2003). The immunohistochemical results provide clear evidence of locations where dopaminergic neurons traversing the MFB terminate in regions free of noradrenergic terminals. To confirm that these regions are free of noradrenergic terminals, NET uptake inhibitors were used. It has been previously reported that desipramine has little effect on uptake in the nucleus accumbens and that the action of DAT provides uptake (Jones et al., 1995). Since desipramine failed to change the rate of uptake but GBR-12909 did, one can safely assume that the microelectrode was placed in locations where release is dominated by dopamine.

Release in brain slices using local stimulation has been reported to respond differently to changes in stimulation parameters, such as pulse number and frequency, than release measured *in vivo* when stimulating the MFB (Kennedy et al., 1992a). Since the MFB is being stimulated in these brain slice experiments, it may make the changes in release with changes in stimulation pulse number and frequency more similar to that observed *in vivo*. While important differences still exist in the brain slice environment compared to the intact brain, the use of remote stimulation has altered the dopamine response in brain slices to these stimulation manipulations. One reason may be a reduction in the number of terminals responding to the stimulation. The concentrations of released dopamine are much lower with remote stimulation than local stimulation, presumably because fewer terminals are releasing dopamine. The smaller magnitude responses with remote stimulation may allow the terminals to act within their dynamic range.

The small diameter of the microelectrode provides the spatial resolution necessary to probe the heterogeneity of release sites within a brain slice. Investigating this heterogeneity is more challenging with local stimulation since the magnitude of release is dependent on

the separation of the microelectrode from the stimulating electrode (Figure 5.3). This can also be seen in Figure 5.9a, where the magnitude and temporal profile change with the lowering of the electrode into and through the brain slice. These changes in the signal underscore the impact of the distance between the microelectrode and the release sites.

Several factors will impact the distance to sampled release sites. First, the top layers of the brain slice are considered dysfunctional due to the cell damage from slicing. Second, there has been shown to be an oxygen gradient through the slice (Kennedy et al., 1992b). This may be due to cells closer to the surface of the slice consuming oxygen from the buffer for respiration. This would suggest that terminals at the lowest layers of the slice may not be releasing normally. Third, the permeation of the stimulation pulse may limit the depth at which release is elicited. Fourth, extracellular dopamine is quickly cleared by a high-affinity uptake system that will limit the distance released dopamine can diffuse. These factors are relevant during remote stimulation. The axons being stimulated presumably arborize into terminal fields from which the release is sampled. Therefore detected release would be constrained to recording sites within a limited proximity to those terminal fields being stimulated via connected axons.

Due to the way the slices were mounted in the slice chamber, the ventral surface of the horizontal slice is the surface identified at 0 μm depth. As the electrode is lowered in the tissue, it is traversing from ventral regions of the brain in a dorsal direction towards the top of the brain. The differences between samples in the depth at which the greatest release is measured may be attributable to the reproducibility of harvesting a brain slice from exactly the same location in the brain. The mesolimbic pathway is known to curve from ventral to dorsal as it approaches the Acb. Some researchers tilt the brain when taking a horizontal slice to incorporate a greater number of whole neurons (Chuhma et al., 2004). This bias would explain why release is larger in more dorsal recording sites. Lateral heterogeneity is

also consistent with the known anatomy. The distribution of release sites has a positive skew, meaning there are more release sites in a medial direction. This corresponds with the direction of the pathway, as can be seen in the atlas image in Figure 5.5.

There are a number of experiments that can now be attempted with the establishment of a remote stimulation protocol. One can now explore poorly understood pathways such as the tuberoinfundibular pathway which consists of dopamine neurons in the hypothalamus that project to the pituatary gland. Additionally, one can use sagittal slices to encompass the nigrostriatal pathway that curves dramatically dorsal from the substantia nigra (SN, posterior to the VTA) to the caudate putamen (CP) (Figure 5.1). Additionally, dopamine release dynamics can be probed. The stimulation pulse number and frequency experiments show that the dopamine neurons respond differently to the same stimulations when stimulated remotely. Investigating facilitation is just one factor that contributes to release dynamics and only the proof of concept has been illustrated here (Figure 5.12). These processes should be investigated more fully. *In vitro* experiments, such as in brain slices, allow more control to elucidate the underlying mechanisms.

References

Chuhma N, Zhang H, Masson J, Zhuang X, Sulzer D, Hen R, Rayport S (2004) Dopamine neurons mediate a fast excitatory signal via their glutamatergic synapses. J Neurosci 24:972-981.

Di Chiara G, Imperato A (1988) Drugs abused by humans preferentially increase synaptic dopamine concentrations in the mesolimbic system of freely moving rats. Proc Natl Acad Sci U S A 85:5274-5278.

Jones SR, Garris PA, Kilts CD, Wightman RM (1995) Comparison of dopamine uptake in the basolateral amygdaloid nucleus, caudate-putamen, and nucleus accumbens of the rat. J Neurochem 64:2581-2589.

Kawagoe KT, Zimmerman JB, Wightman RM (1993) Principles of voltammetry and microelectrode surface states. J Neurosci Methods 48:225-240.

Kawagoe KT, Garris PA, Wiedemann DJ, Wightman RM (1992) Regulation of transient dopamine concentration gradients in the microenvironment surrounding nerve terminals in the rat striatum. Neuroscience 51:55-64.

Kennedy RT, Jones SR, Wightman RM (1992a) Dynamic observation of dopamine autoreceptor effects in rat striatal slices. J Neurochem 59:449-455.

Kennedy RT, Jones SR, Wightman RM (1992b) Simultaneous measurement of oxygen and dopamine: coupling of oxygen consumption and neurotransmission. Neuroscience 47:603-612.

Kessler MA, Yang M, Gollomp KL, Jin H, Iacovitti L (2003) The human tyrosine hydroxylase gene promoter. Brain Res Mol Brain Res 112:8-23.

Kita JM, Parker LE, Phillips PE, Garris PA, Wightman RM (2007) Paradoxical modulation of short-term facilitation of dopamine release by dopamine autoreceptors. J Neurochem 102:1115-1124.

Matthews C, Holde Kv (1996) In: Biochemistry, 2nd Edition (Benjamin/Cummings, ed), p 1158. Menlo Park, CA: .

Mirenowicz J, Schultz W (1996) Preferential activation of midbrain dopamine neurons by appetitive rather than aversive stimuli. Nature 379:449-451.

Montague PR, McClure SM, Baldwin PR, Phillips PE, Budygin EA, Stuber GD, Kilpatrick MR, Wightman RM (2004) Dynamic gain control of dopamine delivery in freely moving animals. J Neurosci 24:1754-1759.

Paxinos G, Franklin KBJ (2004) The mouse brain in stereotaxic coordinates, Compact 2nd Edition. Amsterdam ; Boston: Elsevier Academic Press.

Paxinos G, Watson C (2007) The rat brain in stereotaxic coordinates, 6th Edition. Amsterdam ; Boston: Elsevier Academic Press.

Schultz W, Dayan P, Montague PR (1997) A neural substrate of prediction and reward. Science 275:1593-1599.

Venton BJ, Zhang H, Garris PA, Phillips PE, Sulzer D, Wightman RM (2003) Real-time decoding of dopamine concentration changes in the caudate-putamen during tonic and phasic firing. J Neurochem 87:1284-1295.

Wightman RM, Robinson DL (2002) Transient changes in mesolimbic dopamine and their association with 'reward'. J Neurochem 82:721-735.

Wightman RM, Amatore C, Engstrom RC, Hale PD, Kristensen EW, Kuhr WG, May LJ (1988) Real-time characterization of dopamine overflow and uptake in the rat striatum. Neuroscience 25:513-523.

Wise RA (2004) Dopamine, learning and motivation. Nat Rev Neurosci 5:483-494.

Wu Q, Reith ME, Wightman RM, Kawagoe KT, Garris PA (2001) Determination of release and uptake parameters from electrically evoked dopamine dynamics measured by real-time voltammetry. J Neurosci Methods 112:119-133.

Zheng J, Wu J, Sun Z (2003) An approach to identify over-represented cis-elements in related sequences. Nucleic Acids Res 31:1995-2005.

Chapter 6

Dopamine and Serotonin Measurement in Mixed Samples

Introduction

Fast-scan cyclic voltammetry (FSCV) with carbon-fiber microelectrodes is a sensitive technique for the detection of serotonin and dopamine. It also provides the spatial and temporal resolution necessary for measuring rapid changes in extracellular concentrations within mouse brain slices (Jones et al., 1999). In this work, a method for determining serotonin and dopamine concentrations in a mixed solution and in various brain regions are discussed.

Serotonin is an important neuromodulator found throughout the brain. It has been widely studied for its role in depression (Lemberger et al., 1985) and the sleep-wake cycle (Medanic and Gillette, 1992). It also has been shown to overlap widely with the distribution of dopaminergic neurons (Lavoie and Parent, 1990; Corvaja et al., 1993; Moukhles et al., 1997) and these systems have been shown to interact (Hery et al., 1980; Nedergaard et al., 1988; Trent and Tepper, 1991; Cobb and Abercrombie, 2003). The ventral tegmental area (VTA) and substantia nigra compacta (SNc) are regions containing dopaminergic cell bodies. The VTA sends out the primary projections of the mesolimbic pathway involved in reward based learning (Schultz et al., 1997) and drug addiction (Di Chiara and Imperato, 1988; Wise, 2004). Moreover, serotonin reduces dopaminergic cell firing in the VTA (Liu et al., 2003). The SNc is part of the nigrostriatal dopamine pathway that is involved in motor movement (Bradbury et al., 1985; Missale et al., 1998; Sealfon,

2000) and Parkinson's disease (Bjorklund and Lindvall, 1984), yet serotonin is the primary neuromodulator present in the region (Bunin et al., 1998).

The mesolimbic dopamine pathway has been linked to the red nucleus (RN) (Bosler et al., 1983) and the interstitial medial longitudinal fasciculus (iMLF), a thalamic region (Toonen et al., 1998). The role of serotonin and dopamine in these regions has been little study, but the function of these regions indicates a role. The RN is involved in the sleep-wake cycle (Licata et al., 2001), a process known to involve serotonin, and the iMLF has been implicated in Parkinson's disease (Racette et al., 2004), which involves the loss of dopaminergic neurons.

Electrochemical measurements and immunohistochemical labeling have been conducted to determine the relative levels of serotonin and dopamine in the VTA, SNc, RN, and iMLF (anatomical locations1 shown in Figure 6.3). Since these regions are present in the same coronal brain slice, they can be probed within the same preparation. GFP transgenic mice express green fluorescent protein (GFP) in their dopaminergic neurons (Kessler et al., 2003). These mice are used because their dopaminergic cells can be easily identified. Their intrinsic fluorescence aides in electrode placement for small, sparsely innervated regions, such as the iMLF, and for finding the RN, a non-dopaminergic region, that is adjacent to fluorescent regions.

Materials and Methods

Chemicals

Bupropion hydrochloride and Citalopram hydrobromide were obtained from Sigma-Aldrich (St Louis, MO, USA). 10 mM stock solutions were prepared by dissolving the appropriate weight of drug into a known volume of deionized water.

Animals

Animals were handled in accordance with protocols approved by the Institutional Animal Care and Use Committee of the University of North Carolina. A transgenic mouse line in which catecholamine containing cells express the gene for the enhanced green fluorescent protein was used (Kessler et al., 2003). Male Sprague-Dawley rats (225-350g; Charles River, Wilmington, MA, USA) were also used. Upon receipt, mice and rats were housed at the University of North Carolina Animal Husbandry Facility in Kerr Hall. Mice and rats were provided food and water ad libitum and were kept under conditions of controlled temperature, humidity, and a 12-h light/dark cycle.

Brain slices

Mice were deeply anesthetized by ether inhalation and decapitated. The brain was immediately removed and placed in ice-cold aCSF. The aCSF solution consisted of (in mM): NaCl 126, KCl 2.5, NaH_2PO_4 1.2, $CaCl_2$ 2.4, $MgCl_2$ 1.2, $NaHCO_3$ 25, HEPES 20, D-glucose 11. The pH was adjusted to 7.4 with 5 M NaOH and the buffer was continuously saturated with 95% O_2/5% CO_2. The cerebellum was sliced off with a razor blade and the brain was mounted on a Teflon block using Krazy Glue ®. Brain slices were made using an NVSL vibratome (World Precision Instruments, Sarasota, FL, USA). Coronal slices containing the midbrain were made 300-μm thick, obtained at -2.8 to -3.3 mm from bregma. For immunohistochemistry, the brain slices were made 200-μm thick. Brain slices were stored in ice-cold aCSF. A single slice was submerged under aCSF maintained at 34°C and continuously flowing (2 mL/min) through a superfusion chamber (Warner Instruments, Hamden, CT, USA). Each brain slice was equilibrated for 30 min prior to obtaining measurements. When pharmacological agents were used, they were added to the buffer to a known concentration and superfused for 30 min prior to measuring their effect.

Rats were used for immunohistochemical experiments. They were sacrificed with urethane (1.5 g/kg, i.p.) and perfusd intracardially with 80 mL 0.9% saline followed by 80 mL of 4% paraformaldehyde. The brain was extracted and sliced as described above for mice.

Electrochemistry

Carbon-fiber cylinder microelectrodes were made as previously described (Kawagoe et al., 1993) using T650 carbon fibers (Amoco, Greenville, SC, USA) cut to a length of 25 μm. Electrodes were epoxied (Miller-Stevenson, Danbury, CT, USA) to ensure a good seal, and dipped immediately in acetone for a few seconds to remove residual epoxy from the carbon fiber. A triangular waveform, starting at -0.4 V, increasing to 1.0 V, and scanning back to -0.4 V, was applied to the carbon-fiber working electrode, versus a Ag/AgCl reference electrode, at a scan rate of 600 V/s. This will be referred to as the normal waveform. A second, serotonin-selective waveform was used, and this will be referred to as the modified waveform. The waveform was used as described previously (Bunin et al., 1998). It consists of scanning from +0.2 V to 1.0 V, down to -0.2 V and back up to 0.2 V at 1000 V/s. An update rate of 10 Hz was used for all experiments. The sensitivity of the waveforms to dopamine and serotonin were tested with flow injection analysis (FIA)

The carbon fiber was inserted until the tip was 60-70 μm below the surface of the brain slice between the prongs of a bipolar stimulating electrode (FHC, Bowdoinham, ME, USA), situated 200 μm apart. To evoke release, a biphasic stimulating current pulse (2 ms each phase, 350 μA in amplitude) was applied to the stimulating electrode. The current arising from dopamine and serotonin oxidation (at about 0.6 V) in successive voltammograms was measured and plotted versus time. This current was converted to concentration with post-calibrations.

Immunohistochemistry

Slices were fixed in 2% formaldehyde in Sorenson's buffer (0.15 m Na_2HPO_4/KH_2PO_4 at pH 7.4) for 4 h. The slices were rinsed three times with 1X PBS (Tissue Culture Facility, Chapel Hill, NC, USA). Then, normal goat serum (NGS, Life Technologies, Rockville, MD, USA) was combined with 0.2% BSA/PBS solution (1 : 10, NGS : BSA/ PBS) containing 0.3% Triton-100X. The slices were incubated in this blocking solution for 2 h. The primary antibody solutions were incubated for overnight (15hours) at 4°C with slow agitation and rinsed with PBS. For co-localization experiments, secondary antibody was diluted 1:1000 and incubated overnight with the slices. A primary antibody for TH (Goat, Invitrogen), diluted 1:400, was used with a goat anti-rabbit secondary antibody (Invitrogen) conjugated to Alexa Fluor ® 555. For TPH/GFP double labeling experiments, primary antibodies were diluted into 0.5 mL of PBS and then 5 mL of blocking solution to final dilutions as follows: anti-GFP (Sheep, Invitrogen), 1:200; anti-TPH (Rabbit, Invitrogen), 1:200. The secondary antibodies used were donkey anti-sheep conjugated to Alexa Fluor ® 555 and Donkey anti-rabbit conjugated to FITC. Then, the slices were rinsed with PBS, placed on slides, and examined by confocal microscopy.

Confocal microscopy

Throughout this work, anatomical locations were determined by comparison with a mouse brain atlas (Paxinos and Franklin, 2004). The brain slices containing the desired regions were placed onto microscope slides with glass wells to maintain their structural integrity. Into these wells, Aqua-Poly/Mount (Polysciences, Inc., Warrington, PA) was added. After the slices were placed in mounting medium, they were coverslipped, and sealed with clear nail varnish. The confocal images were collected on a Leica SP2 Laser Scanning Confocal Microscope (Leica Microsystems, Confocal Microscopy, Germany) in the Michael Hooker Microscopy Facility at the University of North Carolina at Chapel Hill. Photomultiplier tubes

were used to detect the fluorescence from the fluorochromes in the multiple-labeling experiments.

Epifluorescent Microscopy

To visualize the fluorescence in brain slices, an upright microscope (Nikon Eclipse E600FN, Melville, NY) was used with a xenon lamp source to excite fluorescence. a Nikon endow GFP bandpass filter set (filter 470 CWL for excitation, 525 CWL for emission, and a 495 LP dichroic mirror) was employed when viewing samples from GFP mice. A CCD camera (Photometrics Sensys, Tucson, Arizona) was used to capture images.

Results

Flow Injection Analysis (FIA)

The normal waveform is sensitive to dopamine and more sensitive to serotonin (Figure 6.1). However with this waveform serotonin quickly fouls the electrode, decreasing its sensitivity (data not shown). The modified waveform prevents this fouling and provides selectivity over dopamine. In fact, 1 μM dopamine is undetectable (Figure 6.1). Figure 2 shows that the oxidative current for serotonin and dopamine are additive in a mixed solution. The current at 0.6 V for a 1 μM dopamine solution and a 1 μM serotonin solution, when added together, equal the current at 0.6 V for a solution containing both 1 μM dopamine and 1 μM serotonin (Figure 6.2b, ratio = 1.05 $\pm$0.05).

This additive property allows the use of both waveforms in a mixed solution to determine the concentration of each analyte. The modified waveform can be used to

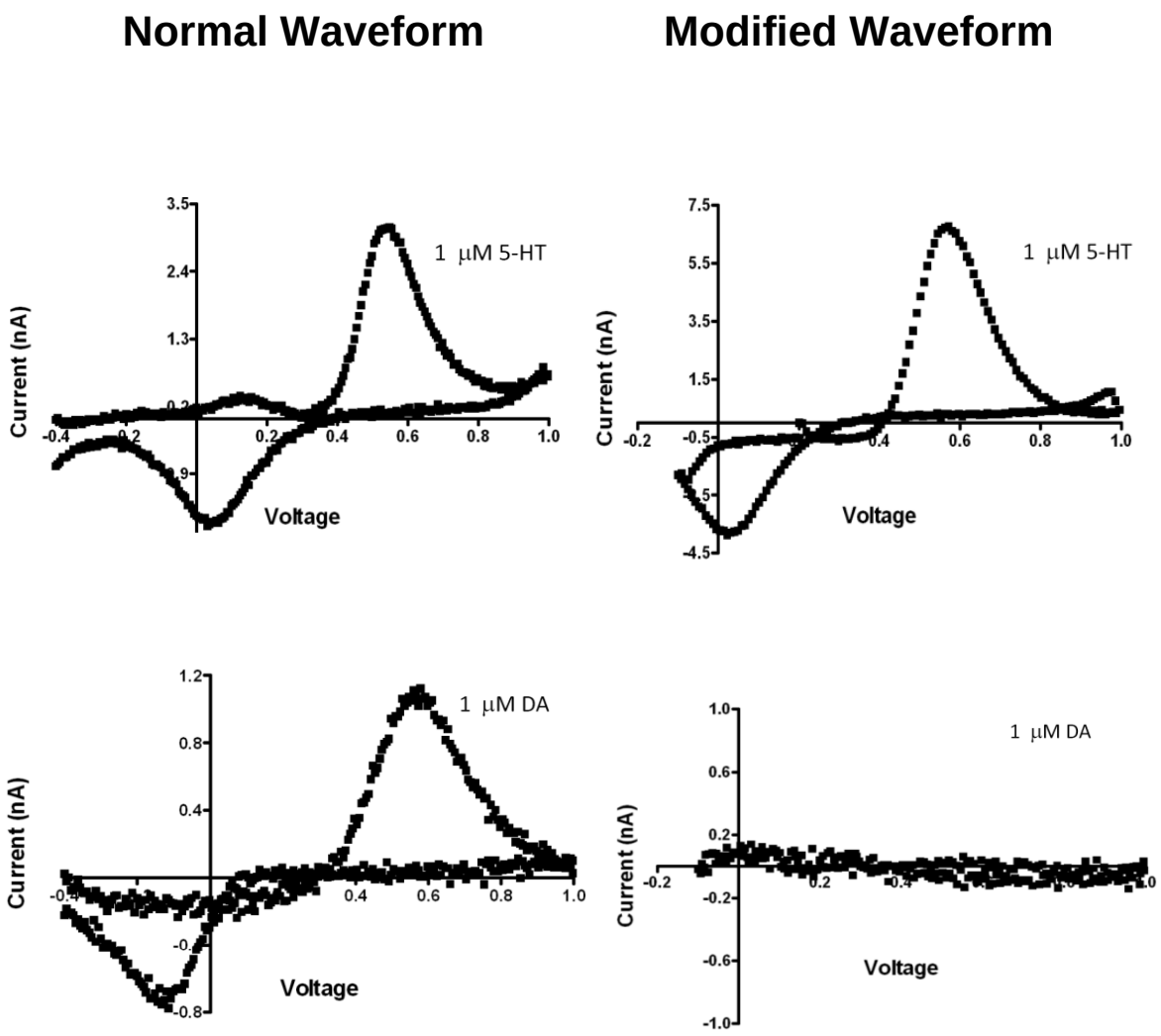

Figure 6.1. Differntial response of DA and 5-HT in a flow cell measured with two different waveforms. The CV's for 5-HT are across the top and the CV's for an equal concentration of DA is shown below. The modified waveform is insensitive to a 1μM dopamine solution.

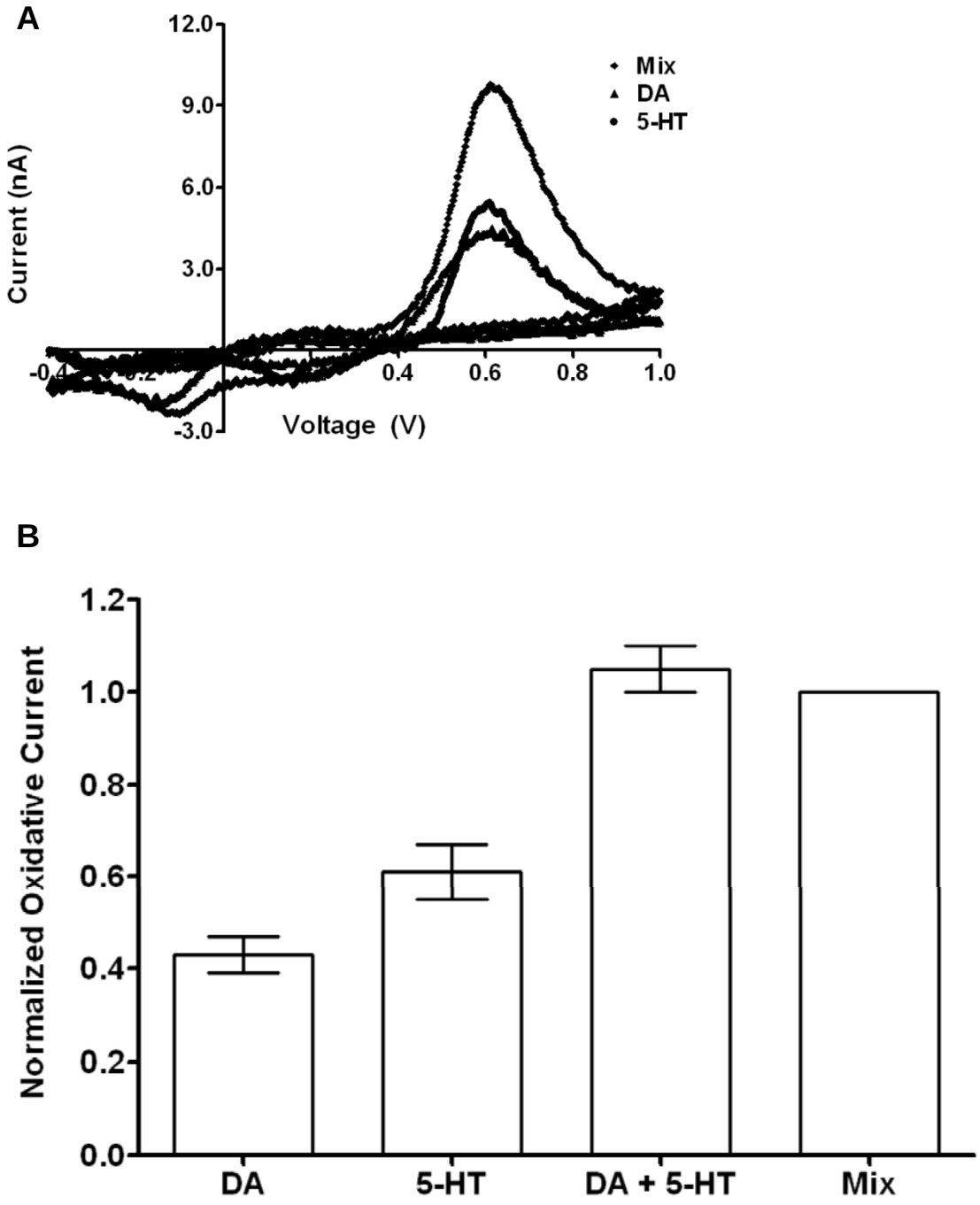

Figure 6.2. FIA of DA and 5-HT comparing their cyclic voltammograms when alone and when mixed. A.) CV's of a 1μM dopamine and a 1 μM serotonin solution are overlayed with the CV of a mixed solution of 1μM dopamine and 1 μM serotonin. B.) The current at 0.6 V for 1μM dopamine and a 1 μM serotonin solution are normalized to that of a mixed solution of both. DA + 5-HT is the result of adding the current from the individual solutions and normalizing it to the mixed solution. These results are essentially identical (1.05 ±0.05).

determine the serotonin concentration. Knowing the sensitivity of the electrode to serotonin with the normal waveform and the concentration of serotonin, one can find the current contribution of serotonin with the normal waveform. Then, the oxidative current from dopamine can be determined and be used to determine the dopamine concentration.

Immunohistochemistry

Tyrosine hydroxylase (TH) was used as a marker for dopaminergic neurons in rat brain slices. Adjacent confocal bright field and fluorescent images correspond to the same location in a brain slice. The oval on the bright field image indicates the area of interest. Figure 6.4a indicates the iMLF and shows the presence of TH. Figure 6.4b indicates the position of the RN which does not label for TH but whose ventral border is outlined by the heavy labeling of the VTA.

In GFP transgenic mice GFP expression is driven by the promoter for TH, the rate-limiting enzyme in catecholamine synthesis and is used as a marker for dopaminergic neurons. Tryptophan hydroxylase (TPH), the rate-limiting enzyme in serotonin synthesis, was used as a marker for serotonergic neurons. In Figure 6.5a, the SNr is heavily labeled for TPH. In contrast, the SNc is labeled for both TPH and GFP. The VTA is labeled for both TPH and GFP as well. In fact, the labeling of TPH can be seen in GFP positive cells.

Serotonin and Dopamine in the Midbrain

The concentration of stimulated (20-pulse, 60Hz) serotonin and dopamine release were measured in the VTA, RN, and iMLF in brain slices from GFP transgenic mice. The determination of concentration was executed using the procedure described above with the normal and modified waveforms. The current traces at 0.6 V is shown for all three regions

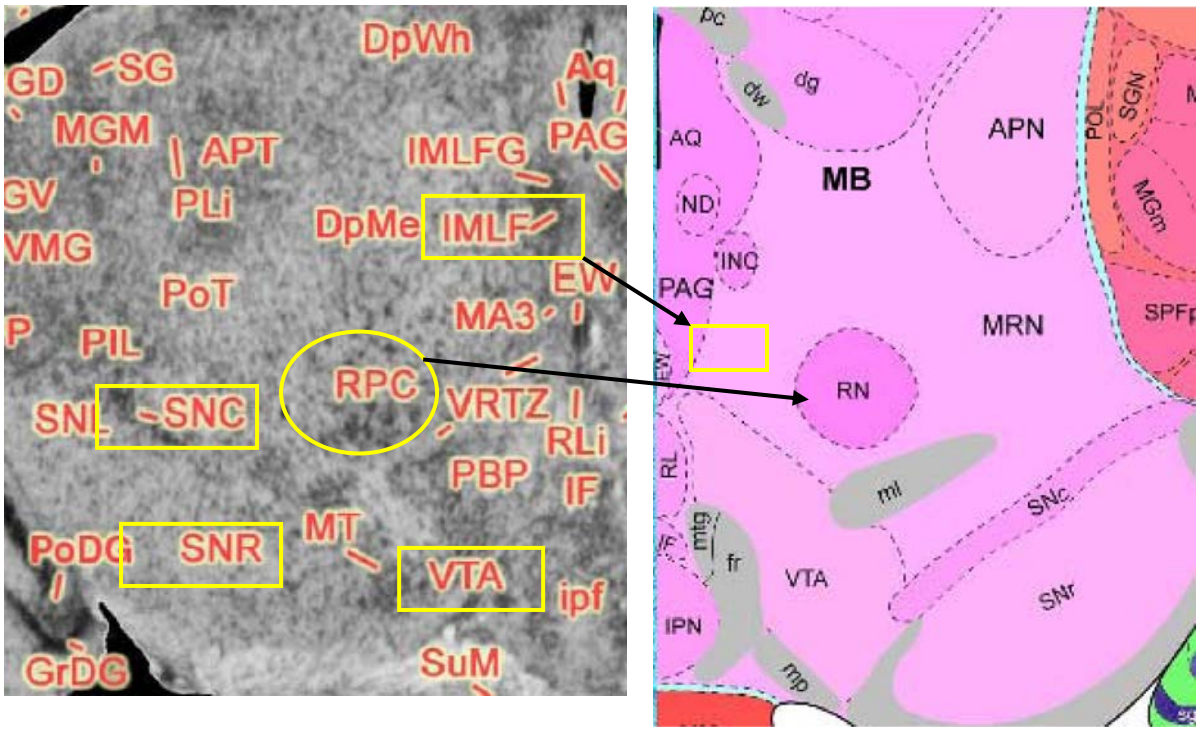

Figure 6.3. Identified target regions (yellow squares and oval). Labeled mouse brain (mbl.org) on the right, and a mouse brain atlas (braininfo.rprc.washington.edu) showing the regions diagrammatically on the left. Note the panels are mirror images because they are taken from opposite sides of the brain. The brain is generally symmetrical about the midline.

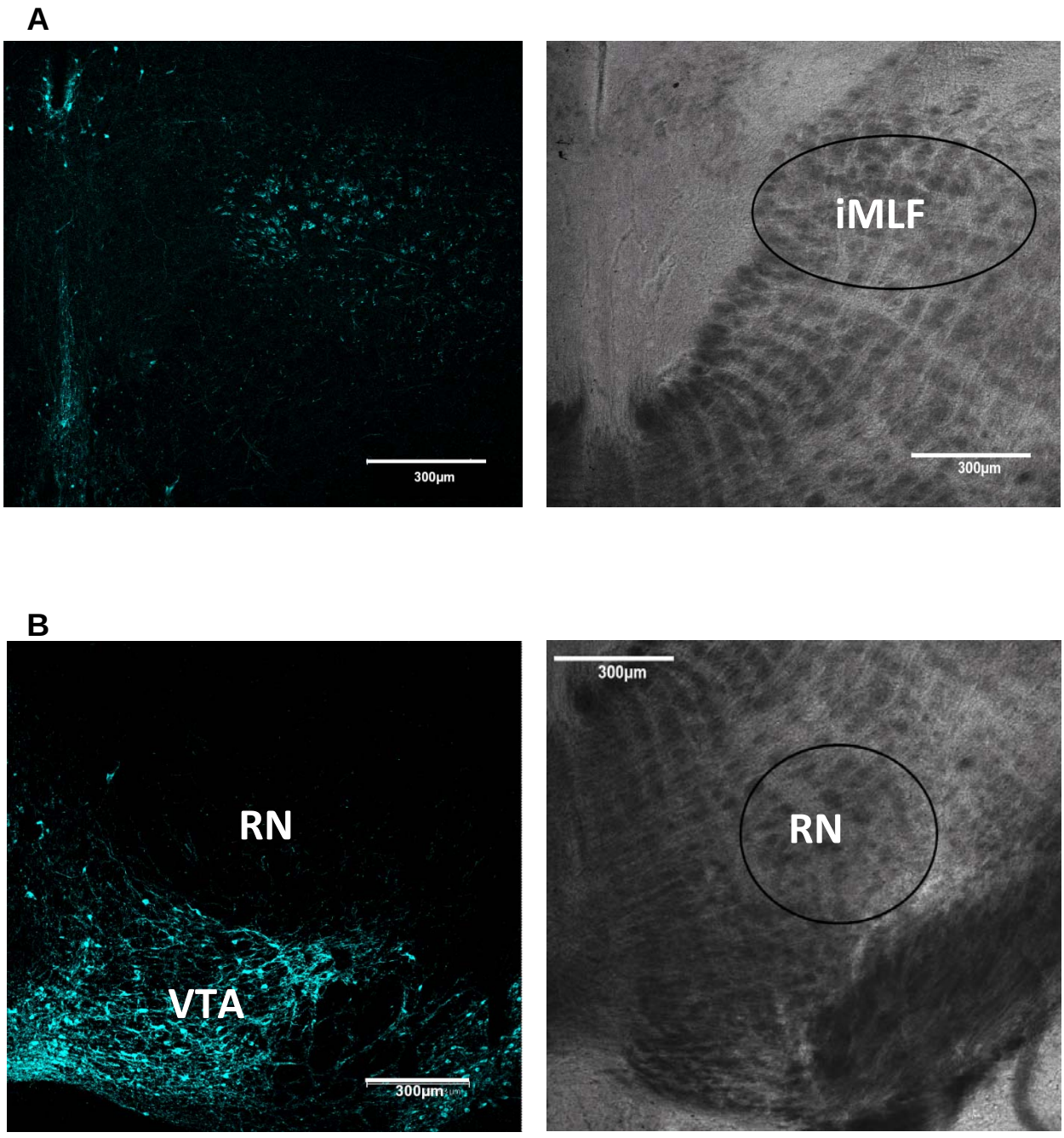

Figure 6.4. TH (cyan) labeling in the midbrain. Confocal fluorescent and bright field images of the A.) iMLF and B.) RN, identified in the ovals encapsulating the region. Adjacent images are from the same slice and location.

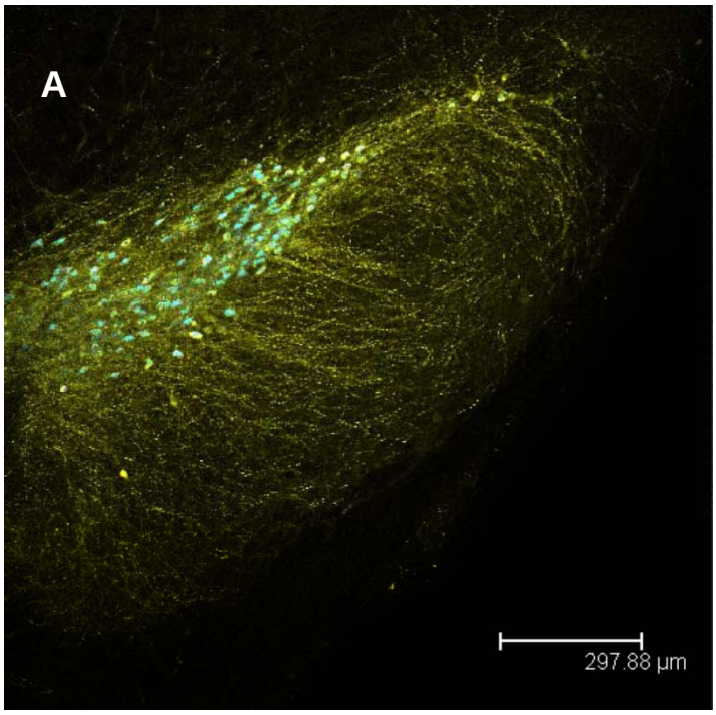

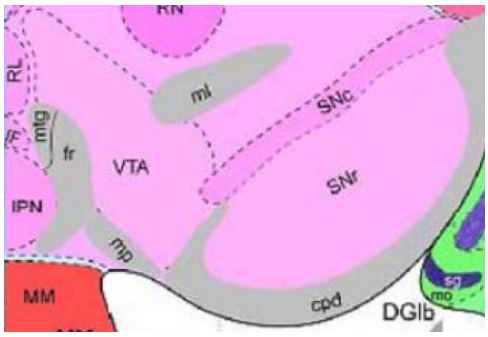

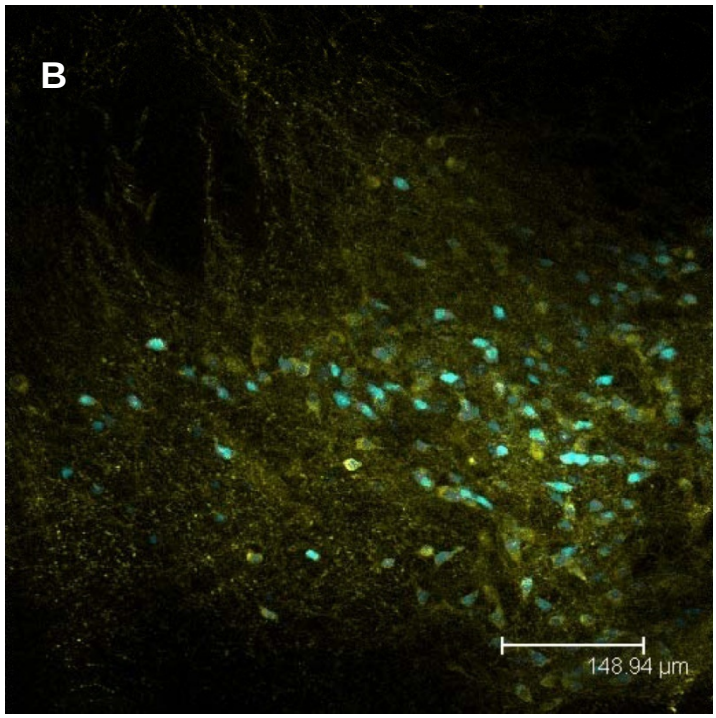

Figure 6.5. GFP and TPH co-localization determined with confocal microscopy. Immuno-histochemical labeling of TPH (yellow) and GFP (cyan) in the A.) SN and B.) VTA. At the right is a mouse brain atlas indicating the location of these areas in a brain slice.

using both waveforms (Figure 6.6a). The cyclic voltammograms (CV) for each waveform taken at the peak of release are shown below the trace for the corresponding region (Figure 6.6b). Stimulated release is largest in the VTA, followed by the iMLF, then the RN. The difference in magnitude of release measured by the two waveforms is largest in the VTA and the normal waveform CV looks the most like dopamine. There is very little difference in the traces in the RN using either waveform, and the CV's confirm that release is mostly serotonergic. The results across five mice are displayed in Figure 6.6c. They show that dopamine release is largest in the VTA and serotonin release is largest in the iMLF. There is three times as much serotonin as dopamine in the RN. Interestingly, there is some small amount of dopamine release measured in the RN despite the weak TH labeling.

Fluorescence and Release in the SNc

Cells expressing GFP can be indentified in the SNc and an oxidation current at 0.6 V is generated upon a 10-pulse, 60 Hz stimulation (Figure 6.7). However, there is no relationship between the fluorescence intensity and current (Figure 6.7c, $r^2 = 0.001$). To determine if the release measured is dopaminergic or serotonergic, the serotonin selective modified waveform was used at each position. From the CV's in Figure 6.7b, one can see that serotonin is being measured (CV from position 2 shown as an example). Moreover, the current observed decreases from positions ventral to dorsal (Figure 6.7e). The most ventral position, 2, is nearest the SNr, a region that labeled heavily for TPH. The labeling of the SNc in Figure 6.5a reveals that the dopaminergic cells are surrounded by serotonergic terminals. Across all positions the serotonin concentration measured in this slice is 237 $\pm$2 nM. In fact, serotonin constitutes 72 $\pm$4% of the signal measured with the normal waveform.

Remote Stimulation of the VTA

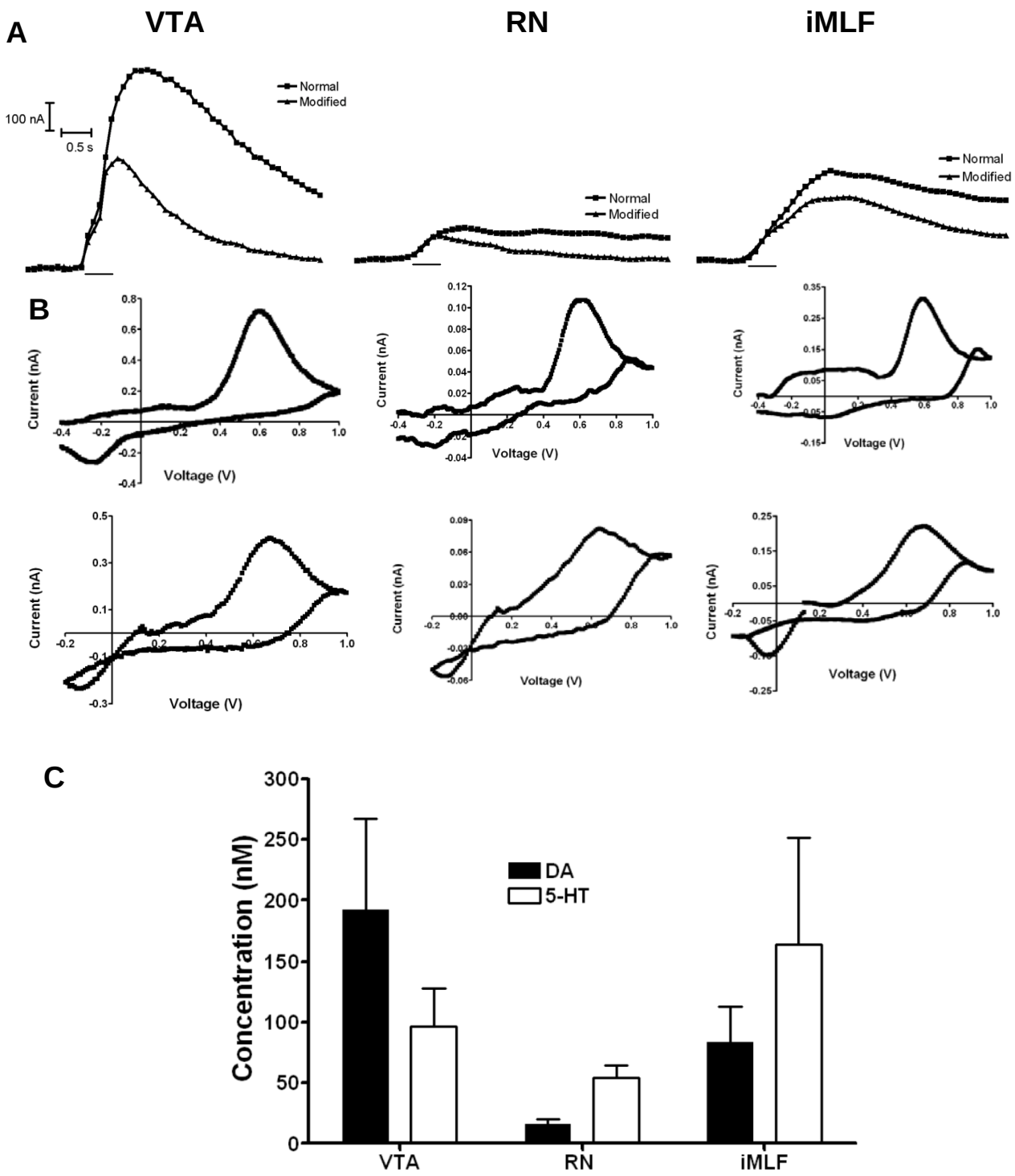

Figure 6.6. Dopamine and serotonin release in the midbrain. A.)Total current traces at 0.6 V for each waveform in the same location across three regions. B.) The corresponding CV's are below the traces. CV's recorded using the normal waveform are in the first row and those using the modified waveform are below them in the second row. C.) A summary of dopamine and serotonin concentrations measured across all three regions for n = 5 mice.

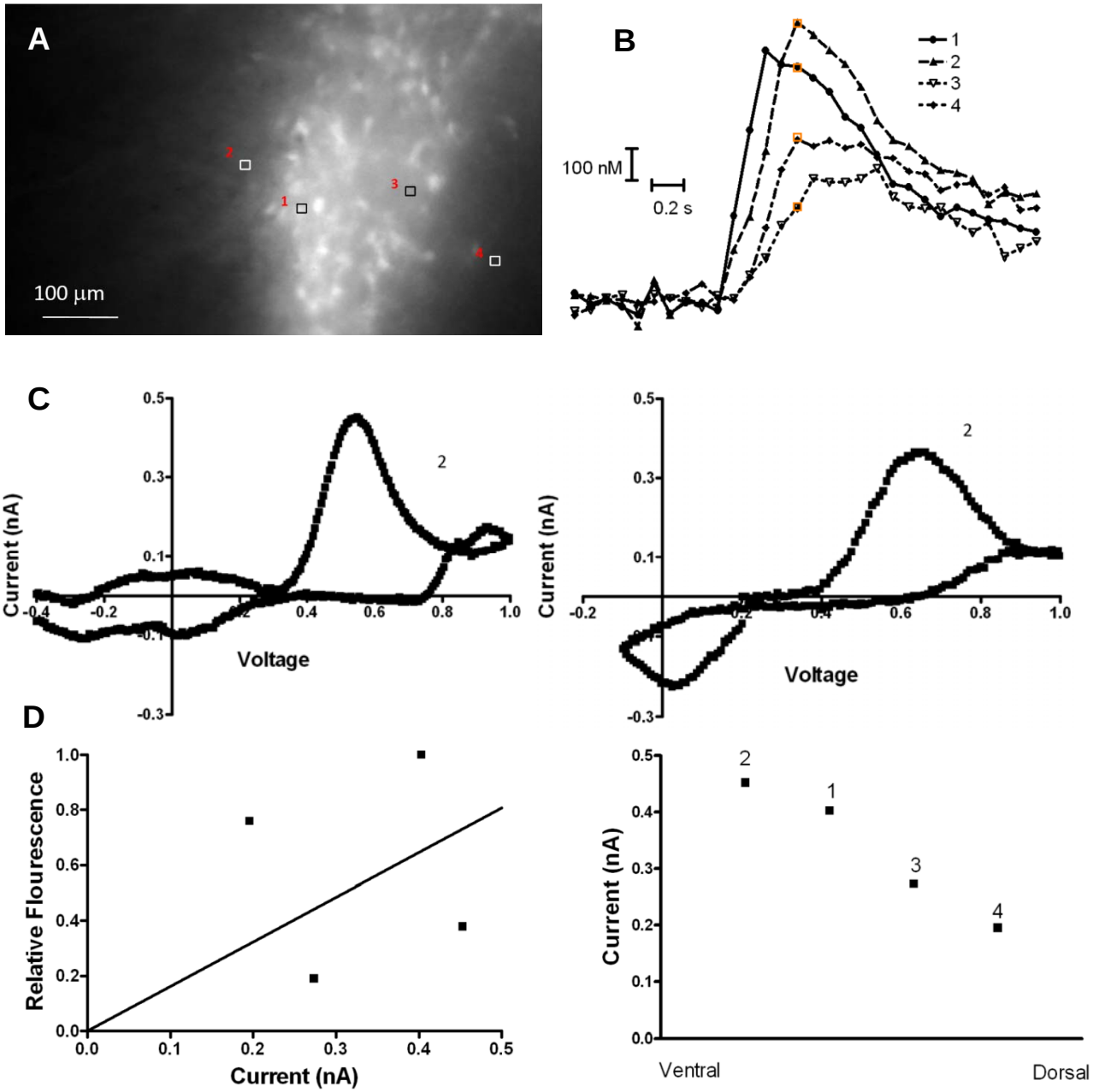

Figure 6.7. SNc relationship between fluorescent intensity and dopamine release. A) Epifluorescent image of a GFP mouse brain slice containing the SNc. Squares indicate electrode location for the corresponding traces. B) Stimulated release (20-pulse, 60 Hz) at the corresponding positions. The orange squares indicate the end of the stimulation. C) Based on electrode sensitivity for serotonin with two different waveforms, the released analyte is 72 ±4% serotonin or 237 ±2 nM across all positions. D.) The linear regression of the relative fluorescence in the squares compared to the release at those positions (r^2 = 0.001). Release magnitude is more tightly associated with proximity to the SNr, the black to the left (ventral) in the image.

Stimulating the MFB caused the release of electroactive substances in the VTA (Figure 6.8). The released substance was electrochemically identified as serotonin (Figure 6.8c). This was confirmed with pharmacology. Bupropion (bpr) is a selective inhibitor of the dopamine transporter (DAT). Addition of 500 nM bpr did not alter the magnitude or time course of the signal. However 500 nM citalopram, a selective inhibitor of the serotonin transporter (SERT), increased the magnitude of the signal and eliminated uptake. The uptake was very weak in the control file and did not change with the addition of bpr. The trace remains constant after stimulation in the presence of citalopram, indicating that uptake is absent. The magnitude of the signal is greater when uptake is absent because extracellular serotonin is not cleared between stimulation pulses.

Discussion

Using the normal waveform and the serotonin-selective modified waveform, the concentrations of dopamine and serotonin can be determined for a mixed solution. The modified waveform is relatively insensitive to dopamine and can therefore be used to determine the concentration of serotonin. Knowing the concentration of serotonin allows the dopaminergic concentration to be calculated. The ability to determine the concentrations of dopamine and serotonin in a mixed solution has been exploited in regions of the rodent brain that contain both neuromodulators. The VTA is considered a dopaminergic cell body region and serotonin has not been previously detected in this region electrochemically (Cragg et al., 1997; John et al., 2006). The presence of a serotonin receptor (5-HT_{2C}) in the VTA has been reported with immunohistochemical experiments (Bubar and Cunningham, 2007) and the protein for 5-HT_{2C} has been detected in the VTA

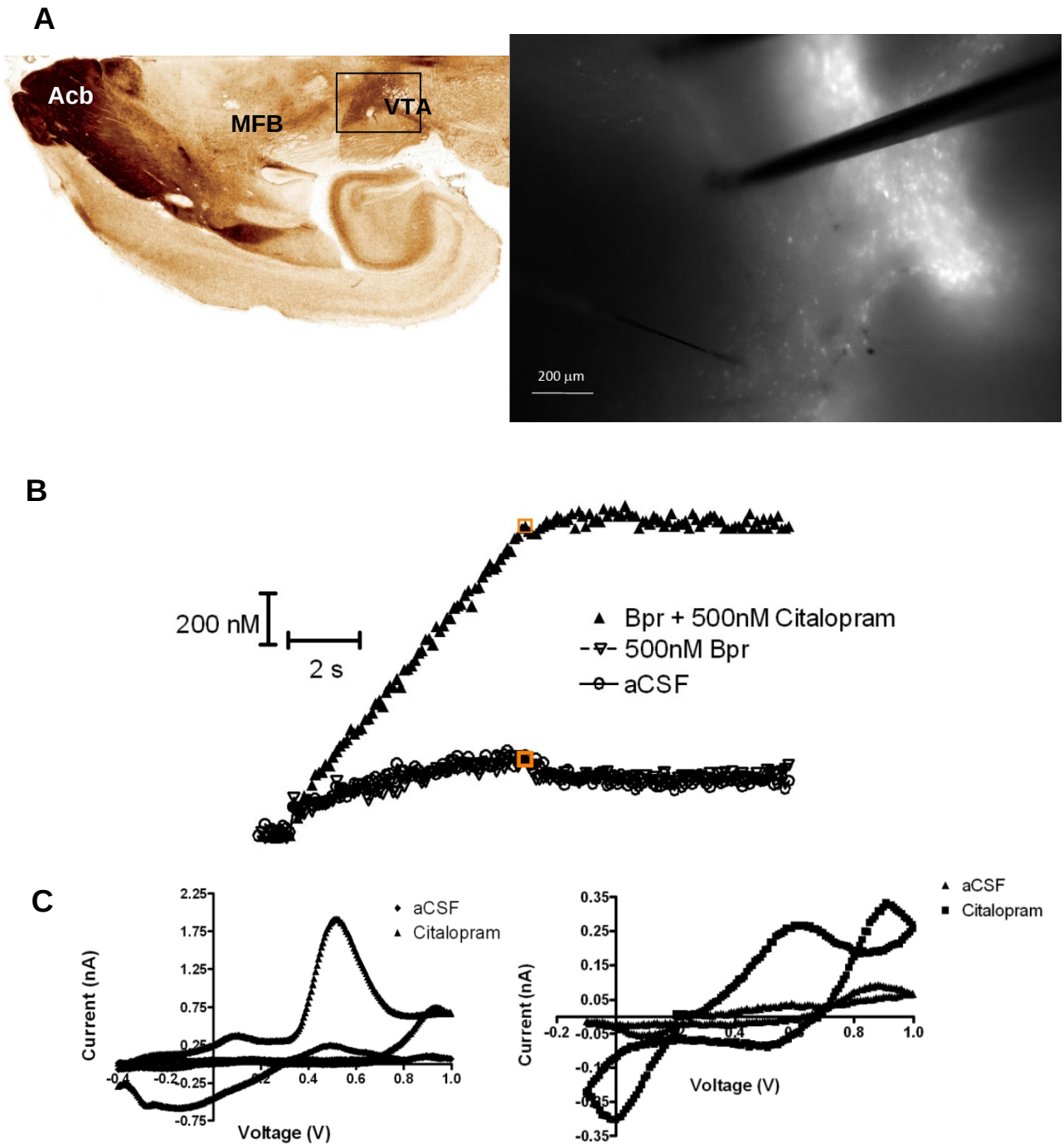

Figure 6.8. Remote stimulation of the VTA. A.) A representation of the region from the rat brain atlas (Paxinos and Watson, 2007) and an epifluorescent image showing electrode placement. B.) Traces recorded pre-drug (aCSF), with the addition of 500 nM Bupropion, and 500 nM Citalopram in the presence of 500nM Bupropion. C.) CV's recorded at the peak of release pre-drug and post-Citalopram. These CV's identify the analyte as serotonin.

(Abramowski et al., 1995; Clemett et al., 2000). The presence of a receptor demands an endogenous ligand to bind and activate it. The waveform used most recently by Jones and coworkers distinguishes between dopamine and serotonin by the potential of the reduction peaks for each analyte (Jones et al., 1996). Theyreport that release in the VTA is exclusively dopaminergic. The modified waveform used here is more sensitive to serotonin because the oxidation peak is measured and dopamine interference is eliminated. However, release is mostly dopaminergic, but it does contain a serotonin component (approximately 33% of the total current with the normal waveform, Figure 6.6c).

Although the iMLF labeled for TH, the majority of the electrochemical signal is serotonin. In cats, serotonergic neurons from the median raphe nucleus (MRN) extend to the iMLF (Jacobs and Azmitia, 1992). Serotonin suppression of cholinergic burst firing regulates rapid eye movement (REM) during sleep in rats, (Luebke et al., 1992) and it is these saccadic movements that become impaired in Parkinson's disease for some humans (Mosimann et al., 2005). Lesions of the iMLF in monkeys leads to loss of all rapid eye movements (Henn et al., 1989). This is a region that has not been study previously with electrochemistry. However, electrochemistry with microelectrodes could elucidate the connection between the iMLF, the dopamine systems, and symptoms of Parkinson's disease.

The modified waveform has been used by our lab previously to measure serotonin in the SNc and the dorsal raphe (DR), which are known serotonergic regions (Bunin et al., 1998). Our measurements in the SNc confirm the earlier work and add the presence of a small concentration of stimulated dopamine release. Using only one waveform, the dopaminergic currents would go unidentified since the majority of the current arises from serotonin oxidation. Those results have been extended by measuring serotonin and

dopamine in the RN, another known serotonergic region. This region also releases small concentrations of dopamine, which has not been reported previously.

The small concentrations of dopamine in these regions could possibly be attributed in error. If the concentration of serotonin being released and measured changed between the applications of the different waveforms, then the current considered due to serotonin would be wrong, and thus, the difference in current would be assigned to dopamine oxidation in error. Additionally, the strength of the method is dependent on the quality of the calibrations using the two waveforms. If one of the three calibrations is inaccurate, then the determination of one or both of the analytes would be in error as well. Nevertheless, serotonin has definitively been measured electrochemically in regions heretofore unreported.

GFP transgenic mice have been used throughout these experiments to facilitate electrode placement. The intrinsic fluorescence of dopaminergic neurons aids in determining the location of the target structure. Moreover, these mice can be used to do novel experiments involving remote stimulation of release measured in the VTA. Initially our hypothesis was that antidromic stimulation, action potentials propagating towards the cell bodies, would cause dopamine release from cell bodies in the VTA. However the results here indicate that serotonin is being released from terminals. The modified waveform measures a CV indicative of serotonin, and citalopram inhibits uptake. Serotonergic axons are heavily labeled within the MFB (Azmitia and Gannon, 1983). We hypothesize that axons within the MFB are being stimulated and are releasing the serotonin being detected.

The use of FSCV with multiple waveforms applied to a carbon-fiber microelectrode is a powerful technique for measuring multiple analytes in a mixed environment, such as exists in many areas of the brain. Moreover, the modified waveform is sensitive to small

concentrations of serotonin and was used to detect serotonin in regions where it had not been previously reported. These electrochemical approaches can be used to probe novel regions, such as the iMLF and RN, and novel contexts, such as remotely stimulating the VTA.

References

Abramowski D, Rigo M, Duc D, Hoyer D, Staufenbiel M (1995) Localization of the 5-hydroxytryptamine2C receptor protein in human and rat brain using specific antisera. Neuropharmacology 34:1635-1645.

Azmitia E, Gannon P (1983) The ultrastructural localization of serotonin immunoreactivity in myelinated and unmyelinated axons within the medial forebrain bundle of rat and monkey. J Neurosci 3:2083-2090.

Bjorklund A, Lindvall O (1984) Dopamine-containing systems in the CNS. Handbook Chem Neuroanat 2:55-113.

Bosler O, Nieoullon A, Onteniente B, Dusticier N (1983) In vitro radioautographic study of the monoaminergic innervation of cat red nucleus. Identification of serotoninergic terminals. Brain Res 259:288-292.

Bradbury AJ, Costall B, Kelly ME, Naylor RJ, Smith JA (1985) Biochemical correlates of motor changes caused by the manipulation of dopamine function in the substantia nigra of the mouse. Neuropharmacology 24:1155-1161.

Bubar MJ, Cunningham KA (2007) Distribution of serotonin 5-HT2C receptors in the ventral tegmental area. Neuroscience 146:286-297.

Bunin MA, Prioleau C, Mailman RB, Wightman RM (1998) Release and uptake rates of 5-hydroxytryptamine in the dorsal raphe and substantia nigra reticulata of the rat brain. J Neurochem 70:1077-1087.

Clemett DA, Punhani T, Duxon MS, Blackburn TP, Fone KC (2000) Immunohistochemical localisation of the 5-HT2C receptor protein in the rat CNS. Neuropharmacology 39:123-132.

Cobb WS, Abercrombie ED (2003) Differential regulation of somatodendritic and nerve terminal dopamine release by serotonergic innervation of substantia nigra. J Neurochem 84:576-584.

Corvaja N, Doucet G, Bolam JP (1993) Ultrastructure and synaptic targets of the raphe-nigral projection in the rat. Neuroscience 55:417-427.

Cragg SJ, Hawkey CR, Greenfield SA (1997) Comparison of serotonin and dopamine release in substantia nigra and ventral tegmental area: region and species differences. J Neurochem 69:2378-2386.

Di Chiara G, Imperato A (1988) Drugs abused by humans preferentially increase synaptic dopamine concentrations in the mesolimbic system of freely moving rats. Proc Natl Acad Sci U S A 85:5274-5278.

Henn V, Hepp K, Vilis T (1989) Rapid eye movement generation in the primate. Physiology, pathophysiology, and clinical implications. Rev Neurol (Paris) 145:540-545.

Hery F, Soubrie P, Bourgoin S, Motastruc JL, Artaud F, Glowinski J (1980) Dopamine released from dendrites in the substantia nigra controls the nigral and striatal release of serotonin. Brain Res 193:143-151.

Jacobs BL, Azmitia EC (1992) Structure and function of the brain serotonin system. Physiol Rev 72:165-229.

John CE, Budygin EA, Mateo Y, Jones SR (2006) Neurochemical characterization of the release and uptake of dopamine in ventral tegmental area and serotonin in substantia nigra of the mouse. J Neurochem 96:267-282.

Jones SR, O'Dell SJ, Marshall JF, Wightman RM (1996) Functional and anatomical evidence for different dopamine dynamics in the core and shell of the nucleus accumbens in slices of rat brain. Synapse 23:224-231.

Jones SR, Gainetdinov RR, Hu XT, Cooper DC, Wightman RM, White FJ, Caron MG (1999) Loss of autoreceptor functions in mice lacking the dopamine transporter. Nat Neurosci 2:649-655.

Kawagoe KT, Zimmerman JB, Wightman RM (1993) Principles of voltammetry and microelectrode surface states. J Neurosci Methods 48:225-240.

Kessler MA, Yang M, Gollomp KL, Jin H, Iacovitti L (2003) The human tyrosine hydroxylase gene promoter. Brain Res Mol Brain Res 112:8-23.

Kuhr WG, Wightman RM (1986) Real-time measurement of dopamine release in rat brain. Brain Res 381:168-171.

Lavoie B, Parent A (1990) Immunohistochemical study of the serotoninergic innervation of the basal ganglia in the squirrel monkey. J Comp Neurol 299:1-16.

Lemberger L, Fuller RW, Zerbe RL (1985) Use of specific serotonin uptake inhibitors as antidepressants. Clin Neuropharmacol 8:299-317.

Licata F, Li Volsi G, Di Mauro M, Fretto G, Ciranna L, Santangelo F (2001) Serotonin modifies the neuronal inhibitory responses to gamma-aminobutyric acid in the red nucleus: a microiontophoretic study in the rat. Exp Neurol 167:95-107.

Liu Z, Bunney EB, Appel SB, Brodie MS (2003) Serotonin reduces the hyperpolarization-activated current (Ih) in ventral tegmental area dopamine neurons: involvement of 5-HT2 receptors and protein kinase C. J Neurophysiol 90:3201-3212.

Luebke JI, Greene RW, Semba K, Kamondi A, McCarley RW, Reiner PB (1992) Serotonin hyperpolarizes cholinergic low-threshold burst neurons in the rat laterodorsal tegmental nucleus in vitro. Proc Natl Acad Sci U S A 89:743-747.

Medanic M, Gillette MU (1992) Serotonin regulates the phase of the rat suprachiasmatic circadian pacemaker in vitro only during the subjective day. J Physiol 450:629-642.

Missale C, Nash SR, Robinson SW, Jaber M, Caron MG (1998) Dopamine receptors: from structure to function. Physiol Rev 78:189-225.

Mosimann UP, Muri RM, Burn DJ, Felblinger J, O'Brien JT, McKeith IG (2005) Saccadic eye movement changes in Parkinson's disease dementia and dementia with Lewy bodies. Brain 128:1267-1276.

Moukhles H, Bosler O, Bolam JP, Vallee A, Umbriaco D, Geffard M, Doucet G (1997) Quantitative and morphometric data indicate precise cellular interactions between serotonin terminals and postsynaptic targets in rat substantia nigra. Neuroscience 76:1159-1171.

Nedergaard S, Bolam JP, Greenfield SA (1988) Facilitation of a dendritic calcium conductance by 5-hydroxytryptamine in the substantia nigra. Nature 333:174-177.

Paxinos G, Franklin KBJ (2004) The mouse brain in stereotaxic coordinates, Compact 2nd Edition. Amsterdam ; Boston: Elsevier Academic Press.

Racette BA, Esper GJ, Antenor J, Black KJ, Burkey A, Moerlein SM, Videen TO, Kotagal V, Ojemann JG, Perlmutter JS (2004) Pathophysiology of parkinsonism due to hydrocephalus. J Neurol Neurosurg Psychiatry 75:1617-1619.

Schultz W, Dayan P, Montague PR (1997) A neural substrate of prediction and reward. Science 275:1593-1599.

Sealfon SC (2000) Dopamine receptors and locomotor responses: molecular aspects. Ann Neurol 47:S12-19; discussion S19-21.

Toonen M, van Dijken H, Holstege JC, Ruigrok TJ, Koekkoek SK, Hawkins RK, Teune TM, vd Burg J, De Zeeuw CI (1998) Light microscopic and ultrastructural investigation of the dopaminergic innervation of the ventrolateral outgrowth of the rat inferior olive. Brain Res 802:267-273.

Trent F, Tepper JM (1991) Dorsal raphe stimulation modifies striatal-evoked antidromic invasion of nigral dopaminergic neurons in vivo. Exp Brain Res 84:620-630.

Wise RA (2004) Dopamine, learning and motivation. Nat Rev Neurosci 5:483-494.